nagra.

TECHNICAL REPORT 23-08

Diffusion Databases for Opalinus Clay, Confining Geological Units and Bentonite: Methods, Concepts and Upscaling of Data

October 2024

Nagra | National Cooperative for the Disposal of Radioactive Waste
Hardstrasse 73 | 5430 Wettingen | Switzerland
T. +41 56 437 11 11 | info@nagra.ch | nagra.ch

nagra.

TECHNICAL REPORT 23-08

Diffusion Databases for Opalinus Clay, Confining Geological Units and Bentonite: Methods, Concepts and Upscaling of Data

October 2024

M. A. Glaus[1], D. A. Kulik[1, 2], G. D. Miron[1], L. R. Van Loon[1, 3], R. A. J. Wüst[4], J. K. Becker[4] & X. Li[4]

[1]PSI, 5232 Villigen, Switzerland

[2]Congineer GmbH, 5200 Brugg, Switzerland

[3]CWL Solutions GmbH, 5314 Kleindöttingen, Switzerland

[4]Nagra

Nagra | National Cooperative for the Disposal of Radioactive Waste
Hardstrasse 73 | 5430 Wettingen | Switzerland
T. +41 56 437 11 11 | info@nagra.ch | nagra.ch

The report titled "Diffusion Databases for Opalinus Clay, Confining Geological Units and Bentonite: Methods, Concepts and Upscaling of Data" presents the modelled diffusion databases derived from Nagra's extensive exploration campaigns which were part of the Swiss Sectoral Plan for Deep Geological Repositories.

The electronic look-up tables and data are part of Nagra's data management system and available upon request from Nagra.

The experimental (laboratory) diffusion data utilised in the modelling approach is presented in NAB 23-26 titled "Diffusion Measurements of HTO, 36Cl- and 22Na+ on Rock Samples of Opalinus Clay and Confining Geological Units from Deep Boreholes of Northern Switzerland: Jura Ost, Nördlich Lägern and Zürich Nordost".

The authors express their gratitude to Dr. N. Maes, Dr. L. Van Laer, and Dr. M. Aertsens for the careful review and quality assurance of this document. They extend sincere thanks to several key individuals who contributed significantly to this work, specifically P. Bunic and S. Frick for their technical support and the numerous experimental data acquired over the years. The graphic design team at Nagra are also acknowledged for their efforts in finalising the document and figures. The authors extend special thanks to Nagra for providing financial support, which enabled the successful completion of this study.

ISSN 1015-2636

Abstract

Safety analysis for the deep geological disposal of radioactive waste in consolidated sedimentary rocks relies on the use of appropriate parameter values for diffusion and retention properties of dose-relevant radionuclides. The effective diffusion coefficients (D_e) and accessible porosity (ε_{acc}) values for radionuclides are among the most important parameters for a quantitative description of transport processes in clay-rich host rocks for which advective and dispersive transport is assumed to be negligible.

This report describes the methods used for the compilation of diffusion databases (DDB) of element-specific D_e and ε_{acc} values for the Mesozoic rocks in Northern Switzerland as well as compacted bentonite using the appropriate reference porewater compositions. The methods are based on the procedures applied in previous safety analysis but aim at a generic implementation of electrostatic effects of the diffusion of charged species in charged porous media. Such effects are described here using the so-called «Mean-Potential Donnan Layer» (MPDL) approach to quantify the equilibrium distribution of charged species between the bulk porewater and the Donnan phase (a defined volume of charged solution near the charged rock surfaces).

Recent empirical relationships are used here to derive the total porosity and the geometrical factor as a function of the total clay content in rock. These empirical relationships produce narrower uncertainty bands in the prediction of D_e of uncharged tracers in clay rock and are more broadly applicable compared to the extended Archie's relationship applied in previous safety analysis. For bentonite, the extended Archie's relationship is still used here because the target bulk dry density of bentonite – and thus the total porosity – is predefined.

The empirical geometrical relationships and the MPDL approach are implemented in the so-called ClaySorDif model (as an extension of the existing ClaySor sorption model) realised in a Python/Jupyter notebook environment based on GEMS codes. The model calibration uses the results of an extensive series of diffusion measurements on rock samples obtained from Nagra's deep drilling campaign in Northern Switzerland. The use of such a consistent tool and data chain for the derivation of solubility, sorption and diffusion data is thus unique in the literature. The DDBs are generated as look-up tables of diffusion parameters for a range of the total clay content in rock and the selected reference porewaters as the primary input variables. Their applicability is restricted to a temperature of 25 °C and the diffusion direction perpendicular to the bedding. The same procedures as in previous safety analysis are proposed here to consider the effects on diffusion of temperature and the orientation of the clay particles. A comprehensive comparison exercise shows that the results produced by the MPDL model based on GEMS produce almost the same results as a previous implementation of the electrostatic model in PHREEQC. Both models differ slightly in their approaches to quantifying the excess negative charge acting on the Donnan equilibrium distribution of charged species.

The D_e and ε_{acc} values are inherently linked to the speciation of a given radioelement. Low D_e and ε_{acc} values result for elements that are predominantly present as anionic species, which is the case e.g. for Np or Th. The highest values for D_e are found for elements predominantly present as cationic species, such as Cs^+, alkaline earth metal cations (e.g. Sr^{2+}, Ra^{2+}) or the trivalent actinides (e.g. Am^{3+}). Halogenides (e.g. I^-) generally exhibit rather low D_e and ε_{acc} values.

The predictions by ClaySorDif are compared with the predictions made in previous safety analysis. The results for sediments with moderate to high clay contents do not differ significantly. Only for more calcareous rocks, for which the geometrical relationships are known to be less applicable, are discrepancies noted in some cases. It should also be emphasised that the scope of the previous diffusion models with respect to surface diffusion was limited to radioelements undergoing cation exchange processes. Anion exclusion effects were assumed to be identical for all types of anions, regardless of their charge numbers. The present model is free of such

restrictions. It accounts for the full speciation of a given element, irrespective of its redox state, which facilitates the compilation of diffusion data for any desired geochemical constellation of rock and porewater composition without the need to make subjective decisions.

The D_e and ε_{acc} values in the look-up tables computed in ClaySorDif are linked to geophysical borehole log data and produce highly resolved borehole depth profiles of D_e and ε_{acc}, as shown in a dedicated chapter of this report. The profiles calculated are further processed in statistical approaches to estimate not only representative mean values for given abstracted rock units used in transport models for safety and performance analysis, but also their ranges of uncertainty and variability.

Zusammenfassung

Die Sicherheitsanalyse für die geologische Tiefenlagerung radioaktiver Abfälle in Sedimentgesteinen beruht auf der Anwendung geeigneter Parameterwerte für die Diffusions- und Rückhalteeigenschaften dosisrelevanter Radionuklide. Die Werte für die effektiven Diffusionskoeffizienten (D_e) sowie für die zugängliche Porosität (ε_{acc}) von Radionukliden gehören zu den wichtigsten Parametern, mit welchen Transportprozesse im tonreichen Wirtgestein eines geologischen Tiefenlagers quantitativ beschrieben werden. Dabei wird davon ausgegangen, dass bei den Transportprozessen der advektive sowie der dispersive Transport vernachlässigt werden können.

Dieser Bericht beschreibt die Methoden, die zur Erstellung von Diffusionsdatenbanken (DDB) mit elementspezifischen D_e- und ε_{acc}-Werten für die mesozoischen Gesteine der Nordschweiz und für kompaktierten Bentonit unter Einbezug der Zusammensetzungen der Referenzporenwässer verwendet wurden. Die Methoden basieren auf den Verfahren, die in früheren Langzeitsicherheitsnachweisen verwendet wurden, zielen aber auf eine generische Umsetzung der elektrostatischen Diffusionsphänomene geladener Spezies in geladenen porösen Medien ab. Solche Effekte werden hier mit dem sogenannten «Mean-Potential Donnan Layer» (MPDL) Ansatz beschrieben, um die Gleichgewichtsverteilung geladener Spezies zwischen dem Porenwasser und der Donnan-Phase (ein definiertes Volumen geladener Lösungen in der Nähe geladener Gesteinsoberflächen) quantifizieren zu können.

Hierzu werden neue empirische Beziehungen verwendet, um die Gesamtporosität und den Geometriefaktor als Funktion des Gesamttongehalts im Gestein abzuleiten. Diese empirischen Beziehungen ermöglichen eine engere Prognose von D_e für ungeladene Tracer im Tongestein. Sie haben im Vergleich zur erweiterten Archie-Gleichung, die in früheren Sicherheitsanalysen angewandt wurde, ein breiteres Spektrum an Anwendungsmöglichkeiten. Für Bentonit wird hier wiederum die erweiterte Archie-Gleichung verwendet, da angestrebte Trockendichte des Bentonits – und damit die Gesamtporosität – vorgegeben sind.

Die empirischen geometrischen Beziehungen und der MPDL-Ansatz sind im sogenannten ClaySorDif-Modell (Erweiterung des bestehenden ClaySor-Sorptionsmodells) in einer Python/Jupyter-Notebook-Umgebung auf der Grundlage von GEMS-Codes implementiert. Die Kalibrierung des Modells stützt sich auf die Ergebnisse einer umfangreichen Reihe von Diffusionsmessungen an Gesteinsproben, die im Rahmen der Tiefbohrkampagne der Nagra in der Nordschweiz gewonnen wurden. Die Verwendung einer derart einheitlichen Instrumenten- und Datenkette zur Ableitung von Löslichkeits-, Sorptions- und Diffusionsdaten ist somit in der Literatur einzigartig. Die DDBs werden in Form von Nachschlagetabellen der Diffusionsparameter, welche als Funktion des Gesamttongehalts des Gesteins und ausgewählter Referenzporenwässer ausgedrückt werden, erstellt. Ihre Anwendbarkeit ist auf eine Temperatur von 25 °C und die Diffusionsrichtung senkrecht zur Tonschichtung limitiert. Die gleichen Verfahren wie in den früheren Langzeitsicherheitsnachweisen werden auch hier vorgeschlagen, um die Auswirkungen von Temperatur und der Orientierung der Tonplättchen auf die Diffusion zu berücksichtigen. Ein umfassender Quervergleich zeigt, dass die Ergebnisse des MPDL-Modells auf der Grundlage von GEMS beinahe die gleichen Ergebnisse liefern wie eine frühere Implementierung des elektrostatischen Modells in PHREEQC. Die zwei Modelle unterscheiden sich leicht in ihren Ansätzen zur Quantifizierung der negativen Überschussladung, die auf die Donnan-Gleichgewichtsverteilung der geladenen Spezies einwirkt.

Die D_e- und ε_{acc}-Werte sind eng mit der Speziation eines bestimmten Radionuklids verbunden. Elemente, die überwiegend als anionische Spezies vorliegen, wie z. B. Np oder Th, haben niedrige D_e- und ε_{acc}-Werte. Die höchsten D_e-Werte ergeben sich für Elemente, die überwiegend als kationische Spezies vorliegen, wie Cs^+, Erdalkalimetallkationen (z. B. Sr^{2+}, Ra^{2+}) oder dreiwertige Actiniden (z. B. Am^{3+}). Halogenide (z. B. I^-) weisen generell eher niedrige D_e- und ε_{acc}-Werte auf.

Die Prognosen von ClaySorDif werden mit denen aus früheren Langzeitsicherheitsnachweisen verglichen. Für Sedimentgesteine mit mässig hohem bis hohem Tongehalt unterscheiden sich die Ergebnisse nicht wesentlich. Lediglich bei kalkreichen Gesteinen, auf die geometrische Verhältnisse bekanntermassen weniger zutreffen, werden in einigen Fällen nennenswerte Abweichungen festgestellt. Erwähnenswert ist, dass der Anwendungsbereich früherer Diffusionsmodelle in Bezug auf die Oberflächendiffusion auf Kationenaustauschprozesse beschränkt war. Zudem wurde davon ausgegangen, dass die Ausschlusseffekte von Anionen für alle Arten von Anionen gleich sind, unabhängig von ihrer Ladungszahl. Das vorliegende Modell ist frei von solchen einschränkenden Annahmen. Es berücksichtigt die vollständige Speziation eines gegebenen Elements, unabhängig von seinem Redoxzustand. Dies erleichtert die Zusammenstellung von Diffusionsdaten für jede gewünschte geochemische Konstellation der Gesteins- und Porenwasserzusammensetzung, ohne dass subjektive Entscheidungen getroffen werden müssen.

Die D_e- und ε_{acc}-Werte der in ClaySorDif berechneten Nachschlagetabellen werden mit den Bohrlochdaten verknüpft und ergeben hochauflösende Tiefenprofile von D_e und ε_{acc}, was in einem eigenen Kapitel dieses Berichts ausführlich gezeigt wird. Die erzeugten Profile werden in statistischen Verfahren weiterverarbeitet, um nicht nur repräsentative Mittelwerte für bestimmte abstrahierte Gesteinseinheiten abzuschätzen, die in Transportmodellen für die Beurteilung der Langzeitsicherheit und die Prüfung der Barrierenwirksamkeit verwendet werden, sondern auch deren Bandbreite von Unsicherheiten und Variabilität aufzuzeigen.

Table of Contents

List of Tables

List of Figures

List of Acronyms

Andra	Agence nationale pour la gestion des déchets radioactifs (the French national agency for the management of radioactive waste)
2SPNE SC/CE	Two-site protolysis non-electrostatic surface complexation and cation exchange
BOZ	Bözberg borehole
BPW	Bentonite porewater
BUL	Bülach borehole
CEC	Cation exchange capacity
ClaySor	GEMS implementation of the 2SPNE SC/CE clay sorption model
ClaySorDif	Implementation of ClaySor and diffusion model in GEMS and Python in JupyterLab
CRZ	Containment-providing rock zone
DDB	Diffusion database
DL	Donnan layer
D_wDB	Database for diffusion coefficients in bulk water
EDL	Electrical double layer
Eh	Standard redox potential
FCC	Free charge capacity
Fm.	Formation
FP	Fission product
GEMS	Gibbs energy minimisation software (for geochemical modelling)
HTO	Tritiated water (H^3HO)
kgw	Kilogram of water
JO	Jura Ost (siting region)
LES	Laboratory for Waste Management (*Labor für Endlagersicherheit*)
LUT	Look-up table
MAR	Marthalen borehole
MPDL	Mean (electrostatic) potential in Donnan layer
Mont	Montmorillonite
Nagra	National Cooperative for the Disposal of Radioactive Waste
NL	Nördlich Lägern (siting region)
NTB	Nagra Technical Report
OPA	Opalinus Clay

PA	Performance assessment
pCO_2	Partial pressure of CO_2
pH	$-\log_{10}(a_H)$, negative logarithm of proton activity
PSI	Paul Scherrer Institute
PW	Porewater
RBG	General licence application (*Rahmenbewilligungsgesuch*)
RN	Radionuclide
S:L	Solid-to-liquid ratio
SDB	Sorption database
SGT	Sectoral Plan for Deep Geological Repositories (*Sachplan geologische Tiefenlager*)
SGT-E2	Stage 2 of the SGT
SGT-E3	Stage 3 of the SGT
SIT	Specific ion-interaction theory (aqueous electrolyte activity model)
SPW	Synthetic porewater
STA	Stadel borehole
TBO	Deep borehole (campaign)
TDB	Thermodynamic database
TRU	Trüllikon borehole
ZNO	Zürich Nordost (siting region)

List of Symbols

a	Activity of species in bulk aqueous phase [–]
A_{DL}	Area of (permanent charge) surface carrying the Donnan layer [m^2]
A_p	Pore surface area [m^2]
A_{sp}	Specific surface area [m^2 kg^{-1}]
c	Concentration in bulk aqueous phase [mol m^{-3}], also [mol dm^{-3}] where specifically noted. When referring to concentrations of a given chemical species, the index i is used as a subscript or the species symbol is inserted in brackets.
c_{DL}	Concentration in Donnan layer [mol m^{-3}], also [mol dm^{-3}] where specifically noted
c_T	Total concentration [mol m^{-3}], also [mol dm^{-3}] where specifically noted.
CBC	Cation binding capacity [eq kg^{-1}]; parameter of ClaySorDif model
CEC	Cation exchange capacity [eq kg^{-1}]
CEC_{100}	Cation exchange capacity [eq kg^{-1}] extrapolated to W_c = 100 wt.%.
CEC_{vol}	Cation exchange capacity referred to volume of porewater [eq m^{-3}]
$Coul$	Coulomb term $(F\Psi_D)/(RT)$ [–] of (electro)chemical potential
D_a	Apparent diffusion coefficient [m^2 s^{-1}]
D_e	Effective diffusion coefficient [m^2 s^{-1}]. In the context of the present report of presenting weighted effective diffusion coefficients for a given element ($D_{e,elem}$), the symbol D_e may also be used for simplicity to represent $D_{e,elem}$ values as long as no confusion arises with $D_{e,i}$ and $D_{e,n}$.
$D_{e,elem}$	Weighted effective diffusion coefficient [m^2 s^{-1}] for a given element
$D_{e,i}$	Effective diffusion coefficient [m^2 s^{-1}] for charged species
$D_{e,n}$	Effective diffusion coefficient [m^2 s^{-1}] for neutral species
D_w	Diffusion coefficient in bulk water [m^2 s^{-1}]
d_{DL}	Donnan layer thickness [m]
d_p	Pore width [m] in planar pores approximation
$E_{a,wc}$	Activation energy for diffusion in porewater of highly compacted clay [kg m^2 s^{-2} mol^{-1}]
F	Faraday constant, 96485.33 [C mol^{-1}]
FCC	Free charge capacity [eq kg^{-1}] parameter of ClaySorDif model
f_{cm}	Fraction of clay mineral (illite) related to total clay [–], assumed to be equal to 0.64 in ClaySorDif calculations
f_{cr}	Total clay mass fraction in clay rock [–]
f_{DL}	Pore volume fraction of Donnan layer [–]
f_{free}	Pore volume fraction of free porewater [–]
G	Geometrical factor [–]

I	Effective ionic strength [mol (d)m^{-3}] or [mol kg^{-1}]
J	Diffusive flux [mol m^{-2} s^{-1}]
k	Boltzmann constant [J K^{-1}]
m_{clay}	Mass of clay [kg]
m_{rock}	Mass of rock [kg]
q_η	Ratio of viscosity of free and Donnan layer water [–]
R	Molar gas constant [J mol^{-1} K^{-1}]
R_{d}	(Sorption) distribution factor [m^3 kg^{-1}]
r_{h}	Hydrodynamic radius [m]
r_{iSL}	Solid-to-liquid ratio of illite in rock material [kg m^{-3}] (or, alternatively as [kg kgw^{-1}])
r_{SL}	Solid-to-liquid ratio of rock material [kg m^{-3}] (or, alternatively as [kg kgw^{-1}])
T	Absolute temperature [K]
V_{DL}	Volume of Donnan layer [m^3]
V_{free}	Volume of free water [m^3]
V_{p}	Pore volume [m^3]
W_{c}	Total clay content (in rock) [wt.%], $W_{\text{c}} = f_{\text{cr}}$ 100 [wt.%]
z	Charge number [formula charge]
γ	Activity coefficient [–]
χ	Mole fraction [–]
χ_i	Mole fraction [–] of charged species
χ_n	Mole fraction [–] of neutral species
α	Rock capacity factor [–]
ε_{acc}	Diffusion-accessible porosity [–]
ε_{AN}	Anion-accessible porosity [–]
ε_{tot} or ε	Total porosity [–]
ϵ (ϵ_0)	Dielectric permittivity [-] (of vacuum [F m^{-1}])
η	Viscosity [kg s^{-1} m^{-1}]
κ^{-1}	Debye length [m]
Ψ_{D}	Donnan potential [J C^{-1}, usually in V]
ρ_{bb}	Bulk dry density of bentonite [kg m^{-3}] (mass of solid divided by total volume, including the pore volume of bentonite)
ρ_{br}	Bulk dry density of porous rock [kg m^{-3}] (mass of solid divided by total volume, including the pore volume of porous rock)
ρ_{cm}	Clay mineral (illite) density [kg m^{-3}]

ρ_{ga}	Material (or grain) density of accessory minerals [kg m^{-3}] (mass of solid divided by volume of solid)
ρ_{gc}	Material (or grain) density of clay [kg m^{-3}] (mass of solid divided by volume of solid)
ρ_{gr}	Material (or grain) density of porous rock [kg m^{-3}] (mass of solid divided by volume of solid)
$[\widehat{\sigma_{DL}}]$	Average total charge concentration in DL porewater [mol dm^{-3}]
$[\sigma_{clay}]$	Volume density of clay permanent charge acting on DL porewater [mol dm^{-3}]

1 Introduction

In Switzerland, legal regulations (Nuclear Energy Act (KEG 2003) and Nuclear Energy Ordinance (KEV 2004)) and guidelines are in place for the management of radioactive waste. The Nuclear Energy Ordinance (KEV) classifies Switzerland's radioactive waste into low- and intermediate-level waste, alpha-toxic waste and high-level waste, the latter comprising spent fuel and vitrified high-level waste from reprocessing. The Nuclear Energy Act (KEG) requires the disposal of all these types of radioactive waste in deep geological repositories. The feasibility of this disposal solution was demonstrated for low- and intermediate-level waste in Nagra (1985) and for long-lived intermediate-level waste and high-level waste in Nagra (2002).

The Sectoral Plan for Deep Geological Repositories (SGT) regulates the search for suitable siting regions for deep geological repositories in Switzerland. This site selection process is conducted in three stages (BFE 2008). Stages 1 (SGT-E1) and 2 (SGT-E2) have already been completed and Nagra is currently in Stage 3 (SGT-E3).

Diffusion is the main transport mechanism for radionuclides in the aqueous phase of clay-rich geological (Opalinus Clay and containment-providing rock zone CRZ) and engineered porous media. The use of adequate transport models and parameter values for diffusion is thus an indispensable requirement for a robust and reliable assessment of the potential radiological consequences for the biosphere (Maes et al. 2021). This report describes the methods and data generated for the diffusion databases (DDB) for the Mesozoic rocks in Northern Switzerland and MX-80 bentonite and their respective porewater compositions.

1.1 Extended state of knowledge due to the new exploration campaign

The exploration campaign of SGT-E3 resulted in extensive core recovery from a total of nine boreholes spread across the three siting regions Jura Ost (JO), Nördlich Lägern (NL) and Zürich Nordost (ZNO) (Fig. 1-1). This formed the basis for detailed investigations of sorption (Marques Fernandes et al. 2024a) and diffusion (Van Loon et al. 2024) properties of the Opalinus Clay host rock as well as the CRZ[1] (see Fig. 1-2). The systematic sampling and analytical programme greatly enhanced previous investigations and allowed the compilation of comprehensive datasets. These investigations significantly expanded the understanding of the sorption and diffusivity behaviour of the dominant rock units within the CRZ and established new scientific approaches for transport parameter determination (e.g. sorption coefficients, R_d, and effective diffusion coefficients, D_e, etc.) and, at the same time, reduced inherent uncertainties.

In all three siting regions, between the Opalinus Clay and the regional lower and upper bounding aquifers, a stratigraphic sequence of mainly diffusion-dominated sedimentary units composed of clay, carbonate, anhydrite or siliciclastic material is present (Fig. 1-2) (Nagra 2024b). Within the CRZ, diffusion is the main control on the transport of radionuclides through the rock matrix, with transport parameters determined by:

1. rock matrix, rock composition, diagenetic history;
2. sorption properties;
3. porosity (and permeability);
4. temperature (high temperature increases kinetic energy of molecules) and pressure (high confining pressure influences pore throats/pathways);
5. pore-fluid properties (ionic strength, density, etc.).

[1] The CRZ is defined as the units between the Malm (NL/ZNO) and Klingnau/Hauptrogenstein (JO) aquifers above the Opalinus Clay and the Keuper/Muschelkalk aquifers below the Opalinus Clay.

Furthermore, all radioactive waste undergoes decay, making the time frame of consideration important. The derivation and application of the above parameters within the various transport models allow the assessment of post-closure behaviour and performance of a deep geological repository for radioactive waste. The sorption and diffusion characteristics of individual radionuclides within these systems are key parameters, playing an important role in radionuclide and tracer migration, and thus dose consequence assessments (see Nagra 2024c).

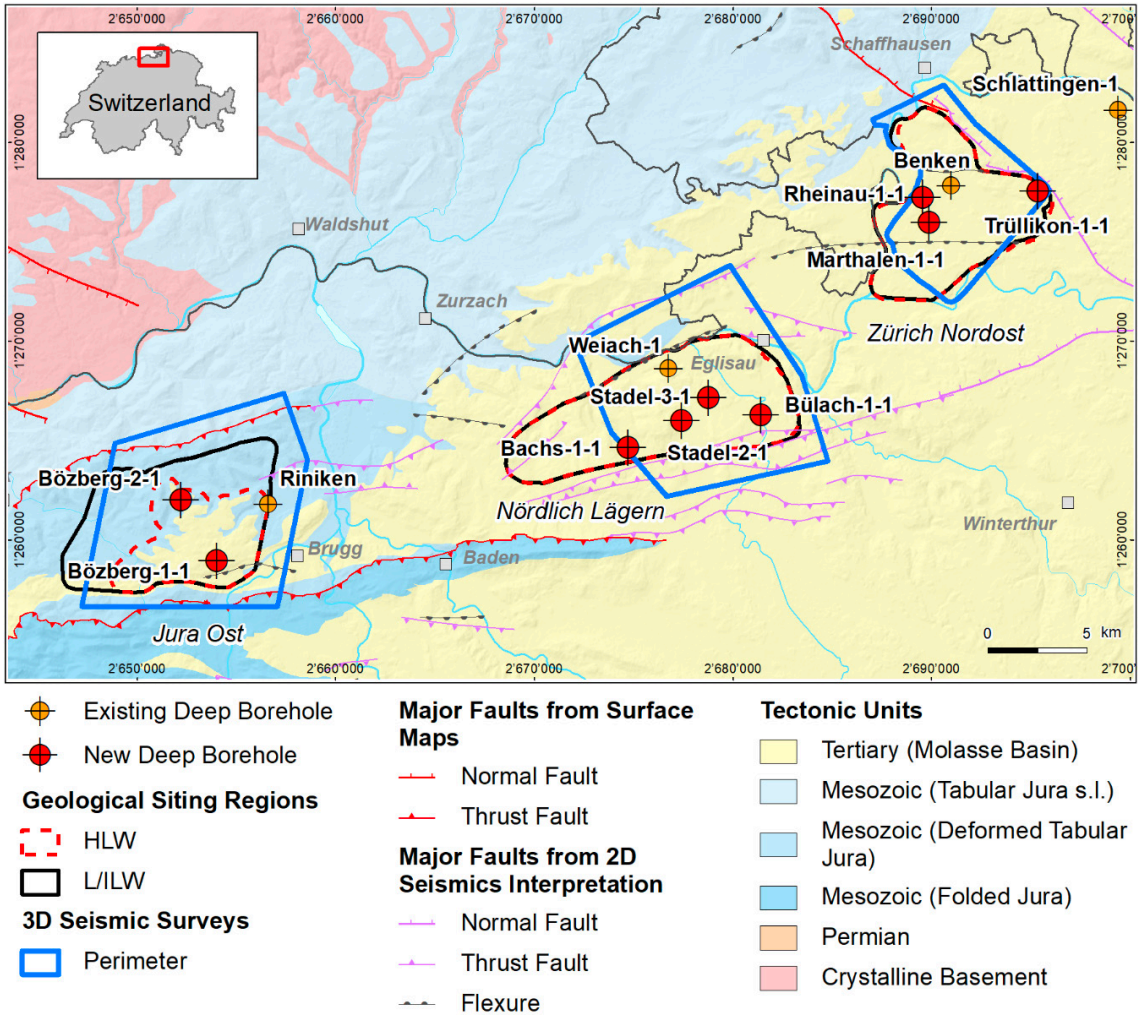

Fig. 1-1: Locations of siting regions and boreholes referred to in this report

From Mäder & Wersin (2023)

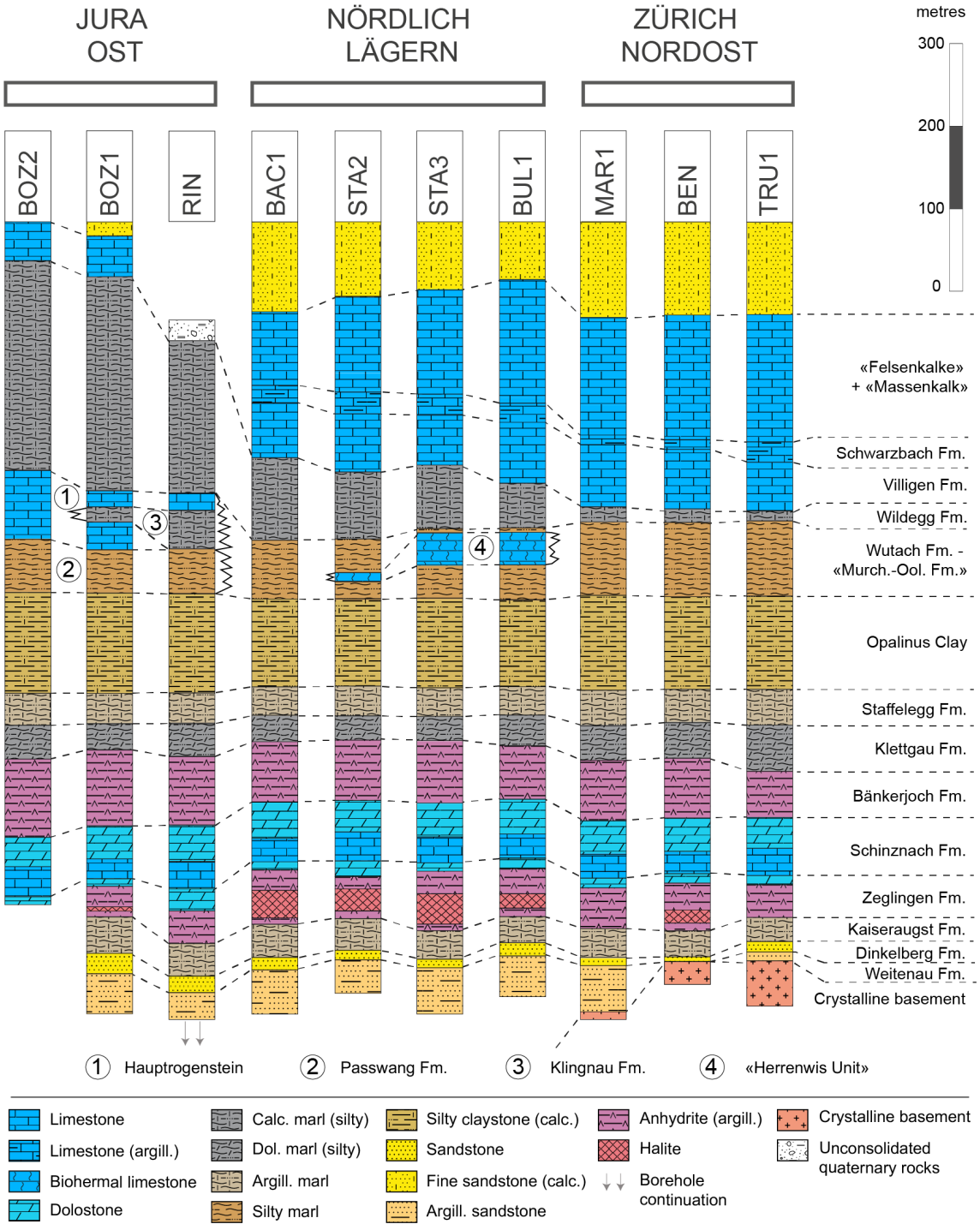

Fig. 1-2: Lithostratigraphic overview and correlation of Mesozoic sediments observed in the recently (2018-2022) drilled boreholes. Details of the CRZ are found in (Nagra 2024a)

Boreholes are aligned to the centre of the Opalinus Clay. Simplified lithological legend according to Naef et al. (2019). Lithostratigraphy on the right side according to Jordan & Deplazes (2019). The confining rock units are found between the Schinznach Fm. and the Villigen Fm.

1.2 Purpose of the report and strategy used for the compilation of diffusion data

The Laboratory for Waste Management (LES) at the Paul Scherrer Institute (PSI) compiles diffusion data for clay rock and bentonite for any relevant constellation of rock and porewater composition and dose-relevant radioelement for application in safety and performance assessments. The purpose of the present report is to describe the methods used to evaluate the parameters in these compilations. The methods previously applied in SGT-E2 for the corresponding calculations (Van Loon 2014) are extended here by the use of an electrostatic model to calculate effective diffusion coefficients (D_e [$m^2 s^{-1}$]) and accessible porosities (ε_{acc} [-]) for all elements under evaluation, based on aqueous speciation data and rock characteristics. The most important differences in the procedures and the use of basic input data for the parameter evaluation between past and present data compilations are also addressed.

To provide an integrated view of diffusive transport of radionuclides in dense clay-rich rocks, including the retardation induced by sorption processes at the clay surface, the use of a coherent chain of models and modelling tools is necessary for: a) a traceable description of the results, and b) a minimisation of intrinsic uncertainties and errors. The concepts and methods detailed in this report aim at fulfilling this purpose and represent one of the most substantial advances realised in this respect. They offer a consistent description of diffusion and sorption based on the use of the same thermodynamic input data for speciation and solubility of radionuclides. While the current model for the description of sorption, i.e. the two-site protolysis non-electrostatic surface complexation and cation-exchange model (2SPNE SC/CE) (Bradbury & Baeyens 1997, Bradbury & Baeyens 2009), involves purely non-electrostatic processes for radionuclide sorption at the planar and edge surfaces of clay minerals, the description of surface diffusion and anion exclusion can be accomplished via the implementation of an electrostatic extension of such models.

Most lithologies in the CRZ comprise negatively charged clay components, and a large part of dose-relevant radionuclide species may be present as ionic species in the aqueous porewater of such clays after breaching of containment. Diffusion of trace radionuclide species under such conditions is strongly influenced by charge effects: while anions are repelled from the negatively charged clay surfaces and diffuse at lower mass transfer rates (fluxes) compared to uncharged tracers, cations are attracted to these and can diffuse at enhanced mass transfer rates, provided that the surface-associated species exhibit the necessary molecular mobility to enable random thermal motion (Tinnacher et al. 2016). The use of D_e, commonly defined as the proportionality factor between concentration gradients in the bulk aqueous phase, as the driving force for diffusion and the observed fluxes implies that these values have a strongly conditional character and depend on many chemical characteristics of the clay surface and the porewater. Note that various, sometimes even contradictory, definitions for diffusion coefficients in porous matrices exist in the literature. A comprehensive overview of this has been given by Shackelford & Daniel (1991). The present report is based on the same definitions as used by Van Loon et al. (2024). For the application of the numerical values of the diffusion parameters in safety analysis (dose calculations), it is essential that these definitions are taken into account when utilising the values in various forms of the transport equation.

A further peculiarity is the experience that D_e values for cationic species in negatively charged clays can even exceed their molecular diffusion coefficients in bulk water (D_w). Such cases are occasionally dismissed as “unphysical”. However, it is the inadequate concept behind the neglection of the relevant driving forces for diffusion that is unphysical, rather than the use of such values in a proper context. An appropriate approach to D_e values of charged radionuclide species in charged clay-rich rocks thus involves physical, geometrical and chemical influencing factors (cf. Fig. 1-3).

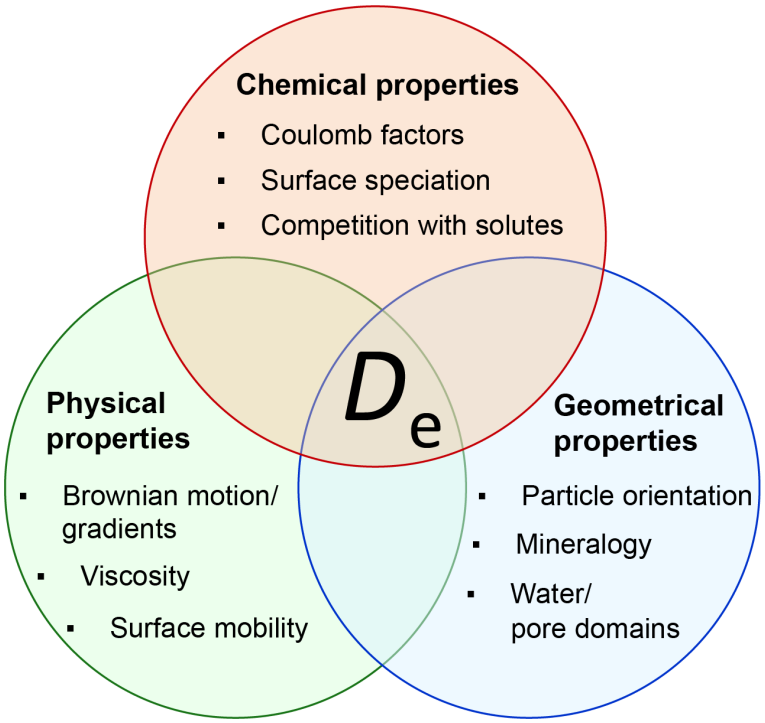

Fig. 1-3: Schematic representation of the typically relevant influencing factors required for a proper description of diffusive transport of charged species in charged porous media

A practicable approach for the implementation of the model scheme shown in Fig. 1-3 for clay-rich rocks has been proposed in Van Loon et al. (2023) and Glaus et al. (2024) using an electrostatic approach to incorporate chemical factors for diffusion of charged species in charged porous media. In these works, diffusion data for tritiated water (HTO), $^{36}Cl^-$ and $^{22}Na^+$ tracers from more than a hundred representative rock samples from the Opalinus Clay and the confining geological units (Fig. 1-2) were used to set up and calibrate an approach to predicting diffusion data for these tracers as a function of the total clay content of the rock and the composition of the rock porewater as the main independent variables. The present report enhances this concept with a modified implementation of thermodynamic calculations for the prediction of diffusion data for all dose-relevant elements. The applicability of the electrostatic approach described in Glaus et al. (2024) to chemical elements other than those used for the model calibration has already been confirmed in previous and more recent work (Van Loon et al. 2025 *in prep.,* Glaus et al. 2021, Appelo et al. 2010). The importance of an unbiased distinction between geometrical and chemical effects for the diffusion of (un)charged species in compacted smectites has also been shown in a recent publication (Fox et al. 2024). Without such a fundamental process understanding, experimental data gained from laboratory-scale experiments cannot be upscaled indiscriminately to deep geological repository conditions.

Reducing the complex interactions that impact the specific diffusion properties of a given chemical species in a given geochemical environment (rock composition, porewater composition, connectivity of pore network, etc.) to the total clay content of the rock means that the predicted diffusion data are inherently subject to considerable, albeit acceptable, uncertainties. The advantage of such an approach is that it can readily be implemented in the form of look-up tables (LUTs), which may subsequently be directly linked to available borehole data. Compiling LUTs based on such simplified parameter schemes is therefore the strategy chosen for SGT-E3. It not only allows the prediction of diffusion properties as a function of borehole log data but also

permits the application of statistical methods for the assessment of related uncertainties. Furthermore, it also allows specific diffusion properties and their variabilities to be assigned to abstracted lithological units, which can then be directly compared across the different siting regions. Algorithms for the prediction of diffusion data based on basic rock properties are implemented here in a programmed environment. They can generate diffusion parameters for any type of radioelement and geochemical composition without the use of subjective decisions, as was the case in previous stages of the SGT. This approach is particularly dedicated to the situation encountered in the far-field of a deep geological repository hosted in clay-rich rocks. The situation for the near-field (bentonite) is also covered by this approach. For this specific case, the target clay content of bentonite and its degree of compaction are predefined. As will be shown in subsequent sections of this report, the parametrisation of the geometrical factors also differs for the case of bentonite. For all these reasons, the application of the approach detailed in this report is different for clay-rich rocks and bentonite.

1.3 Definitions and scope of application of the results

The diffusion of a solute, i (with aqueous concentrations c_i) in porous media that undergoes chemical interaction with the solid is typically described for transient states by Fick's second law in the following form for one-dimensional diffusion in the direction of the x-coordinate (Tournassat & Steefel 2015):

$$\frac{\partial(c_i\alpha)}{\partial t} = D_\mathrm{e}\frac{\partial^2 c_i}{\partial x^2} \tag{1-1}$$

where α is the rock capacity factor [–] defined as the ratio of the total concentration of species i in the solid phase (the sum of the concentrations in pore solution and concentrations of solid phase species) to the aqueous concentration, c_i. As highlighted in Section 1.2, D_e is a direct scaling factor relating the tracer flux (J, [mol m^{-2} s^{-1}]) and the respective tracer concentration gradient $\frac{\partial c_i}{\partial x}$ in the bulk aqueous phase according to Fick's first law:

$$J = -D_\mathrm{e}\frac{\partial c_i}{\partial x} \tag{1-2}$$

In the case of linear and reversible sorption, α can be treated as a constant in Eq. (1-1), which then extends to:

$$\frac{\partial c_i}{\partial t} = \frac{D_\mathrm{e}}{\alpha}\frac{\partial^2 c_i}{\partial x^2} = D_\mathrm{a}\frac{\partial^2 c_i}{\partial x^2} \tag{1-3}$$

with D_a being the apparent diffusion coefficient [m^2 s^{-1}]. According to the definition of α, the following relationship shown in Eq. (1-4) between α and the sorption distribution coefficient (R_d, [m^3 kg^{-1}]) exists:

$$\alpha = \varepsilon_\mathrm{acc} + R_\mathrm{d}\rho_\mathrm{br} \tag{1-4}$$

where ε_acc is the diffusion-accessible porosity [–] and ρ_br is the dry bulk density of the porous rock (mass of solid divided by total volume, including pore volume). The R_d value characterises the distribution of a solute between a solid and solution phase and is defined as the amount of

substance bound to the solid phase (normalised per unit of dry mass of the solid) divided by the amount of substance in the solution phase (normalised per unit of solution volume).

A comprehensive set of data for describing the diffusive transport of a reactive species in porous media thus comprises compilations of (i) D_e, (ii) ε_{acc}, and (iii) R_d for each element. The former two items are normally provided in diffusion databases (DDB) and the latter in sorption databases (SDB). Note that the latter (Marques Fernandes et al. 2024b) use a purely non-electrostatic approach for R_d values based on the 2SPNE-SC/CE model. While the methods for the two approaches differ in this respect, consistency regarding the results is ensured as outlined in this report.

In summary, D_e determines the maximum possible fluxes for a given geometrical situation involving a radionuclide source and a target domain, while the rock capacity factors determine the temporal evolution of the radionuclide fluxes. The pore volume of the rock matrix and the availability of binding sites for uptake can be seen as a capacity which has to be filled before the maximum values of radionuclide fluxes can be reached. This behaviour is of importance for the time evolution of the diffusive mass transfer of radionuclides from a deep geological repository to the biosphere. Regarding the literature from the past decades, a contentious discussion on the nature and the conceptual understanding of the diffusion of radionuclides in argillaceous rocks has ensued (see e.g. Oscarson (1994)). The systematic investigation of the influences of various parameters related to surface and porewater properties on the diffusion of radionuclides in charged argillaceous rocks has, however, unambiguously demonstrated that these factors have a strong influence on the diffusion parameters used in a safety analysis. Diffusion measurements on model clay minerals have shown that the D_e of anions and cations may differ by several orders of magnitude (Glaus et al. 2010) and that such situations cannot be excluded without an in-depth understanding of the relevant chemical processes involved. For these reasons, the present approach aims at developing a generic procedure that can be applied to any type of radionuclide and geochemical situation.

1.4 Structure of the report

The methods used for generating diffusion data are comprehensively described in Chapter 2. The sections on the “physical” and “geometrical” aspects repeat the model features described in Van Loon et al. (2023) and Glaus et al. (2024). As explained in the previous section, separate realisations of the same conceptual approach are used for clay rock and bentonite. The implementation of chemical influencing factors in terms of an electrostatic model is described in detail in a separate section of Chapter 2. This differs in some respects from the model implementation in the geochemical code PHREEQC (Parkhurst & Appelo 2013) described in Glaus et al. (2024); the chemical foundation is, however, the same. The results (D_e and ε_{acc}) are presented in representative tabular and graphical form for selected cases (clay content, porewater composition) in Chapter 3. A comprehensive collection of the LUTs is available electronically from Nagra for both clay rocks and bentonite. The chapter also summarises the most important features of generic influencing factors, such as temperature and particle orientation. These aspects are taken without modification from previous work (Van Loon 2014). A detailed comparison of results obtained by the approaches chosen for the present work and those realised previously in PHREEQC (Glaus et al. 2024) are also presented in Chapter 3. Furthermore, a comprehensive comparison of the present results and those produced for previous safety analysis (Van Loon 2014) is provided in Chapter 4. Chapter 5 provides a quality check of the data in terms of plausibility cases. Chapter 6 rounds off the report with a statistical analysis of the diffusion parameters for the abstraction of lithostratigraphic model units used for safety and performance assessment modelling. It provides detailed insight into how the LUTs are linked to borehole log data and on the methods used to average these data to produce representative diffusion properties for the model units. The variabilities and uncertainties involved are also characterised.

2 Methods for estimating effective diffusion coefficients and accessible porosities

The present section explains the concept and implementation of the model used to evaluate the diffusion properties of the dose-relevant elements for the purpose of compiling LUTs for the different study areas (Fig. 1-1) and their respective model porewaters. As shown in Fig. 1-3, such a model comprises physical, geometrical and chemical information. The separation into these different categories facilitates the representation and traceability of the contents. However, the boundaries are not entirely clear in all respects.

An appropriate approach to "chemical correction factors" applied for D_e values is the use of electrostatic factors describing the enrichment of cationic species at the surfaces of negatively charged clay materials and the respective depletion of anionic species (Glaus et al. 2015, Ochs et al. 2001, Appelo & Wersin 2007, Birgersson & Karnland 2009). Different chemical concepts can be applied for such purposes, with the common baseline that they involve chemical equilibration between the species present in the bulk aqueous phase and those present at the clay surface. These concepts have been summarised in recent literature (Glaus et al. 2024, Maes et al. 2021, Krejci et al. 2023).

Fig. 2-1 shows a schematic view of the electrostatic description of cation enrichment and anion depletion in an electrical double layer. In view of the geometrical extension of the pore space in argillaceous clay rocks (Keller et al. 2011, Mazurek et al. 2023), it is reasonable that such concepts are applicable for larger pores up to macropores, while, from a formal point of view, overlapping double layers would be more appropriate to represent the nanopores of smectites or clay rocks. For simplicity, the concept shown in Fig. 2-1 is applied for all pore types in the present report.

The assumption that all or part of the ionic species in the double layer undergo Brownian motion to some degree and are considered "mobile" for diffusion, leads to additional concentration gradients for diffusion, which are superimposed on those in the free aqueous phase. The concept shown in Fig. 2-1 assumes that ions in free water (blue charge signs) and the ion swarm in the Donnan layer (DL) (green charge signs) are mobile, while some of these (red signs) may be present as immobile surface complexes. The blue domain in Fig. 2-1 represents free water with bulk properties where charge neutralisation is achieved through solution anions and cations. The green domain represents the DL, a charged solution phase exhibiting the opposite net charge of the clay surface. The local concentration gradients parallel to the clay surface in the different domains result in individual flux contributions (J_i) if there is a concentration difference of a tracer cation species.

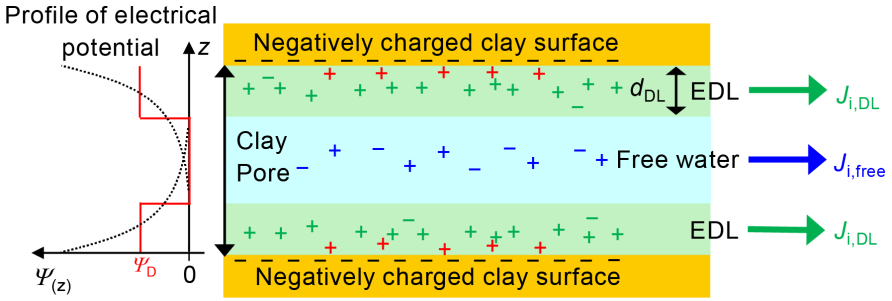

Fig. 2-1: Schematic representation of the Donnan approach for an electrical double layer (EDL) for a planar pore geometry

Details on the symbols and colours are given in the main text. Depending on the assumptions made for the electrical potential (left), the green domain is termed Donnan layer or, in a more general sense, as diffuse layer. Sketch adapted from Maes et al. (2021).

The conceptual and technical details of the electrical double layer (EDL) model have been presented in previous publications (Glaus et al. 2015, Glaus et al. 2024). The physical and geometrical aspects of the model are reiterated here for completeness (cf. Sections 2.1 and 2.2). The novel aspect introduced in the present report is the chemical speciation-based implementation of the electrostatic model in the GEMS software (Section 2.3). Independent of the technical implementation, the D_e values can be expressed using the following type of equation, which is derived from the superposition of parallel fluxes (cf. Fig. 2-3) in the bulk aqueous phase and the Donnan volume:

$$D_e = \frac{\varepsilon_{tot}}{G} D_w \left(f_{free} + f_{DL} \frac{c_{DL}}{c} q_\eta \right) \quad (2\text{-}1)$$

The ratio c_{DL}/c represents the concentration ratio of charged species between the DL and the free aqueous phase. ε_{tot} is the total porosity, G [–] the geometry factor, f_{free} [–] the volume fraction of free porewater, f_{DL} [–] the volume fraction of the Donnan layer, D_w [m^2 s^{-1}] the diffusion coefficient in bulk water, and q_η [–] the ratio of the viscosities of free and EDL water. Note that the application of Eq. (2-1) is restricted to prerequisites such as a rapid attainment of the thermodynamic equilibrium between the DL and free porewater species compared to the dynamics of diffusion. The parameter influences mentioned in Fig. 1-3 are not directly recognisable in Eq. (2-1). Their functional dependencies on the chosen control variables, the total clay content and the porewater composition, will be explained in detail in the subsequent sections.

An important assumption for the application of Eq. (2-1) is the identity of G factors for all species and a given orientation of diffusion with respect to the bedding of the clay platelets. This assumption is almost blindly accepted by most researchers and has been rather poorly documented by experimental results. One of the rare studies in which the applicability has been demonstrated is the work of Aldaba et al. (2014). For uncharged species such as HTO, the concentration ratio c_{DL}/c equals 1 and, assuming $q_\eta = 1$, Eq. (2-1) can be reduced to:

$$D_e = \frac{\varepsilon_{tot}}{G} D_w \quad (2\text{-}2)$$

because:

$$f_{free} + f_{DL} = 1 \quad (2\text{-}3)$$

For the present case of an electrostatic description of ion speciation in the Donnan layer, the calculation of ε_{acc} ($<\varepsilon_{tot}$) for anions requires some explanation. The concept of diffusion-accessible porosity for anions (the symbol ε_{AN} is specifically used here to denote ε_{acc} of anions), or "anion exclusion" in the opposite sense, involves the assumption that the concentrations of anionic species in the accessible pore fraction equal the respective concentrations in the bulk aqueous phase, while a given part of the pore space is devoid of anions. This concept is fundamentally different from the Donnan approach in which anions are present in the Donnan layer at lower concentrations compared to those in free pore volume (cf. Fig. 2-1). A comparison of the two models is shown in Fig. 2-2. The results of the species distribution of anions between the Donnan layer and the bulk aqueous phase can readily be converted into an anion-exclusion model from which ε_{acc} values are derived. Background information on this has been given in two recent publications (Glaus et al. 2024, Zwahlen et al. 2024). The technical details for this conversion are given in Section 2.3 of the present report. This circumstance emphasises another advantage of the electrostatic approach for the compilation of diffusion data: the evaluation of parameters for anion exclusion is directly based on chemical speciation. For a non-electrostatic description of species

uptake in the clay phase, ε_{acc} values are based mostly on arbitrary assumptions for anion exclusion that cannot readily be related to changing chemical conditions. This fact is particularly significant in the case of representatives of the transition metals, lanthanides and actinides which all have a strong tendency to form solution complexes with inorganic constituents of the porewater such as carbonate anions. Depending on the coordination number of such complexes, the overall charge of these can even be negative. Using fixed values for anion exclusion is not an appropriate approach for such cases.

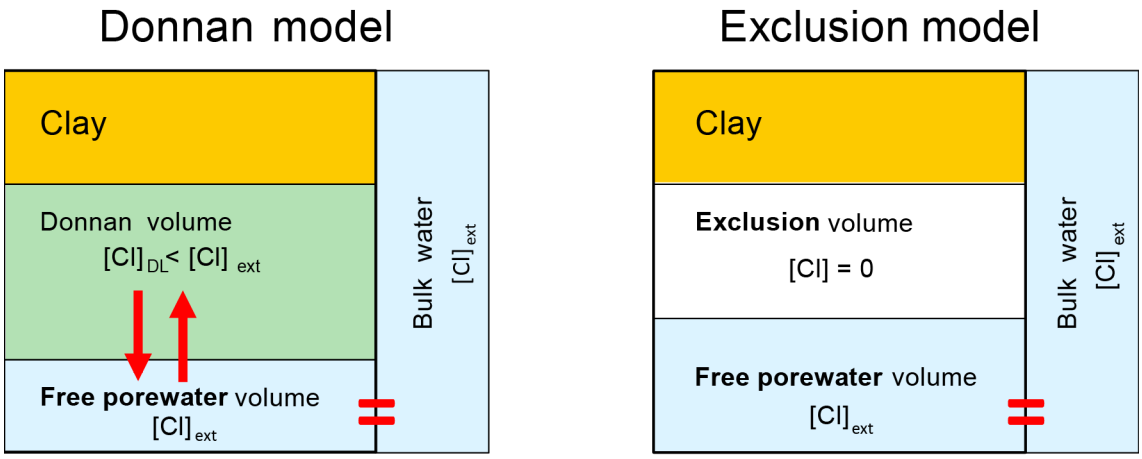

Fig. 2-2: Schematic representation of anion exclusion for chloride

The clay phase (including the porewater) is framed in bold, the external solution phase is symbolised by the blue rectangle to the right. Results of the Donnan model can readily be converted to an anion exclusion model by readjusting the amount of chloride in the Donnan volume (green) to a corrected value, resulting in the same concentration as in the external solution ($[Cl]_{ext}$, blue). For both cases, the total amount of chloride in the pore space is the same. Brackets denote species concentrations.

2.1 Physical aspects

The physical basis for the diffusion of solutes in the bulk solution phase is given by the Stokes-Einstein law, which has been applied previously in SGT-E2 (Van Loon 2014). The diffusion coefficient (of a solute) in water, D_w, can be expressed as a function of absolute temperature (T), the viscosity of the solvent (η) and the hydrodynamic radius of the solute (r_h):

$$D_w = \frac{kT}{6\pi\eta r_h} \tag{2-4}$$

where k is the Boltzmann constant.

For the purposes of this study and to facilitate further development and use of the ClaySorDif model and codes, the D_w values (specified at 1 bar and 25 °C) for all considered chemical elements and their relevant ionic aqueous species have been collected in the D_wDB database, stored in JSON format, and loaded into a Python dictionary during operation of the ClaySorDif code (see below). The D_w values were mostly taken from Li & Gregory (1974). A recent compilation of molecular diffusion coefficients for a series of species available from Andra was made within the framework of Andra's Cigéo project (Andra 2022). Note that these data sources are not fully comprehensive in terms of all known aqueous species of a given element, and, for many species,

rather simple analogies are used to derive their D_w values. Despite this, the ranges of values are comparatively narrow and, as such, it may be concluded that the lack of species-specific data does not lead to a significant bias in the predicted D_e values.

It is further assumed that the same diffusion parameters apply for all isotopes of a given element. Thus, this assumption ignores the effect of isotopic mass differences on the diffusion parameters. As will be outlined in Section 2.3.2, the numeric values of the diffusion parameters for a given element are based on those of their most important chemical species, which involves an arbitrarily chosen level of truncation. For almost all the elements, this truncation has no severe impact on the calculation of radioactive doses.

In view of the general lack of knowledge of q_η values, these are simply assumed to equal unity. It is known, however, that these factors are normally below 1 for fluids in narrow pores (Glaus et al. 2015, Gimmi & Kosakowski 2011, González Sánchez et al. 2008). This assumption is therefore conservative in the sense that D_e values are more likely to be over- than underestimated.

2.2 Geometrical aspects

For the reasons mentioned in Section 1.2, the details of the approaches for clay rock and bentonite differ in some respects. Therefore, these cases are treated in separate sections.

2.2.1 Clay rock

In the following, an average pore radius (or pore width) will be derived from the specific surface area using the assumption that the porosity in a complex mineral composition of sedimentary rocks is mainly determined by the clay phase. The specific surface area is commonly defined as surface area per unit mass of solid. Multiplying this quantity with the solid-to-liquid ratio produces its variant based on per unit pore volume. The comparison of this quantity with the geometrical characteristics of the pores allows the average pore width to be derived. All these basic input quantities can be related to the total clay content as the basic input variable.

In view of the long extension of clay particles compared with their thickness, the assumption of infinitely long planar pores is well justified. The pore width (d_p [m]) for a planar pore with much longer lateral dimensions compared to thickness is related to the inverse ratio of the pore surface area (A_p [m^2]) and pore volume (V_p [m^3]), and thus to the specific surface area (A_{sp} [m^2 (kg clay)$^{-1}$]) and the solid-to-liquid ratio of rock material (r_{SL} [(kg rock) m^{-3}]), according to:

$$d_p = \frac{2V_p}{A_p} = \frac{2}{A_{sp} r_{SL} f_{cr}} \tag{2-5}$$

where f_{cr} is the clay mass fraction [(kg clay) (kg rock)$^{-1}$]:

$$f_{cr} = \frac{m_{clay}}{m_{rock}} \tag{2-6}$$

where m_{clay} and m_{rock} are the clay mass [kg clay] and the rock mass [kg rock], respectively.

Note that r_{SL} is related to the total mass of rock per unit pore volume. It is derived from the bulk dry density of the rock (ρ_{br} [kg m^{-3}]) and rock porosity ε_{tot} by:

$$r_{SL} = \frac{\rho_{br}}{\varepsilon_{tot}} \tag{2-7}$$

The bulk dry density can, in turn, be expressed as a function of the material (or grain) density (ρ_{gr} [kg m^{-3}]):

$$\rho_{br} = (1 - \varepsilon_{tot})\rho_{gr} \quad (2\text{-}8)$$

The combination of Eqs. (2-7) and (2-8) then yields:

$$r_{SL} = \frac{(1-\varepsilon_{tot})}{\varepsilon_{tot}}\rho_{gr} \quad (2\text{-}9)$$

The use of Eq. (2-9) implies that the grain density of the clay minerals and the accessory minerals is rather similar. This assumption is not valid to the same extent for all rocks. However, the bias induced in the diffusion data can be safely ignored in all cases compared to more important sources of uncertainty. The restriction that porosity is present only in clay minerals is realised in Eq. (2-5) by the introduction of the clay mass fraction (f_{cr}), defined as the mass ratio between clay and rock. As will be outlined in more detail in Section 2.3, illite was chosen as the representative clay mineral for these calculations. A representative value for A_{sp} was chosen as 100,000 m^2 kg^{-1} for this clay mineral (Glaus et al. 2015).

A schematic representation of these geometrical boundary conditions for the EDL model for a planar pore situation is shown in Fig. 2-3. The Donnan layer thickness (d_{DL} [m]) is assumed to be a multiple (n_{DL}) of the Debye length ($1/\kappa$, which is, among other factors, a primary function of the ionic strength, cf. Appelo & Postma (2005), and further expressions, cf. Eqs. (2-38) and (2-39). Thus, the fractional contributions (f_{DL} and f_{free}) of the volume of Donnan layer water (V_{DL}) and of free porewater (V_{free}) can be calculated as follows:

$$f_{DL} = \frac{V_{DL}}{V_p} = \frac{2d_{DL}}{d_p} \quad (2\text{-}10)$$

and

$$f_{free} = \frac{V_{free}}{V_p} = 1 - f_{DL} \quad (2\text{-}11)$$

Further explanations for the calculation of d_{DL} are provided in subsequent sections (Section 2.3).

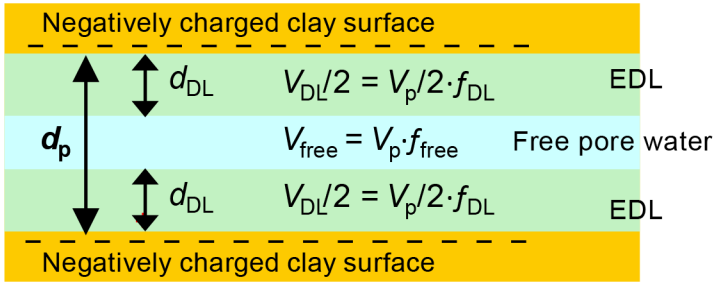

Fig. 2-3: Schematic representation of the volumetric subdivision of the pore space into a domain containing free porewater and Donnan porewater making up the Donnan volume

For the implementation of the model in PHREEQC (Appelo & Wersin 2007) or in GEMS (Section 2.3), it is important to prevent situations where $2d_{DL} > d_p$, as this can result in negative values of f_{free}. To address this issue for such conditions, f_{free} is arbitrarily truncated to 0.01 and d_{DL} to $0.99d_p/2$.

The dependence of diffusivity on porosity has been described in previous studies (Glaus et al. 2010, Van Loon & Mibus 2015) using Archie's relationship or an extended form of it. The latter is shown in Eq. (2-12):

$$D_e = A_1 {\varepsilon_{tot}}^{m_1} + A_2 {\varepsilon_{tot}}^{m_2} \quad (2\text{-}12)$$

where A_i and m_i are empirical parameters characteristic of the porous medium. Note the structural similarity between Eq. (2-2) and Eq. (2-12). If only the contribution of a single component (i = 1) is considered ($A_2 = 0$, as in the conventional Archie's relationship) and the identity of D_w and A_1 is assumed, a simple relationship between G and m_1 can be established:

$$G = {\varepsilon_{tot}}^{1-m_1} \quad (2\text{-}13)$$

For such simple cases, the parametrisation in terms of Archie's relationship can readily be implemented in the form of Eq. (2-2) by the conversion shown in Eq. (2-13).

The diffusion measurements of HTO in a comprehensive series of samples of Mesozoic sedimentary rock formations of Northern Switzerland (Van Loon et al. 2023) have shown that the applicability of Eq. (2-12) is not fully realised. To obtain a better agreement between experimental data and the model, empirical relationships between ε and the G-factor, respectively, and the total clay content of rock (W_c [wt.%]), where $W_c = f_{cr}$ 100 wt.%), were introduced instead (Van Loon et al. 2023):

$$G = a_1 + e^{a_2 W_c} \quad (2\text{-}14)$$

$$\varepsilon_{tot} = a_3(1 - e^{-a_4 W_c}) \quad (2\text{-}15)$$

Note that the parameter symbols used in the original publications (Van Loon et al. 2023, 2024) are changed in the present report to avoid confusion with the parameters from Archie's relationship. A summary of the parameter values used for Eqs. (2-14) and (2-15) is given in Tab. 2-1.

Tab. 2-1: Parameter values and uncertainties on a 1σ and 3σ confidence level used for Eq. (2-14) and Eq. (2-15)

As taken from Van Loon et al. (2023) and Van Loon et al. (2024).

Parameter	Best value	1σ	3σ
a_1	10.0	2.0	6.0
a_2	0.0515	0.0016	0.0047
a_3	0.1444	0.0063	0.0188
a_4	0.0398	0.0045	0.0134

The combination of Eq. (2-2) and Eqs. (2-14) and (2-15) yields the following relationship between D_e and W_c for a conservative non-interacting tracer:

$$D_e = D_w \frac{\varepsilon_{tot}}{G} = D_w \frac{a_3(1-e^{-a_4 W_c})}{a_1+e^{a_2 W_c}} \quad (2\text{-}16)$$

Fig. 2-4 shows the experimental results along with the model curves (solid line) based on Eq. (2-16) and the parameter values given in Tab. 2-1. The dashed curves indicate the upper and lower bounds of the model based on the 3σ confidence levels.

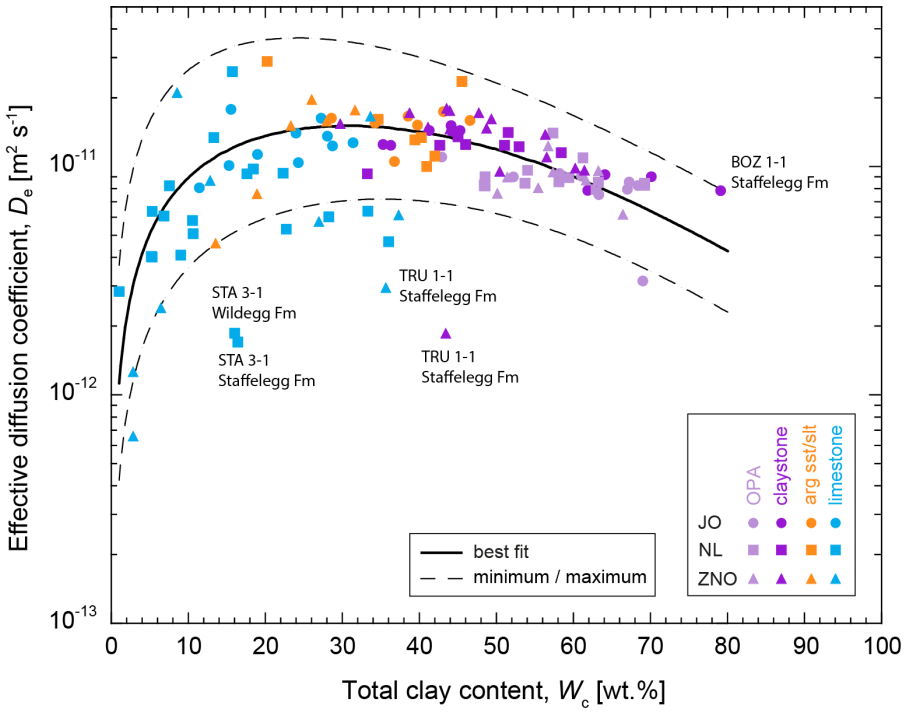

Fig. 2-4: Empirical relationship for the dependence of D_e values (diffusion direction perpendicular to bedding) of HTO on the W_c for rock samples originating from Nagra's deep borehole campaign in different study areas (see the different symbols) and different Mesozoic sedimentary formations (see the different colour codes)

Plot taken from Van Loon et al. (2023).

The empirical parameters used for the model curves in Fig. 2-4 are based on the measurements performed on samples from Nagra's deep borehole campaign in the Mesozoic sediments of Northern Switzerland (Van Loon et al. 2023), as illustrated in Fig. 1-1 and Fig. 1-2.

A detailed analysis of the data shown in Fig. 2-4 revealed that no specific dependence of the diffusion data can be established for the different study areas (Van Loon et al. 2023). The data fit into one single functional relationship. Whether the relationship can be applied to similar sedimentary formations in other locations is an open question. In view of the hypothesis that the parameter values critically depend on the extent of particle orientation and cementation, and the fact that the sedimentary and burial history of other formations may differ from the situation in Northern Switzerland, such a generalisation is uncertain.

Note that the functional dependence of $\varepsilon_{\mathrm{tot}}$ and ρ_{br} on W_c is also used for the calculation of r_{SL}. The combination of Eqs. (2-9) and (2-15) thus yields:

$$r_{SL} = \frac{(1-a_3(1-e^{-a_4 W_c}))}{a_3(1-e^{-a_4 W_c})}\rho_{\mathrm{gr}} \tag{2-17}$$

An average value for ρ_{gr} of 2,700 kg m^{-3} was used for these purposes (Glaus et al. 2024).

A representative case for illustrating the behaviour of the various geometrical characteristics and their dependence on W_c is shown in Tab. 2-2 for the conditions of the synthetic porewater used in the experiments with rock samples from the Bülach borehole (BUL 1-1). The ionic strength of this porewater is 0.505 M according to the composition published in Van Loon et al. (2023). As can be seen from the evolution of the volume fractions of free and DL water, the limiting case of $2d_{DL} > d_p$ is reached for W_c values above ~70%. The parameter values are also shown beyond the range of experimentally available data (W_c > 80%), to better illustrate the limiting behaviour.

Interestingly, the average pore diameter decreases with increasing W_c. Such behaviour would not be expected *a priori*. It can be explained by the non-linear dependence of the porosity on the W_c content. Also note the importance of the factor f_{cr} in Eq. (2-5). If this factor was omitted, very small pore diameters would result, ranging between 0.04 nm (at W_c = 1%) and 1.2 nm (at W_c = 91%). Such small pore diameters contradict the experimental results obtained by Mazurek et al. (2023), where a clustering of smaller pores with a diameter distributed around ~3 nm in clay-rich samples and larger pores clustering around ~50 nm in limestones were observed. This shows that the assumption of pores being restricted to clay-mineral domains is (i) more realistic than the assumption of the pore surface being distributed across all types of mineral constituents, and (ii) that this simple approach does not realistically consider the presence of larger pores. The model approach chosen here must be regarded as a comparatively approximate treatment of reality.

Tab. 2-2: Dependence of various characteristics of pore and EDL geometry on W_c for the conditions of the artificial porewater of the Bülach borehole

Ionic strength = 0.505 M

W_c [wt.%]	ε_{tot} [–] Eq. (2-15)	r_{SL} [kg dm^{-3}] Eq. (2-9) and Eq. (2-17)	d_p [nm] Eq. (2-5)	f_{DL} [–] Eq. (2-10)	f_{free} [–] Eq. (2-11)
1	0.006	476.6	4.20	0.408	0.592
11	0.051	50.0	3.63	0.471	0.529
21	0.082	30.3	3.14	0.544	0.456
31	0.102	23.7	2.72	0.628	0.372
41	0.116	20.5	2.37	0.720	0.280
51	0.125	18.8	2.08	0.821	0.179
61	0.132	17.8	1.84	0.929	0.071
71	0.136	17.2	1.64	0.990	0.010
81	0.139	16.8	1.47	0.990	0.010
91	0.141	16.5	1.33	0.990	0.010

2.2.2 Bentonite

Bentonite is composed of clay (montmorillonite) and accessory minerals (quartz, feldspars, etc.). For the sake of simplicity, the material properties of all accessory minerals are treated as a uniform quantity. The reference bentonite bulk dry density ρ_{bb} is set to 1,450 kg m^{-3} (Curti 2021). For the sake of formal analogy, the total clay mass fraction in bentonite is also termed f_{cr}. The target value of f_{cr} in bentonite is set to 0.81, with most of the clay consisting of smectite with traces of illite.

As the bulk dry density of bentonite is known and it is not influenced by site-specific features, the diffusivity of conservative tracers in compacted bentonite can simply be derived from an Archie-type relationship (cf. Eq. (2-12)). The total porosity of compacted bentonite can be derived from its bulk dry density, the material (or grain) density of clay (ρ_{gc}) and the respective material (or grain) density of accessory minerals (ρ_{ga}) as follows:

$$\varepsilon_{tot} = 1 - \frac{\rho_{bb}\left(f_{cr}\rho_{ga} + (1-f_{cr})\rho_{gc}\right)}{\rho_{gc}\rho_{ga}} \qquad (2\text{-}18)$$

ρ_{gc} is taken as 2,800 kg m^{-3} and ρ_{ga} as 2,600 kg m^{-3}. The porosity resulting from the target bulk dry density of 1,450 kg m^{-3} is 0.475. The relationship given in Eq. (2-18) is completely different from the respective expression of clay rock (cf. Tab. 2-2). Porosity increases linearly with f_{cr} in Eq. (2-18), whereas it shows a limiting behaviour for clay rock (Eq. (2-15)). It must be kept in mind that the latter equation is intended to be applicable across the entire range of available data, whereas Eq. (2-18) is only applied for the target conditions of compacted bentonite. Also note that the functional relationship of Eq. (2-15) links the total porosity of the rock with the clay content in the case of clay rock, and the limiting porosity for the limiting case of no clay in the rock is assumed to be zero. For bentonite, the range of target bulk dry density is on a completely different scale and, for a (formal) zero-clay content, such a bentonite would exhibit a porosity of ~0.44. Furthermore, the total clay content of bentonite is relatively high at 81 wt.%. As such, the corresponding porosity of 0.475 is much larger than the clay rock value in Tab. 2-2 (0.139). This also shows that the "geometrical" approach to diffusion in clay rock (Eq. 2-16) is not applicable for bentonite.

The parameter values taken for Eq. (2-12) are $A_1 = (9.8 \pm 2.0) \times 10^{-11}$ m^2 s^{-1}, $A_2 = (9.3 \pm 3.2) \times 10^{-10}$ m^2 s^{-1}, $m_1 = 1.8 \pm 0.2$, $m_2 = 3.2 \pm 0.48$. These parameter values were specifically fitted to the results of diffusion experiments obtained from a commercial bentonite, named Volclay KWK (Glaus et al. 2017). The parameter uncertainties also include the results from measurements on pure montmorillonite (Glaus et al. 2017; Bestel et al. 2018). Uncertainty bands for the functional relationship between D_e and ε are obtained by crosswise combination of these parameter uncertainties (at the 2σ level). The data and model curves are shown in Fig. 2-5. The $D_{e,HTO}$ value predicted from Eq. (2-12) for the target porosity of 0.475 is $(1.1^{+0.89}_{-0.54})\times10^{-10}$ m^2 s^{-1}. From this $D_{e,HTO}$ value, a geometry factor (G_{HTO}) of $9.6^{+9.2}_{-4.3}$ is derived using Eq. (2-2) and a $D_{w,HTO}$ of 2.24×10^{-9} m^2 s^{-1}. The application range of this model is restricted to the target bulk dry density of the bentonite (1,450 kg m^{-3}) which is within the range of measured values.

For a very simplistic pore geometry model, it can be assumed that the total specific surface area (interlayers + interparticle space) is 770,000 m^2 kg^{-1}. This value is very close to the theoretical value for bentonite of 750,000 m^2 kg^{-1} mentioned in Karnland et al. (2006) and in good agreement with the limiting values for low d-spacing and stacking numbers (Delavernhe et al. 2015). For the given bulk dry density, the clay-to-liquid ratio is 2,470 kg m^{-3}, and the average pore width (d_p) ~1 nm (which is in rather good agreement with measured data of d-spacing). Such small pore widths mostly lead to the situation in which the Donnan layer thickness (d_{DL}) must be truncated to fulfil the requirement $d_{DL} < 0.99\ d_p/2$.)

Otherwise, the same formalisms are applied to derive the volume fractions of free and Donnan layer (V_{DL}) water as in the case of clay rock (Section 2.3).

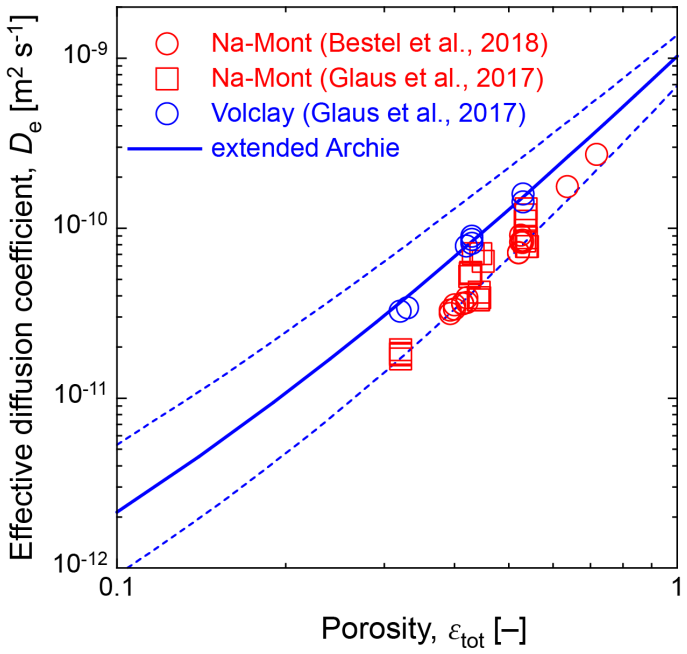

Fig. 2-5: Relationship between D_e values for HTO and porosity for smectite clay minerals ("Mont" = montmorillonite) and bentonite

The fit curves and the uncertainty bands were specifically adapted for the Volclay KWK data. The fit curves are extended beyond the range of available data in order to better show the "non-linear" behaviour of the model (on the double-log scale).

2.3 Chemical aspects: Mean-potential Donnan layer model

Chemical aspects of transport in argillaceous rocks include several interrelated components forming a consistent tool and data chain (Fig. 2-6) that was created to reduce overall uncertainties in the results that feed into Nagra's safety analysis.

Fig. 2-6: Consistent tool and data chain used in this work

Modified after Kulik et al. (2023). RN = radionuclides, FP = fission products.

The PSI/Nagra TDB2020 (Hummel & Thoenen 2023), model porewaters (Mäder & Wersin 2023, Curti 2023), GEMS calculations of radionuclide solubility limits (Kulik & Miron 2024), radionuclide sorption R_d values from the ClaySor model (Marinich et al. 2024, Marques Fernandes et al. 2024b) and effective diffusion coefficients D_e from the ClaySorDif model (this report) form the links in this consistent workflow that delivered the databases of R_d and D_e values, including their uncertainties. The following sections describe the aspects of this workflow that are relevant for the generation of the DDB.

2.3.1 Definition of the chemical system (solid and porewater scenario)

2.3.1.1 Reference porewater for clay rocks

The data from three borehole locations (Fig. 1-1) in the three siting regions in Northern Switzerland were used by Mäder & Wersin (2023) for defining the model porewater compositions for the Opalinus Clay. Because NL and ZNO have similar porewater chemistry, they are reported as a single NL-ZNO porewater.

Geochemical assumptions made by Mäder & Wersin (2023) as listed below were all implemented in GEMS calculations of model porewater equilibria (at 1 bar, 25 °C) using the PSI/Nagra TDB 2020 (Hummel & Thoenen 2023) with the specific ion-interaction theory (SIT) aqueous activity model (see Kulik & Miron (2024) for details):

1. The following were fixed based on the available data: NL-ZNO siting regions: 8.5 g dm^{-3} Cl and 2.2 g dm^{-3} S; JO siting region: 3.0 g dm^{-3} Cl and 2.6 g dm^{-3} S.
2. Na-Ca-Mg composition is based on the sum of Ca and S, the calcite dolomite equilibrium Ca/Mg ratio, and the Na/Ca ratio suggested by (clay) ion-exchange equilibria.
3. Exchange composition is defined based on measured data. An exchange capacity of 0.147 eq kg^{-1} for the NL-ZNO siting regions and 0.148 eq kg^{-1} for the JO siting region (ca. 0.66 kg illite of CEC = 0.225 eq kg^{-1}) were chosen operationally, solely for initiating the model.
4. Equilibria set by mineral-saturation constraints that make "geochemical sense", with some arbitrary choices of endmembers of solid solutions where the data are lacking.
   - 4.1. Calcite-dolomite equilibrium is imposed.
   - 4.2. pCO_2 is imposed at $10^{-2.2}$ bar (reference case) or $10^{-1.8}$ bar (high-pCO_2 variant); this fixes pH and alkalinity.
   - 4.3. Siderite equilibrium fixes $[Fe^{II}]_{aq}$ at given pH and alkalinity.
   - 4.4. Pyrite equilibrium at given sulphate and $[Fe^{II}]_{aq}$ fixes sulphide and the redox potential, and thus also $[Fe^{III}]_{aq}$.
   - 4.5. Quartz is used to fix $[Si]_{aq}$ aqueous concentration.
   - 4.6. Kaolinite is used to fix $[Al]_{aq}$ at given $[Si]_{aq}$ and pH.
   - 4.7. Celestite fixes $[Sr]_{aq}$ at given sulphate concentration.
   - 4.8. Fluorite is used to fix $[F]_{aq}$ at given Ca concentration.
   - 4.9. Barite fixes $[Ba]_{aq}$ at given sulphate concentration.
   - 4.10. Rhodochrosite is used to fix $[Mn^{II}]_{aq}$ at given pH and alkalinity.

For consistency with the porewater data, Kulik & Miron (2024) added Br to model reference porewaters using the known Cl/Br mole ratios in saline groundwaters (Davis et al. 1998). They noted that at constant addition of K as KCl and KBr, even significant variations of Br concentration have almost no effect on the chemical state of the porewater. In all cases, the composition, pH, pCO_2 and Eh of all porewater types listed in Mäder & Wersin (2023), calculated in PHREEQC using the PSI/Nagra TDB 2020, could be closely reproduced in GEMS calculations at low illite S:L ratios, with relative differences of 1% or less.

The reference porewater models should be used not only for estimating solubility limits, but also for seamless calculations of the R_d and D_e values at realistic porosities of compacted clay rock. Therefore, the "backbone" ClaySor model for illite (Marinich et al. 2024), involving the exchange of major cations (Ca^{2+}, K^+, Mg^{2+}, Na^+, Sr^{2+}) on planar sites and the protolysis of amphoteric edge sites, was added to the chemical system. In order to check how the porewater models perform at various solid-to-liquid mass ratios (r_{SL}), up to those typical in Opalinus Clay, the GEMS calculations were first conducted at very low r_{SL} to set the composition of ion exchange, and then at high r_{SL} and realistic porosity of Opalinus Clay containing 50% clay with 64% illite content, i.e. at the reference mass ratio r_{iSL} = 6.14 kg kgw^{-1} (kgw: kg of water) for illite with an assumed material density of 2,730 kg m^{-3} (formula definition is given in Section 2.3.3, Eq. (2-42) below). This system composition (for the NL-ZNO and JO siting regions in the reference and high-pCO_2 cases) has been adjusted by model titrations (at 1 bar, 25 °C) to compensate for the effects of protolysis charge on edge sites and to reproduce the model porewater compositions from Mäder & Wersin (2023) as closely as possible (Kulik & Miron 2024).

The concentrations of the most important constituents are shown in Tab. 2-3. The purpose of this table is to show the differences compared to the synthetic porewaters used for the diffusion measurements (see Tab. 2-4 in Section 2.3.4). The detailed composition with respect to minor elements can be taken from the aforementioned references.

Tab. 2-3: Composition with respect to major elements of the porewaters (concentrations are given as [M]) used for the compilation of D_e values

The suffixes "Ref" and "hpCO_2" denote the reference and the high-pCO_2 porewater variants.

Element	**NL-ZNO-Ref**	**NL-ZNO-hpCO_2**	**JO-Ref**	**JO-hpCO_2**
Na	2.02×10^{-1}	2.02×10^{-1}	1.29×10^{-1}	1.21×10^{-1}
K	1.16×10^{-3}	1.16×10^{-3}	8.32×10^{-4}	8.21×10^{-4}
Ca	2.70×10^{-2}	2.69×10^{-2}	7.60×10^{-3}	7.89×10^{-3}
Mg	1.59×10^{-2}	1.58×10^{-2}	4.47×10^{-3}	4.65×10^{-3}
Sr	3.80×10^{-4}	3.84×10^{-4}	1.93×10^{-4}	1.94×10^{-4}
Cl	2.50×10^{-1}	2.67×10^{-1}	8.50×10^{-2}	9.20×10^{-2}
Total SO_4	2.34×10^{-2}	2.34×10^{-2}	2.77×10^{-2}	2.75×10^{-2}
Total inorganic C	2.06×10^{-3}	3.47×10^{-3}	3.20×10^{-3}	5.15×10^{-3}
pH Ionic strength (M)	7.07 0.33	6.87 0.34	7.34 0.168	7.14 0.169

2.3.1.2 Bentonite porewater

The solubility limit calculations for model bentonite porewaters (BPW) are described elsewhere (Hummel et al. 2023). These were performed for two variants of BPW as derived by Curti (2023): (i) a reference porewater (E3-BPW-Ref), which is a representative water with $\log_{10}pCO_2$ = -2.2, and (ii) a variant representing the elevated pCO_2 (E3-BPW-high-pCO_2) with $\log_{10}pCO_2$ = -1.8. The high-pCO_2 variant was selected in order to test the impact of enhanced carbonate complexation on the solubility limits in BPW. These porewaters were assumed to exist in equilibrium with barite, calcite, dolomite, celestine, kaolinite, gypsum, quartz, rhodochrosite, magnetite and pyrite. The last two minerals also comprise a redox buffer determining the anoxic Eh of the porewater. The "backbone" ClaySor model for montmorillonite, involving the exchange of five major cations (Ca^{2+}, K^+, Mg^{2+}, Na^+, Sr^{2+}) at the planar sites and the protolysis of amphoteric edge sites (Marinich et al. 2024), was added for a seamless application of BPW models for R_d calculations at the realistic porosity of the compacted bentonite. The development of surface charge on montmorillonite edge sites at high S:L ratios had to be compensated by titration with NaOH or HCl in order to maintain the composition of the model reference bentonite porewater (Curti 2023).

2.3.2 Mean-potential Donnan layer model

To account for the impact of the permanent charge induced by surfaces of clay minerals (illite, montmorillonite) on ion concentration and mobility in porewater, various EDL models have been used (see an overview by Tournassat & Steefel 2015). The mean-potential Donnan layer (MPDL) model represents one of the simplest and most convenient, and has been implemented in popular codes such as PHREEQC (Appelo & Wersin 2007), FLOTRAN (Gimmi & Alt-Epping 2018), CrunchClay (Tournassat & Steefel 2021) and ORCHESTRA (Jenni et al. 2021).

In order to retain the consistency of the current tool chain (Fig. 2-6) based on GEMS (GEM software collection, https://gems.web.psi.ch), and to provide Nagra and the GEMS user community with all relevant extensions for waste disposal in clay rocks and bentonite, the MPDL model was implemented as described below. The MPDL model is based on a planar representation of pores in argillaceous rocks and on a discrete distribution of electrostatic potential (cf. Fig. 2-1, red line). In the MPDL model, a mean electrostatic potential Ψ_D $[V]$ acts on the aqueous ions in the porewater of the Donnan layer (DL) of volume V_{DL} (cf. Eq. (2-10) and Fig. 2-3):

$$V_{DL} = d_{DL} A_{DL} = V_P f_{DL} \text{ [dm}^3\text{]} \quad (2\text{-}19)$$

where d_{DL} is the thickness of the DL (e.g. Glaus et al. 2015); A_{DL} is the area of (permanent charge) surface carrying the DL and f_{DL} is the volume fraction of DL porewater. The exact relationship between A_{DL} and the pore surface area, A_p, depends on assumptions about pore geometry; in this model, $A_{DL} \approx A_p$.

The DL equilibrium is found by iteratively adjusting the Coulomb term:

$$Coul = (F\Psi_D) / (RT) \quad (2\text{-}20)$$

Here, F is the Faraday constant (96,485 C mol^{-1}); R is the universal gas constant (8.3145 J K^{-1} mol^{-1}); T is the absolute temperature (K). The iterations run until the charge balance:

$$-[\sigma_{clay}] - \widehat{[\sigma_{DL}]} = 0 \quad (2\text{-}21)$$

is achieved with the desired precision. Here, $[\sigma_{clay}]$ is the volume density of clay permanent charge acting on DL porewater (molarity, [mol dm^{-3}]) obtained from the input free charge capacity (FCC) parameter (cf. Section 2.3.3) and the S:L ratio (see below). $\widehat{[\sigma_{\mathrm{DL}}]}$ is the optimised total charge molarity in DL porewater [mol dm^{-3}], computed over all charged aqueous species as:

$$\widehat{[\sigma_{\mathrm{DL}}]} = \sum_{z_i \neq 0} z_i c_{i,\mathrm{free}} exp\left(-z_i \cdot \widehat{Coul}\right) \frac{\gamma_{i,\mathrm{free}}}{\gamma_{i,\mathrm{DL}}} \tag{2-22}$$

where z_i is the charge number of ion *i*. The Coulomb term of (aqueous) species in DL is part of the electrochemical potential related to the species activity $a_i = c_i \gamma_i$, expressed via the molar concentration c_i and the activity coefficient γ_i. Hence, the concentration ratio of species *i* in the DL to its counterpart in "free" porewater not affected by clay mineral charge includes a ratio of activity coefficients:

$$\frac{c_{i,\mathrm{DL}}}{c_{i,\mathrm{free}}} = exp\left(-z_i \cdot \widehat{Coul}\right) \frac{\gamma_{i,\mathrm{free}}}{\gamma_{i,\mathrm{DL}}} \tag{2-23}$$

The definition of the activity coefficient of an aqueous species in the DL porewater remains an open scientific issue; hence, it is commonly assumed that:

$$\frac{\gamma_{i,\mathrm{free}}}{\gamma_{i,\mathrm{DL}}} = 1 \tag{2-24}$$

Gimmi & Alt-Epping (2018) and Tournassat & Steefel (2021) have shown, in full agreement with the current MPDL calculations, that the apparent ionic strength in DL porewater:

$$\widehat{I_{\mathrm{DL}}} = \frac{1}{2} \sum_{z_i \neq 0} z_i^2 c_{i,\mathrm{DL}} \tag{2-25}$$

can be quite high (i.e. 10 M or more). As the ionic strength of the reference model porewaters ranges between 0.2 and 0.5 M, the assumption that $\gamma_{i,\mathrm{DL}} = \gamma_{i,\mathrm{free}}$ is probably not correct. Therefore, more research is required in this area.

The dependence of D_e on the concentration ratio $\frac{c_{i,\mathrm{DL}}}{c_{i,\mathrm{free}}}$ has already been introduced in Eq. (2-1). The corresponding notation for an ion *i* can be specifically expressed according to:

$$D_{e,i} = \frac{\varepsilon}{G} D_{\mathrm{w},i} \left(f_{\mathrm{free}} + f_{\mathrm{DL}} \frac{c_{i,\mathrm{DL}}}{c_{i,free}} q_\eta \right) \tag{2-26}$$

The concentration ratio $\frac{c_{i,\mathrm{DL}}}{c_{i,\mathrm{free}}}$ is obtained from the MPDL Coulomb term using (Eqs. (2-20) and (2-23)) under the usual assumption (Eq. (2-24)) that the ratio of activity coefficients of the *i*-th aqueous species in free and in DL porewater is unity:

$$\frac{c_{i,\mathrm{DL}}}{c_{i,free}} = \exp\left(-z_i \widehat{Coul}\right) = exp\left(\frac{-z_i F \Psi_{\mathrm{D}}}{RT}\right) \tag{2-27}$$

It follows that, in the DL porewater influenced by the negative permanent charge of the clay surface, cationic species are enriched compared to their concentrations in "free porewater" ($\frac{c_{i,\mathrm{DL}}}{c_{i,free}} > 1$), anionic species are depleted ($\frac{c_{i,\mathrm{DL}}}{c_{i,free}} < 1$) (anion exclusion), and neutral species are generally not affected by the clay charge ($\frac{c_{i,\mathrm{DL}}}{c_{i,free}} = 1$). The initially unknown values of $\widehat{Coul}$ and thus Ψ_{D} are computed by iteration, as mentioned above.

2.3.3 ClaySorDif implementation of MPDL model

The MPDL model calculation (so far at ambient conditions only) starts with the equilibrium "free" (bulk) porewater aqueous speciation, i.e. a vector of $c_{i,\mathrm{free}}$ values for all species of all dissolved elements, computed in GEMS using the appropriate model porewater chemistry at 1 bar, 25 °C (see Tab. B-1 and B-2 in Kulik & Miron 2024). After the MPDL calculation has converged, it yields another, virtual aqueous speciation for the DL porewater, i.e. a vector of $c_{i,\mathrm{DL}}$ values. For an element such as an actinide, the predominant species in porewater may be cationic, anionic or neutral, so they will be affected differently by the electrical potential in the DL, leading to different effective diffusion coefficient $D_{\mathrm{e},i}$ values. However, simple diffusion models use a common $D_{\mathrm{e,elem}}$ value for the total dissolved chemical element. Based on "free" and DL porewater aqueous speciations, $D_{\mathrm{e,elem}}$ is calculated as follows.

First, for each element, the aqueous speciation mole fractions of the charged species $\chi_{i,\mathrm{free}}$ and $\chi_{i,\mathrm{DL}}$ are computed as a function of the total concentration (c_{T}) of the respective element:

$$\chi_{i,\mathrm{free}} = \frac{c_{i,\mathrm{free}}}{c_{\mathrm{T,free}}} (z_{i,\mathrm{free}} \neq 0) \tag{2-28}$$

In practice, only the fractions of "dominantly" charged species with an $\chi_{i,\mathrm{free}}$ > 0.001 are considered. It can safely be assumed that this truncation has no significant impact on the dose calculation of most radioelements under consideration. There is, however, the notable exception of carbon: The most dominant carbon species comprise inorganic carbon and its complexes. C-14-bearing organic species are thus ignored in the calculation according to the mentioned truncation criterion. These species may, however, exhibit rather different diffusion and retardation properties compared to the inorganic species.

The fraction of neutral species (all those unaffected by the electrical potential) is the residual, calculated by:

$$\chi_{n,\mathrm{free}} = 1 - \sum \chi_{i,\mathrm{free}} \tag{2-29}$$

The bulk diffusion coefficient for the element in water is taken from the D_{w}DB database (the source of $D_{\mathrm{w,elem}}$ and $D_{\mathrm{w},i}$ for some elements, see Section 2.1). Unless a separate value is provided in D_{w}DB for neutral aqueous species, the respective bulk diffusion coefficient is assumed to be:

$$D_{\mathrm{w,n}} \approx D_{\mathrm{w,elem}} \tag{2-30}$$

or, if $D_{\mathrm{w,elem}}$ is not available, $D_{\mathrm{w,n}}$ is assumed to be identical to that of HTO, $D_{\mathrm{w,HTO}}$. Note that D_{w} values decrease with increasing hydrodynamic radius according to the Stokes-Einstein equation (Eq. (2-4)). For complex solutes with unknown bulk water-diffusion properties, this assumption is therefore comparatively conservative because the water molecule has a higher D_{w} value compared to other ionic solutes.

The effective $D_{\mathrm{e,n}}$ values of all neutral species of a given element are then calculated as:

$$D_{\mathrm{e,n}} = \frac{\varepsilon_{\mathrm{tot}}}{G} D_{\mathrm{w,n}} \tag{2-31}$$

It is further assumed that the geometrical factor G is identical for all solutes. Again, this assumption is comparatively conservative. G factors significantly larger than those of uncharged reference species can, under given circumstances, be found for anionic species (Chagneau et al. 2015). However, the opposite case, namely G factors less than those of uncharged reference species, has not yet been observed. The mean $D_{\mathrm{e,elem}}$ value for a given element is finally defined as the weighted average of $D_{\mathrm{e},i}$ values over the respective aqueous speciation fractions:

$$D_{\mathrm{e,elem}} = D_{\mathrm{e,n}}\chi_{\mathrm{n,free}} + \frac{\varepsilon_{\mathrm{tot}}}{G}\sum D_{\mathrm{w},i}\chi_{i,\mathrm{free}}\left(f_{\mathrm{free}} + f_{\mathrm{DL}}\frac{c_{i,\mathrm{DL}}}{c_{i,\mathrm{free}}}q_{\eta}\right) \tag{2-32}$$

The contributions of effective diffusion coefficients for neutral species ($D_{\mathrm{e,n}}$) and for ionic species ($D_{\mathrm{e},i}$) in $D_{\mathrm{e,elem}}$can be better seen in a simpler form of Eq. (2-32) below:

$$D_{\mathrm{e,elem}} = D_{\mathrm{e,n}}\chi_{\mathrm{n,free}} + \sum D_{\mathrm{e},i}\chi_{i,\mathrm{free}} \tag{2-33}$$

Eqs. (2-28) to (2-33) are implemented in the ClaySorDif Python code. These equations are approximate with respect to the above assumption that the ratio of activity coefficients of the *i*-th aqueous species in free- and in DL porewater is unity. According to the comparison in this work with PHREEQC calculations that produce comparatively similar results, a similar assumption may also be applied there. This is understandable because no widely accepted model for activity coefficients in Donnan aqueous electrolyte is yet available. In future studies, when such a model exists, the estimation of effective diffusion coefficients of elements can be further improved by considering the more realistic aqueous speciation mole fractions (of ionic and neutral species) in the DL based on its virtual composition obtained from MPDL calculations for each element:

$$\chi_{i,\mathrm{DL}} = \frac{c_{i,\mathrm{DL}}}{c_{\mathrm{T,DL}}}\,(z_{i,\mathrm{DL}} \neq 0) \tag{2-34}$$

$$\chi_{n,\mathrm{DL}} = 1 - \sum \chi_{i,\mathrm{DL}} \tag{2-35}$$

The mean $D_{\mathrm{e,elem}}$ values of a given element will then be computed as:

$$D_{\mathrm{e,elem}} = D_{\mathrm{e,n}}\chi_{n} + \frac{\varepsilon_{\mathrm{tot}}}{G}\sum D_{\mathrm{w},i}\left(f_{\mathrm{free}}\chi_{i,free} + f_{\mathrm{DL}}\frac{c_{i,\mathrm{DL}}}{c_{i,free}}\chi_{i,\mathrm{DL}}q_{\eta}\right) \tag{2-36}$$

where

$$\chi_n = f_{\text{free}}\chi_{n,\text{free}} + f_{\text{DL}}\chi_{n,\text{DL}} \tag{2-37}$$

The remaining task to compute Eq. (2-32) is to find the fractions of "free" (f_{free}) and DL (f_{DL}) porewaters for the given dry density and clay content of argillaceous rock, as well as the dependence of $\frac{\varepsilon_{\text{tot}}}{G}$ on the clay content. This requires determining the mean pore thickness (width) d_{p} [m] (Eq. (2-5)) and the Donnan layer thickness d_{DL} [m], the latter of which is usually assumed to be a multiple (n_{DL}) of the Debye length $\frac{1}{\kappa}$ [m]:

$$d_{\text{DL}} = \frac{n_{\text{DL}}}{\kappa} \tag{2-38}$$

where the default value of n_{DL} is 2, and

$$\frac{1}{\kappa} = \sqrt{\frac{\epsilon\epsilon_0 \cdot RT}{2F^2 \cdot 1000I}} \tag{2-39}$$

(Glaus et al. 2015); ϵ = 78.3 [-] is the relative dielectric permittivity of water at 1 bar, 25 °C, ϵ_0 = 8.85419 × 10^{-12} [F m^{-1}] is the dielectric permittivity of a vacuum, and I [molarity, M, or molality, m] is the effective ionic strength in "free" porewater. Using the numerical values for the constants, Eq. (2-39) can be represented for 25 °C on the nanometer scale as follows:

$$\frac{1}{\kappa} = \frac{0.30382}{\sqrt{I}} \tag{2-40}$$

In either case, the thickness of the DL depends on the ionic strength of the model porewater: a 4-fold increase in I (e.g. from 0.16 to 0.64 m) results in a 2-fold decrease in d_{DL}. It is further assumed that no domain with complete anion-exclusion properties (cf. Glaus et al. (2015)) exists.

The volume fractions of DL f_{DL} and "free" f_{free} porewater are calculated from Eqs. (2-10) and (2-11) respectively, considering the restriction of $f_{\text{DL}} \leq 0.99$ and the fact that, in a planar pore, there are two Donnan layers, one on each side (see Fig. 2-3).

Not all clay minerals in sedimentary rocks have a permanent charge (as routinely measured by CEC (cation-exchange capacity): for instance, kaolinite and chlorite have little to no CEC, while bentonites show a comparatively high CEC (0.8 eq kg^{-1} and above for montmorillonite), and illite and mixed-layer clays exhibit an intermediate CEC (0.1 to 0.3 eq kg^{-1}) (Tournassat & Steefel 2015). As illite is the most abundant clay mineral in the Opalinus Clay, with smectite and mixed layers comprising just a few percent of the clay component, for the current MPDL calculations the illite content in the clay component was fixed at the typical value of f_{cm} = 0.64, assuming illite as the only source of the clay permanent charge.

The MPDL charge volume density acting onto the DL pore volume is calculated as follows:

$$[\sigma_{\text{clay}}] = -\text{FCC}\frac{\rho_{\text{br}} f_{\text{cm}} f_{\text{cr}}\, f_{\text{DL}}}{\varepsilon_{\text{tot}}} \tag{2-41}$$

where FCC [eq kg^{-1}] is the "free charge capacity" of illite that corresponds to the density of "uncompensated" permanent charge on planar surfaces. FCC is treated here as an adjustable parameter independently of CEC; ρ_{br} [kg dm^{-3}] is the bulk dry density of clay rock; the product $f_{\mathrm{cm}}f_{\mathrm{cr}}$ is the mass fraction of illite in dry clay rock; and $\varepsilon_{\mathrm{tot}}$ is the porosity, as calculated from Eq. (2-15). It is expected that FCC ≤ CEC of the clay mineral. In the ClaySor model, the number of ion-exchange sites per 1 kg of illite or montmorillonite is set numerically equal to the CEC and is used to set the planar site balance constraint. Hence, it is more accurate to call this ClaySor parameter a CBC (cation-binding capacity); CBC = CEC, where the CEC value is usually experimentally measured in dilute aqueous electrolyte suspensions of illite or montmorillonite (Tournassat & Steefel 2015).

To assess the chemical equilibrium porewater speciation and perform R_{d} calculations in compacted clay rock, it is best to use the illite-porewater mass ratio defined as:

$$r_{\mathrm{iSL}} = \frac{\rho_{\mathrm{br}} f_{\mathrm{cm}} f_{\mathrm{cr}}}{\varepsilon_{\mathrm{tot}}} = \frac{\rho_{\mathrm{br}} f_{\mathrm{cm}} f_{\mathrm{cr}}}{\mathrm{a}_3(1-e^{-\mathrm{a}_4 W_{\mathrm{cr}}})} \tag{2-42}$$

Conversely, the bulk dry density of clay rock ρ_{br} must also depend on the clay content f_{cr}. In the ClaySorDif model, it is evaluated as follows:

$$\rho_{\mathrm{br}} = [f_{\mathrm{cm}}\rho_{\mathrm{cm}} + (1 - f_{\mathrm{cm}})\rho_{\mathrm{ga}}] \cdot (1 - \varepsilon_{\mathrm{tot}}) \tag{2-43}$$

where ρ_{cm} is the clay mineral (illite) density, and ρ_{ga} is the grain density of the solid Opalinus Clay part other than illite (usually assumed $\rho_{\mathrm{ga}} = \rho_{\mathrm{cm}}$). Both can be called the "material grain density" and range between 2.70 and 2.85 kg dm^{-3} (Tournassat & Steefel 2015).

In the Opalinus Clay and related argillaceous rocks, the total clay content W_{c} is within the 30 to 70 wt.% range (with an average close to W_{c} = 50 wt.% or f_{cr} = 0.5), the porosity is within the $0.085 < \varepsilon_{\mathrm{tot}} < 0.155$ range (with an average close to $\varepsilon_{\mathrm{tot}}$ = 0.12). At W_{c} = 50 wt.%, Eq. (2-15) gives $\varepsilon_{\mathrm{tot}}$ = 0.1247. Taking $\varepsilon_{\mathrm{tot}}$ = 0.125 and fixing $\rho_{\mathrm{cm}} = \rho_{\mathrm{ga}} = 2{,}730$ kg m^{-3} for clay-dominated rocks, Eq. (2-43) yields $\rho_{br} = 2{,}390$ kg m^{-3}. Using Eq. (2-42) and assuming $f_{cm} = 0.64$, the illite-porewater mass ratio becomes $r_{iSL} = 6.14$ kg kgw^{-1}. Taking into account the issues due to the buildup of the illite edge charge upon increasing r_{iSL} (Kulik & Miron 2024), the value $r_{\mathrm{iSL,ref}}$ = 6.14 kg kgw^{-1} was chosen as a reference value to avoid these issues in GEMS calculations of the reference porewaters and solubility limits (Kulik & Miron 2024), ClaySor calculations of R_{d} of radionuclides in model porewaters (Kulik & Miron 2024), and ClaySorDif MPDL calculations (this work).

The uncertainty of the above value of $r_{\mathrm{iSL,ref}}$ can be assessed as follows. Using the above range of measured porosities and Eq. (2-42), the 2,300 kg m^{-3} < ρ_{br} < 2,500 kg m^{-3} range of bulk dry densities for clay rock is estimated. From the average $\varepsilon_{\mathrm{tot}} = 0.125$, $\rho_{\mathrm{br}} = 2{,}390$ kg m^{-3} is calculated, which lies in the middle of the above ρ_{br} interval. The variability of r_{iSL} within the considered range of W_{c} can be found from Eq. (2-42) using the values $f_{\mathrm{cr,min}} = 0.3$ and $f_{\mathrm{cr,max}} = 0.7$, respectively, while keeping $f_{\mathrm{cm}} = 0.64$ constant (though it seems to have its own scatter between 0.5 and 0.7). This leads to 4.57 kg kgw^{-1} < r_{iSL} < 7.91 kg kgw^{-1} and $r_{\mathrm{iSL,ref}} = 6.14 \pm 1.77$ kg kgw^{-1}. Conversion from the illite-porewater ratio to the total solid/porewater ratio is straightforward:

$$r_{\mathrm{SL}} = \frac{r_{\mathrm{iSL}}}{f_{\mathrm{cm}} f_{\mathrm{cr}}} \tag{2-44}$$

For the reference case ($f_{\mathrm{cm}} = 0.64$, $f_{\mathrm{cr}} = 0.5$), this gives $r_{\mathrm{SL,ref}} = 19.19$ kg kgw^{-1}, which is consistent with that directly calculated by dividing $\rho_{\mathrm{br,ref}} = 2{,}400$ kg m^{-3} and $\varepsilon_{\mathrm{tot,ref}} = 0.125$.

Predictions from the MPDL model are not restricted only to D_{e} values. The breakthrough time of an element or ion is influenced by the dimensionless rock capacity factor α. In the case of anion exclusion, i.e. for anionic species ($z_i < 0$, assuming $q_\eta = 1$ and $R_{\mathrm{d}} = 0$), Eq. (1-4) can be expressed as:

$$\alpha_i = \varepsilon_{\mathrm{AN},i} = \varepsilon_{\mathrm{tot}} \left(f_{\mathrm{free}} + f_{\mathrm{DL}} \frac{c_{i,\mathrm{DL}}}{c_{i,\mathrm{free}}} \right) \tag{2-45}$$

The symbol $\varepsilon_{\mathrm{acc}}$ used in Eq. (1-4) for the accessible porosity is explicitly written here as $\varepsilon_{\mathrm{AN},i}$, representing the anion-accessible porosity. The respective conversion of MPDL model results into those of the anion-exclusion approach has been explained in Fig. 2-2. In the absence of clay charge, $\varepsilon_{\mathrm{AN},i}$ is close to the total porosity. At low porosity, high clay charge and relatively low ionic strength, f_{DL} reaches 0.99 and the MPDL concentration ratio $\frac{c_{i,\mathrm{DL}}}{c_{i,free}}$ (especially for a divalent anion) can be much less than 0.1, meaning almost complete anion exclusion. For neutral non-sorbing tracers, $\frac{c_{i,\mathrm{DL}}}{c_{i,free}} = 1$, from which it follows (cf. also Eq. 2-3) that $\alpha = \varepsilon_{tot}$. For neutral sorbing species, the implicit assumption is made that $\varepsilon_{\mathrm{tot}}$ is available for these species.

For sorbing elements (with neutral and cationic aqueous species), the rock capacity factor takes the form of Eq. (1-4). In the simplest case for the clay rock, it is assumed that the element considered is only sorbed on illite, in which case R_{d} is first computed for the equilibrium between illite edges and planar sites and "free" porewater (defined at $r_{iSL,ref} = 6.14$ kg kgw^{-1}) using the ClaySor model (Marinich et al. 2024), and then scaled up to the mass of clay rock by multiplying with the factor $1/(f_{\mathrm{cm}} f_{\mathrm{cr}})$. For elements of the alkali and alkaline earth series that are mainly sorbed by ion exchange on planar permanent-charge sites, ClaySor includes the site-binding model normalised per mass of illite and delivers the same type of R_{d}, which is perhaps a good model for illite. However, for montmorillonite (in bentonite), alternative models have been suggested (Birgersson & Karnland 2009) that represent cation exchange not in terms of site binding (controlled by the CBC parameter as in the ClaySor model) but rather as the excess amount of cation in the DL relative to that in "free" porewater. This kind of representation is possible in ClaySorDif as an alternative to the site-binding ion exchange in the ClaySor model, although its applications require more research in the future aimed at establishing the ionic activity coefficients in the DL porewater.

The ClaySorDif extension for GEMS calculations of clay rock porewater systems described above has been implemented as a Python class ClaySorDif.py which uses the Python interface xGEMS of the GEMS3K code from the GEMS code collection (Kulik et al. 2013). A simplified flow chart of ClaySorDif operation is provided in Fig. 2-7. The required parameters are collected and provided (mainly in JSON input files) according to the scheme shown in Fig. 2-8.

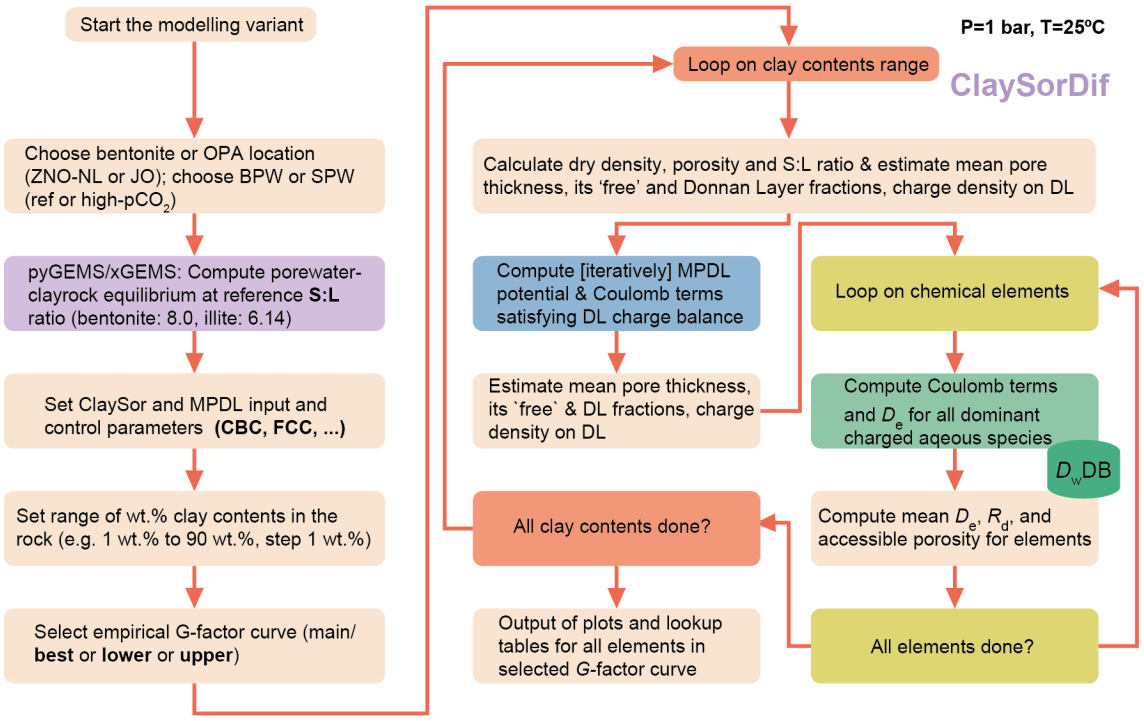

Fig. 2-7: Flow chart of the operation of the ClaySorDif MPDL model Python code

D_wDB is the database of bulk diffusion coefficients in water.

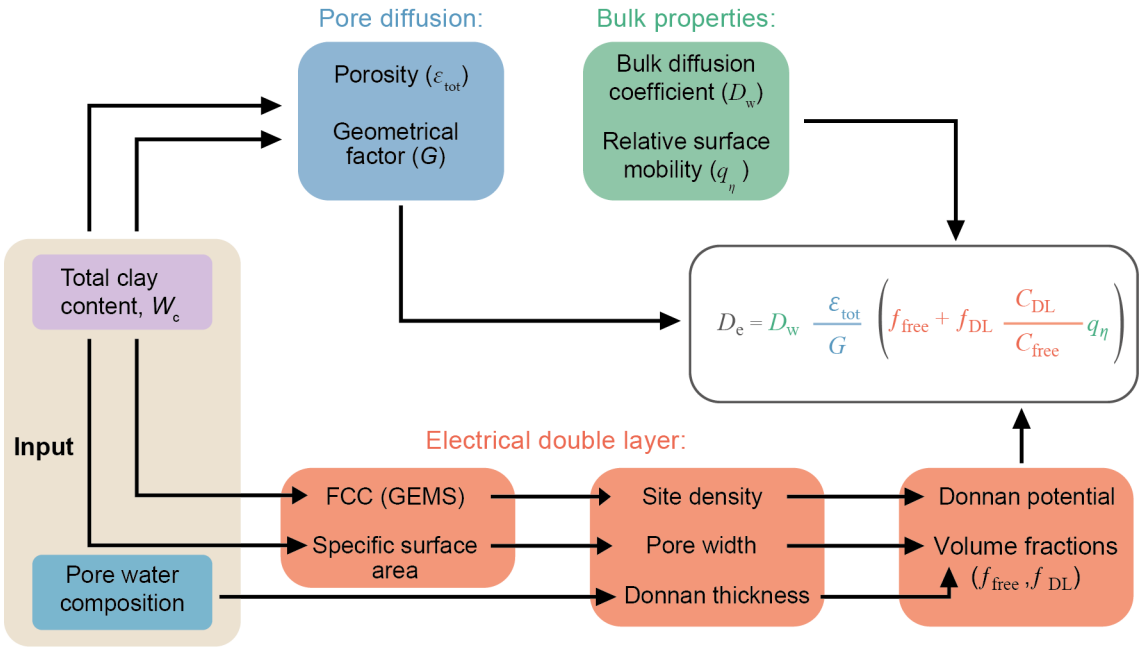

Fig. 2-8: Parameter flow used in D_e calculations in PHREEQC and in GEMS (ClaySorDif)

2.3.4 PHREEQC implementation for comparison and verification

Effective diffusion coefficients, D_e, are calculated in PHREEQC according to the procedures published in Glaus et al. (2015) using the same equations as for the ClaySorDif calculations (see above) and assuming a planar pore geometry. The most significant difference to ClaySorDif simulations lies in assumptions made in PHREEQC regarding charge neutralisation in the EDL at the planar clay mineral surfaces. The negative charge resulting from the isomorphic lattice substitutions is (i) partly neutralised by the surface complexes formed with aqueous solution cations in the Stern layer, while (ii) the remaining excessive negative charge is neutralised by the cations present in the Donnan layer. The thermodynamic equilibrium expressions for the former surface complexes include electrostatic effects caused by the surface potential at the basal clay surfaces. While FCC is merely the adjustable parameter in ClaySorDif calculations (cf. Fig. 2-7, Eq. (2-41)), the thermodynamic equilibrium constants for the formation of the Stern layer surface complexes of cations were fitted in PHREEQC calculations (for a given CEC value providing the site balance constraint) to match the ion-exchange equilibrium distribution between aqueous solution and basal surfaces according to known selectivity coefficients for cation exchange. Thereby, the fractional equivalent occupancy of cations at the basal surfaces is calculated from the sum of cations in the Stern layer plus cations in the Donnan layer.

Note that in PHREEQC calculations of four verification cases described below, and in corresponding ClaySorDif comparison calculations, slightly different forms of Eqs. (2-14) and (2-15) and slightly different parameter values were used:

$$\varepsilon_{\mathrm{tot}} = \mathrm{a}_0 + \mathrm{a}_3(1 - e^{-\mathrm{a}_4 W_c}) \tag{2-46}$$

where a_0 = 0.005, a_3 = 0.1430 and a_4 = 0.0361. The following form of the equation and the subsequent Eq. (2-48) have become obsolete since the publication of Van Loon et al. (2023):

$$G = \mathrm{a}_1 + e^{\mathrm{a}_2 W_c} \tag{2-47}$$

where $\mathrm{a}_1 = 10.0$ and $\mathrm{a}_2 = 0.0516$.

For a non-sorbing inert tracer, such as HTO, the D_e value was calculated as:

$$D_e = \frac{\mathrm{a}_0 + \mathrm{a}_3(1 - e^{-\mathrm{a}_4 W_c})}{\mathrm{a}_1 + e^{\mathrm{a}_2 W_c}} D_w \tag{2-48}$$

Fig. 2-9 shows a comparison between the two scenarios. The discrepancies are only noticeable at very low clay contents for which the applicability of the model is already limited, as illustrated by the increased discrepancy of model predictions and measured D_e for HTO (Van Loon et al. 2023).

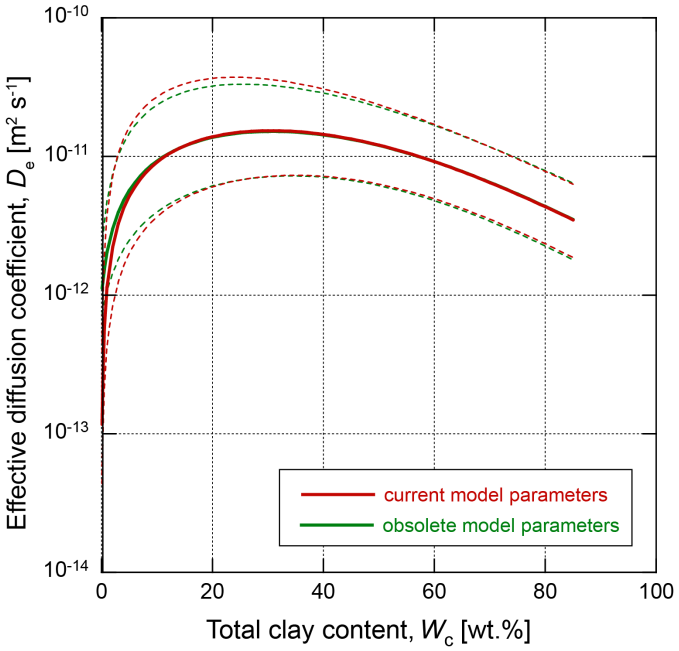

Fig. 2-9: Comparison of D_e values calculated for HTO using the current model parameters (cf. Eq. (2-16), Van Loon et al. 2023) and the obsolete model parameters used for comparing the ClaySorDif model with the PHREEQC calculations (cf. Eq. (2-48)) and for generating the values of the DDBs

PHREEQC modelling was applied recently (Glaus et al. 2024) to the experimental diffusion data for drill core samples from the recent Nagra's recent deep borehole campaign in the siting regions shown in Fig. 1-1. Diffusion measurements were conducted in four synthetic porewaters (SPW) (Tab. 2-4) with compositions mimicking representative porewater data for the respective locations.

The average CEC [mol kg^{-1} of clay] measurements via the Ni-ethylenediamine and the Cs isotope-dilution method on the drill core samples, extrapolated to 100% clay (CEC_{100}), is approximately ~0.21 mol kg^{-1}. For practical reasons, in the PHREEQC implementation, the CEC was expressed per volume of porewater as $\mathrm{CEC_{vol}} = \mathrm{CEC_{100}} f_{cr} r_{\mathrm{SL}}$.

Element-specific bulk diffusion coefficients were taken from the literature (Li & Gregory 1974). The ε_{tot} and G were computed from the clay content measured in samples using Eqs. (2-46) and (2-47). The standard thermodynamic data were taken from the PSI/Nagra TDB 2020 v1-1 exported into PHREEQC.dat format. The surface complexation constants for Stern-layer ion-exchange species are given in Tab. 2-5 (Glaus et al. 2021).

Tab. 2-4: Composition of the SPWs (concentrations are given as [M]) used in the diffusion experiments

Element	SPW-BOZ	SPW-BUL	SPW-STA	SPW-TRU
Na	1.40×10^{-1}	3.43×10^{-1}	1.56×10^{-1}	2.44×10^{-1}
K	7.76×10^{-4}	1.91×10^{-3}	1.91×10^{-3}	1.64×10^{-3}
Ca	9.24×10^{-3}	3.83×10^{-2}	3.50×10^{-2}	2.22×10^{-2}
Mg	3.94×10^{-3}	1.76×10^{-2}	1.76×10^{-2}	1.56×10^{-2}
Sr	1.15×10^{-4}	3.33×10^{-4}	3.33×10^{-4}	2.89×10^{-4}
Cl	8.28×10^{-2}	4.02×10^{-1}	2.19×10^{-1}	2.72×10^{-1}
Total SO_4	4.21×10^{-2}	2.75×10^{-2}	2.22×10^{-2}	2.43×10^{-2}
Total inorganic C	7.05×10^{-4}	4.13×10^{-4}	4.13×10^{-4}	4.87×10^{-4}
pH Ionic strength (M)	7.90 0.190	7.56 0.505	7.56 0.306	7.68 0.354

Tab. 2-5: Surface complexation constants for the formation of dominant Stern-layer species (sites abbreviated as Su)

The constant for Sr^{2+} was adjusted to that of Ca^{2+}.

Species	$\log^{Su}K$	Reaction
Su^-	0	$Su^- = Su^-$
SuNa	-0.7 [a]	$Su^- + Na^+ = SuNa$
SuK	-1.0 [b]	$Su^- + K^+ = SuK$
Su_2Ca	0.104 [b]	$2Su^- + Ca^{2+} = SuCa$
Su_2Mg	0.107 [b]	$2Su^- + Mg^{2+} = SuMg$
Su_2Sr	0.104 [b]	$2Su^- + Sr^{2+} = SuSr$

[a] Taken from Appelo & Wersin (2007) and references cited therein.
[b] Adapted values which produce a similar cation loading to a pure cation-exchange model (Glaus et al. 2021).

The equilibrium porewater compositions from Tab. 2-4 have been reproduced in GEMS calculations for further MPDL calculations and comparisons with PHREEQC results for the same locations and porewaters. However, instead of the model with free charge species on planar surfaces as in PHREEQC calculations, the ClaySor non-electrostatic binding model for ion exchange has been used as such, without introducing the uncompensated permanent-charge exchange site species.

Synthetic porewater (SPW) compositions were checked in PHREEQC and trial GEMS calculations against measured pH, Eh and equilibria with calcite, dolomite (and gypsum depending on the location). In GEM-Selektor trial runs, 1,000 kg of SPW and 1 g of illite were used in the respective systems to obtain equilibrium compositions of illite ion exchange. These were then normalised per 1 g (dry) illite. Illite edges were excluded from calculations at this stage. X-species (ion exchange) was tried and then excluded from GEMS calculations.

Comparison of ClaySorDif with PHREEQC results for the same porewater compositions and $\frac{\varepsilon_{tot}}{G}$ profiles (see Section 3.6) has been used for adjustment of the FCC (free charge density) parameter in the ClaySorDif model to achieve the best match for both experimental and modelling data. The comparison results are provided and discussed in Section 3.6 below.

3 Results

3.1 Look-up tables for clay rock and bentonite

The LUTs generated for clay rocks using the ClaySorDif code are structured using the total clay content of rock (W_c) as the independent variable in the left-most column. The range of values of W_c can be intentionally set in the respective Python scripts. For the present purposes, W_c is adjusted in increments of 1% starting from 1%. Note that the validity of the model predictions is hampered at low W_c values owing to the lack of pertinent representative experimental data. However, no distinct limit can be specified beyond which the predictions can be considered questionable. Caution is recommended when using predictions for W_c values <5%. In light of the finalisation of the DDBs in early 2023 (prior to the editorial processing of this report and the publications of Van Loon et al. (2023) and Glaus et al. (2024)), the empirical geometrical functional relationships of W_c with ε_{tot} and G, as described in Eq. (2-46) and Eq. (2-47), were used instead of those shown in Eq. (2-14) and Eq. (2-15). As demonstrated in Fig. 2-9, the resulting discrepancies are only marginal.

Separate LUTs were produced for D_e[2] and ε_{acc} values. The tables comprise all dose-relevant elements in alphabetical order arranged in the topmost row from left to right. For each element, best-estimate predictions (named D_e_best for D_e and ε_{acc}_best for ε_{acc}, with the respective element name appended) are given along with lower and upper bounding limits (D_e_low, ε_{acc}_low and D_e_up, ε_{acc}_up, respectively) as a function of W_c, which is arranged vertically. Explanations for assessing these uncertainty limits are given in Section 3.5. A typical section of such a table for clay rock is shown in Tab. 3-1 and Tab. 3-2.

The basis for the calculation of geometrical properties is different for bentonite compared to that for argillaceous rocks as outlined in Section 2.2.2. The clay content of the bentonite engineered barrier is taken from the respective reference compositions, and porosities can be readily derived from the target bulk dry density according to Eq. (2-18). These porosity values are subsequently used as input for Archie's relationship in the form of Eq. (2-12). Otherwise, the same formalities of the ClaySorDif model are applied to bentonite as to argillaceous rock. Tab. 3-3 and Tab. 3-4 show the respective data representation for bentonite. The latter tables have only three entries for the clay content, which are related to the target bulk dry density and the target clay content of MX-80 bentonite (81 wt.%) and the upper and lower bounding values (71 and 91 wt.%, respectively).

[2] For simplicity, the symbol D_e is used here and in the column headings of the tables. The values actually represent the weighted effective diffusion coefficients for a given element ($D_{e,elem}$). The respective equations and calculations are explained in Section 2.3.3.

Tab. 3-1: Representative section (W_c of 40 to 65 wt.%) of the NL data entries for D_e [m^2 s^{-1}] of Cl and Cs depicting diffusion parameters for clay rock and reference NL-ZNO porewater

Further explanations are given in the text.

W_c [wt.%]	D_e_low_Cl	D_e_best_Cl	D_e_up_Cl	D_e_low_Cs	D_e_best_Cs	D_e_up_Cs
40	2.00E-12	5.18E-12	1.28E-11	2.19E-11	3.32E-11	5.38E-11
41	1.98E-12	5.02E-12	1.24E-11	2.19E-11	3.31E-11	5.34E-11
42	1.95E-12	4.86E-12	1.20E-11	2.18E-11	3.30E-11	5.29E-11
43	1.92E-12	4.70E-12	1.16E-11	2.17E-11	3.28E-11	5.24E-11
44	1.89E-12	4.53E-12	1.12E-11	2.16E-11	3.26E-11	5.18E-11
45	1.85E-12	4.36E-12	1.08E-11	2.14E-11	3.23E-11	5.12E-11
46	1.82E-12	4.19E-12	1.04E-11	2.13E-11	3.20E-11	5.05E-11
47	1.78E-12	4.02E-12	1.00E-11	2.11E-11	3.17E-11	4.98E-11
48	1.74E-12	3.91E-12	9.62E-12	2.09E-11	3.13E-11	4.91E-11
49	1.70E-12	3.81E-12	9.23E-12	2.06E-11	3.09E-11	4.83E-11
50	1.66E-12	3.70E-12	8.84E-12	2.04E-11	3.05E-11	4.76E-11
51	1.62E-12	3.59E-12	8.47E-12	2.01E-11	3.01E-11	4.68E-11
52	1.58E-12	3.48E-12	8.09E-12	1.98E-11	2.96E-11	4.60E-11
53	1.54E-12	3.37E-12	7.73E-12	1.95E-11	2.91E-11	4.51E-11
54	1.49E-12	3.27E-12	7.37E-12	1.91E-11	2.86E-11	4.43E-11
55	1.45E-12	3.16E-12	7.02E-12	1.88E-11	2.81E-11	4.34E-11
56	1.41E-12	3.06E-12	6.69E-12	1.84E-11	2.75E-11	4.25E-11
57	1.36E-12	2.95E-12	6.35E-12	1.80E-11	2.70E-11	4.16E-11
58	1.32E-12	2.85E-12	6.03E-12	1.76E-11	2.64E-11	4.07E-11
59	1.27E-12	2.75E-12	5.72E-12	1.73E-11	2.58E-11	3.99E-11
60	1.23E-12	2.65E-12	5.42E-12	1.69E-11	2.53E-11	3.89E-11
61	1.19E-12	2.55E-12	5.13E-12	1.64E-11	2.47E-11	3.80E-11
62	1.15E-12	2.45E-12	4.85E-12	1.60E-11	2.41E-11	3.71E-11
63	1.10E-12	2.36E-12	4.59E-12	1.56E-11	2.35E-11	3.62E-11
64	1.06E-12	2.27E-12	4.40E-12	1.52E-11	2.29E-11	3.53E-11
65	1.02E-12	2.18E-12	4.22E-12	1.48E-11	2.23E-11	3.44E-11

Tab. 3-2: Representative section (W_c of 40 to 65 wt.%) of the NL data entries for ε_{acc} [-] of Cl and Cs depicting diffusion parameters for clay rock and reference NL-ZNO porewater

Further explanations are given in the text.

W_c [wt.%]	$\varepsilon_{acc\_low\_Cl}$	$\varepsilon_{acc\_best\_Cl}$	$\varepsilon_{acc\_up\_Cl}$	$\varepsilon_{acc\_low\_Cs}$	$\varepsilon_{acc\_best\_Cs}$	$\varepsilon_{acc\_up\_Cs}$
40	0.02518	0.04819	0.07917	0.08179	0.11500	0.14381
41	0.02538	0.04774	0.07863	0.08293	0.11615	0.14481
42	0.02558	0.04725	0.07803	0.08404	0.11725	0.14577
43	0.02576	0.04671	0.07737	0.08512	0.11831	0.14667
44	0.02593	0.04613	0.07667	0.08617	0.11933	0.14753
45	0.02610	0.04551	0.07593	0.08719	0.12030	0.14834
46	0.02625	0.04485	0.07514	0.08819	0.12124	0.14911
47	0.02639	0.04417	0.07431	0.08916	0.12215	0.14984
48	0.02652	0.04416	0.07344	0.09011	0.12302	0.15053
49	0.02665	0.04413	0.07253	0.09103	0.12385	0.15119
50	0.02676	0.04409	0.07159	0.09193	0.12465	0.15181
51	0.02687	0.04403	0.07062	0.09281	0.12542	0.15240
52	0.02696	0.04397	0.06961	0.09366	0.12616	0.15296
53	0.02705	0.04390	0.06857	0.09449	0.12687	0.15349
54	0.02714	0.04382	0.06750	0.09530	0.12756	0.15400
55	0.02721	0.04373	0.06641	0.09608	0.12821	0.15447
56	0.02728	0.04363	0.06528	0.09685	0.12885	0.15493
57	0.02734	0.04352	0.06414	0.09760	0.12945	0.15536
58	0.02740	0.04341	0.06297	0.09833	0.13004	0.15576
59	0.02745	0.04329	0.06177	0.09903	0.13060	0.15615
60	0.02749	0.04316	0.06056	0.09972	0.13113	0.15651
61	0.02753	0.04303	0.05932	0.10040	0.13165	0.15686
62	0.02756	0.04290	0.05807	0.10105	0.13215	0.15719
63	0.02759	0.04276	0.05691	0.10169	0.13263	0.15750
64	0.02761	0.04261	0.05658	0.10231	0.13309	0.15780
65	0.02763	0.04246	0.05624	0.10292	0.13353	0.15808

Tab. 3-3: Representative section of the data entries for D_e [$m^2 s^{-1}$] of Cl and Cs depicting diffusion parameters for bentonite and bentonite reference porewater

Further explanations are given in the text.

W_c [wt.%]	D_e_low_Cl	D_e_best_Cl	D_e_up_Cl	D_e_low_Cs	D_e_best_Cs	D_e_up_Cs
71	1.89E-11	3.68E-11	6.61E-11	1.60E-10	3.12E-10	5.60E-10
81	1.78E-11	3.46E-11	6.19E-11	1.79E-10	3.49E-10	6.23E-10
91	1.69E-11	3.29E-11	5.86E-11	1.99E-10	3.85E-10	6.87E-10

Tab. 3-4: Representative section of the data entries for and ε_{acc} [-] of Cl and Cs depicting diffusion parameters for bentonite and bentonite reference porewater

Further explanations are given in the text.

W_c [wt.%]	ε_{acc}_low_Cl	ε_{acc}_best_Cl	ε_{acc}_up_Cl	ε_{acc}_low_Cs	ε_{acc}_best_Cs	ε_{acc}_up_Cs
71	0.16761	0.16761	0.16761	0.48009	0.48009	0.48009
81	0.15517	0.15517	0.15517	0.48393	0.48393	0.48393
91	0.14509	0.14509	0.14509	0.48777	0.48777	0.48777

The predictions are made for different porewater conditions. The composition of the porewaters for clay rock is taken from Kulik & Miron (2024) and for bentonite from Curti (2023). Their application for the purpose of compiling the SDB and DDB is explained in detail in (Kulik & Miron 2024, Marques Fernandes et al. 2024b), and in this report.

All predictions for the dose-relevant radionuclides are made using the procedures explained in Chapter 2, with the exception of Ac(III) and Cf(III) for which no valid thermodynamic calculation basis exists. The values for these two radionuclides were taken from the chemical analogue Cm(III) instead.

A graphical representation of the predictions of D_e values for a typical W_c value of 56 wt.% (taken as a representative value for the Opalinus Clay and clay-rich rocks) is shown in Fig. 3-1. As can be seen from the comparison of the two types of porewater, the impact of the carbonate content and the pH on the diffusion parameters is comparatively moderate. For some elements, no impact can be documented at all. The reason is that these elements are predicted to be present as uncharged elemental species. Consequently, no impact of surface diffusion or anion exclusion can be expected in these cases.

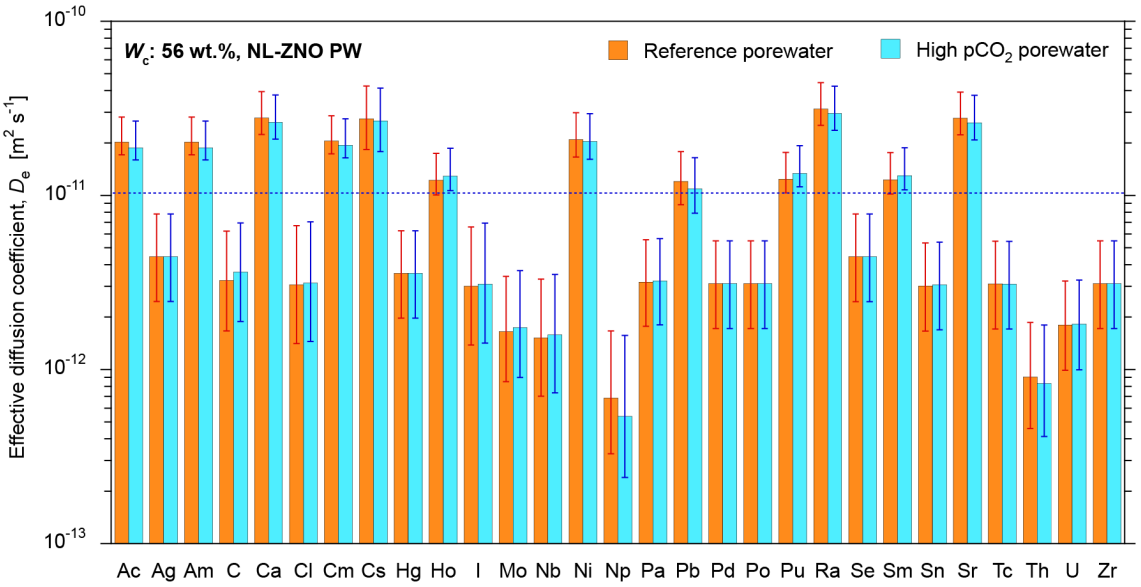

Fig. 3-1: Comparison of the prediction of D_e values for argillaceous rocks with a W_c of 56 wt.% for the NL-ZNO reference porewater (pH = 7.07, I = 0.33 mol kg^{-1}) and its high-pCO_2 variant (pH = 6.87, I = 0.34 mol kg^{-1})

The dashed line indicates the prediction for the uncharged HTO tracer to give an approximate idea of the effects of surface diffusion or anion exclusion.

The comparison with the reference value for HTO (dashed line in Fig. 3-1) does not include the different properties of the tracers with respect to their individual D_w values. Normalising the D_e values for the differences in D_w is not expedient in such a representation because the incremental contribution of each chemical species is accounted for in the element-specific overall D_e values using species-specific D_w values. Significant effects of surface diffusion can be seen predominantly for Cs^+, the alkaline earth metal cations and the trivalent lanthanides and actinides. As already mentioned before, some actinides, such as Np, Th and U, show anionic character owing to the predominance of negatively charged solution complexes with inorganic ligands, such as hydroxide, carbonate or sulphate.

A similar representation of the predictions of the ε_{acc} is shown in Fig. 3-2. The maximum ε_{acc} is attained for uncharged (such as HTO) or positively charged species. A significantly reduced ε_{acc} is observed for negatively charged species, such as inorganic carbon (mainly present as bicarbonate), the halogenides or oxyanions (such as molybdate). Similarly, the predominance of negatively charged complexes, as is the case for Np and Th, leads to a reduced ε_{acc} for the overall effect regarding the respective chemical element.

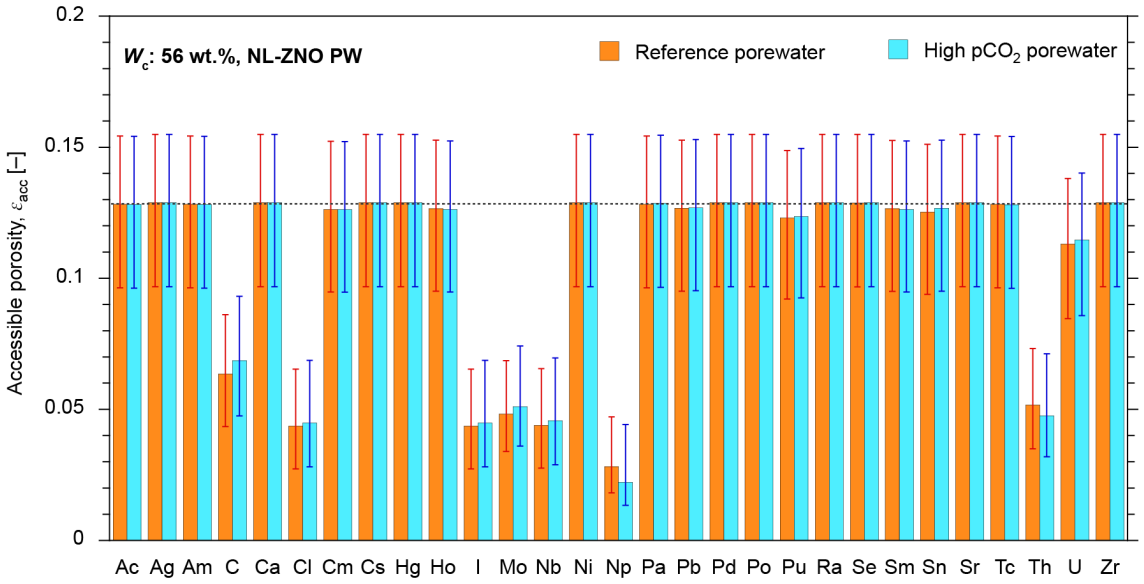

Fig. 3-2: Comparison of the prediction of ε_{acc} values for argillaceous rocks with W_c of 56 wt.% for the NL-ZNO reference porewater (pH = 7.07, I = 0.33 mol kg^{-1}) and its high-pCO_2 variant (pH = 6.87, I = 0.34 mol kg^{-1})

The dashed line indicates the prediction for the uncharged HTO tracer.

The respective D_e and ε_{acc} data for the JO siting region are shown in Fig. 3-3 and Fig. 3-4. The comparison of the data for NL-ZNO and JO shows a larger gap between typical D_e values for predominantly cationic elements and those present as anionic species. This makes sense in view of the lower ionic strength of the JO porewaters. At lower ionic strength, EDL effects are more pronounced compared to higher ionic strength. Similarly, the lowest anion-accessible porosities are found for JO. Again, the explanation for this behaviour is found in the lower ionic strength of the respective porewaters. No significant effect of the difference between the reference and the high-pCO_2 variant porewaters can be seen in either the D_e or ε_{acc} data.

The range of D_e values covered by the results shown for the NL-ZNO and JO cases is rather restricted. The highest values are in the range of a few multiples of 10^{-11} m^2 s^{-1} and the lowest a few multiples of 10^{-13} m^2 s^{-1}, corresponding to a span of approximately two orders of magnitude. Much broader spans between D_e values for cationic and anionic species were observed in experiments with compacted pure clay minerals (cf. e.g. (Glaus et al. 2010)). The reason for the restricted range of values in the present data is mainly found in the relatively high concentrations of alkali and alkaline earth metal cations in the reference porewaters. These conditions lead to a restricted range of Coulomb factors (cf. Eq. 2-20) according to the range of Ψ_D values. In particular, the presence of alkaline earth metal cations in the porewaters leads to comparatively strong competition with cationic tracer species in the Donnan layer, thus keeping the range of their D_e values relatively low.

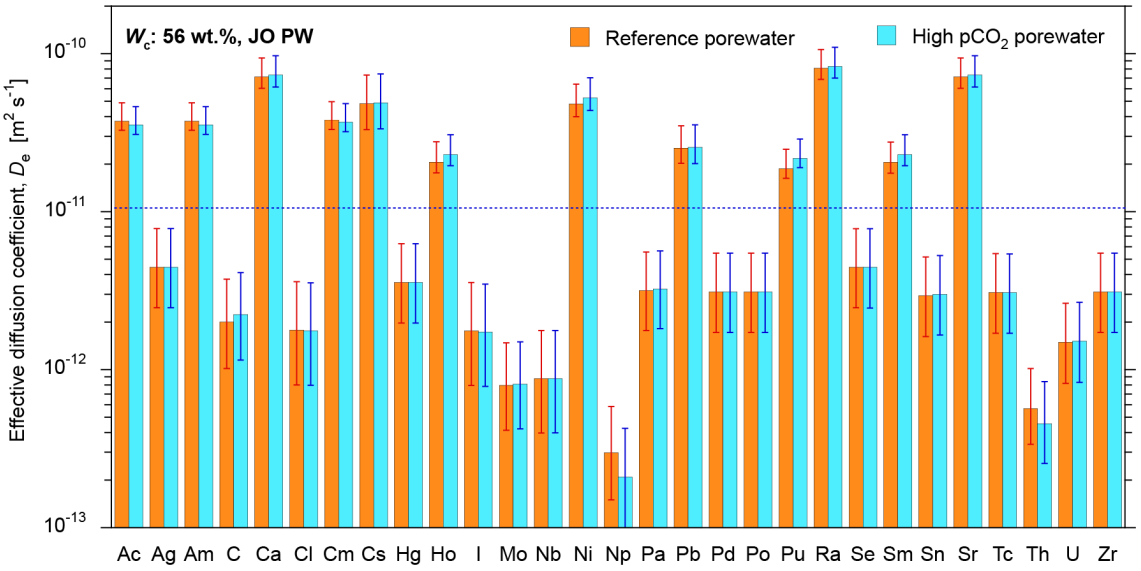

Fig. 3-3: Comparison of the prediction of D_e values for argillaceous rocks with W_c of 56 wt.% for the JO reference porewater (pH = 7.34, I = 0.168 mol kg^{-1}) and its high-pCO_2 variant (pH = 7.14, I = 0.169 mol kg^{-1})

The dashed line indicates the prediction for the uncharged HTO tracer to give an approximate idea of the effects of surface diffusion or anion exclusion.

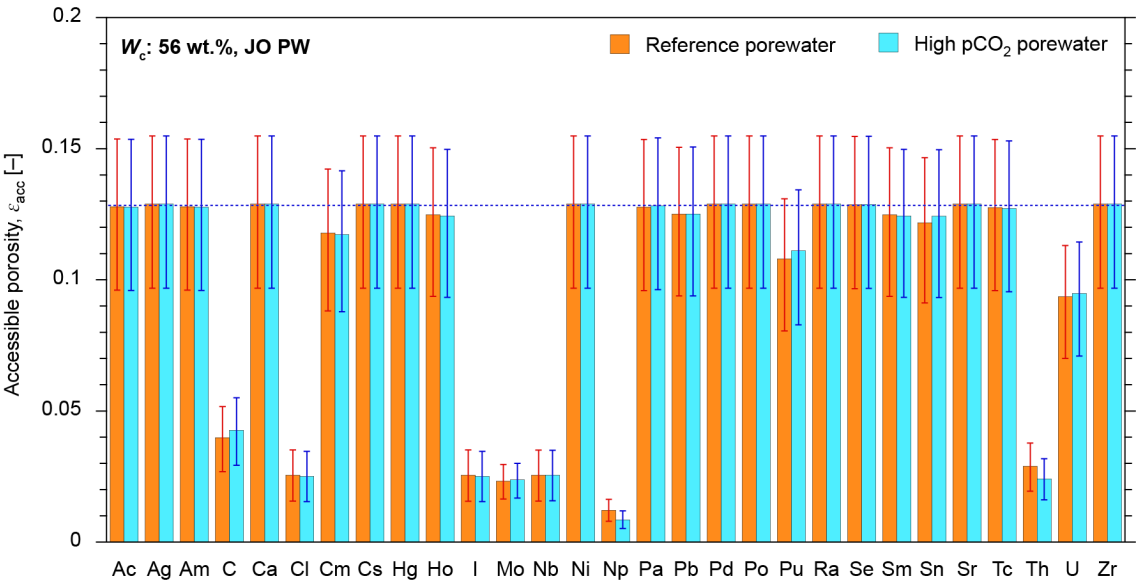

Fig. 3-4: Comparison of the prediction of ε_{acc} values for argillaceous rocks with W_c of 56 wt.% for the JO reference porewater (pH = 7.34, I = 0.168 mol kg^{-1}) and its high-pCO_2 variant (pH = 7.14, I = 0.169 mol kg^{-1})

The dashed line indicates the prediction for the uncharged HTO tracer.

Similar representative cases are shown for a W_c value of 6 wt.% in Fig. 3-5 (D_e values) and Fig. 3-6 (ε_{acc} values) for NL-ZNO and in Fig. 3-7 (D_e values) and Fig. 3-8 (ε_{acc} values) for JO. This low clay content value has been chosen for two reasons: (i) a W_c value of 6 wt.% represents a minor minimum in a binomial frequency distribution of W_c values (while the maximum is seen for 50–60 wt.%), and (ii) this value is likely at the lower edge of validity of the ClaySorDif model (Van Loon et al. 2023). The reference lines for uncharged tracers are lower for the W_c value of 6 wt.% than for the W_c value of 56 wt.% case. Note that the intrinsic uncertainties in the predictions for the W_c value of 6 wt.% are generally larger than those for 56 wt.%. However, this has not been taken into account in the calculation of the bounding values (cf. Section 3.5).

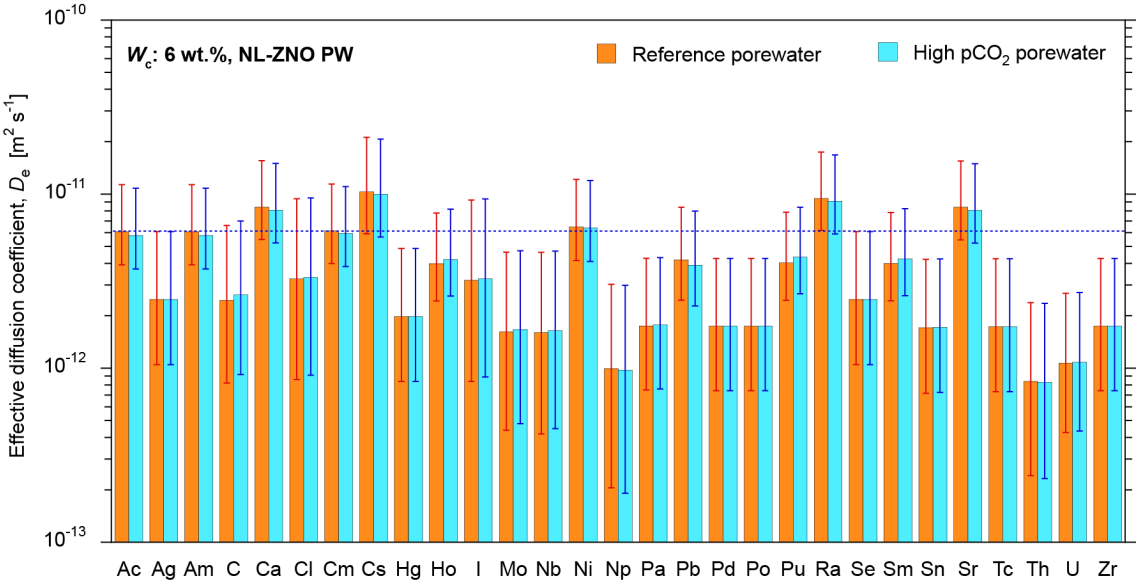

Fig. 3-5: Comparison of the prediction of D_e values for argillaceous rocks with a W_c of 6 wt.% for the NL-ZNO reference porewater (pH = 7.07, I = 0.33 mol kg^{-1}) and its high-pCO_2 variant (pH = 6.87, I = 0.34 mol kg^{-1})

The dashed line indicates the prediction for the uncharged HTO tracer to give an approximate idea of the effects of surface diffusion or anion exclusion.

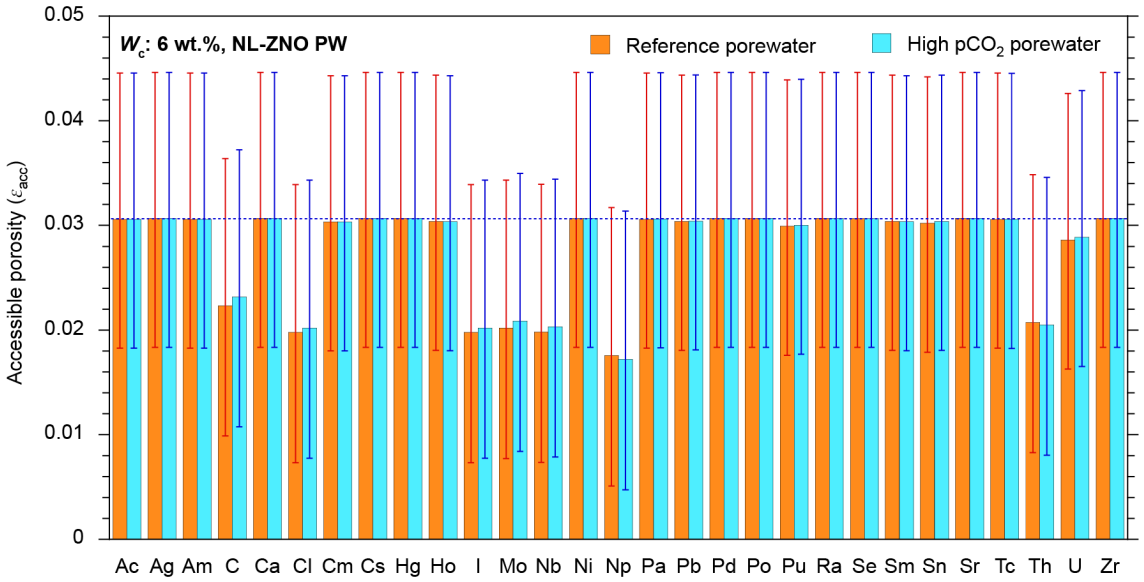

Fig. 3-6: Comparison of the prediction of ε_{acc} values for argillaceous rocks with a W_c of 6 wt.% for the NL-ZNO reference porewater (pH =7.07, I = 0.33 mol kg^{-1}) and its high-pCO_2 variant (pH = 6.87, I = 0.34 mol kg^{-1})

The dashed line indicates the prediction for the uncharged HTO tracer.

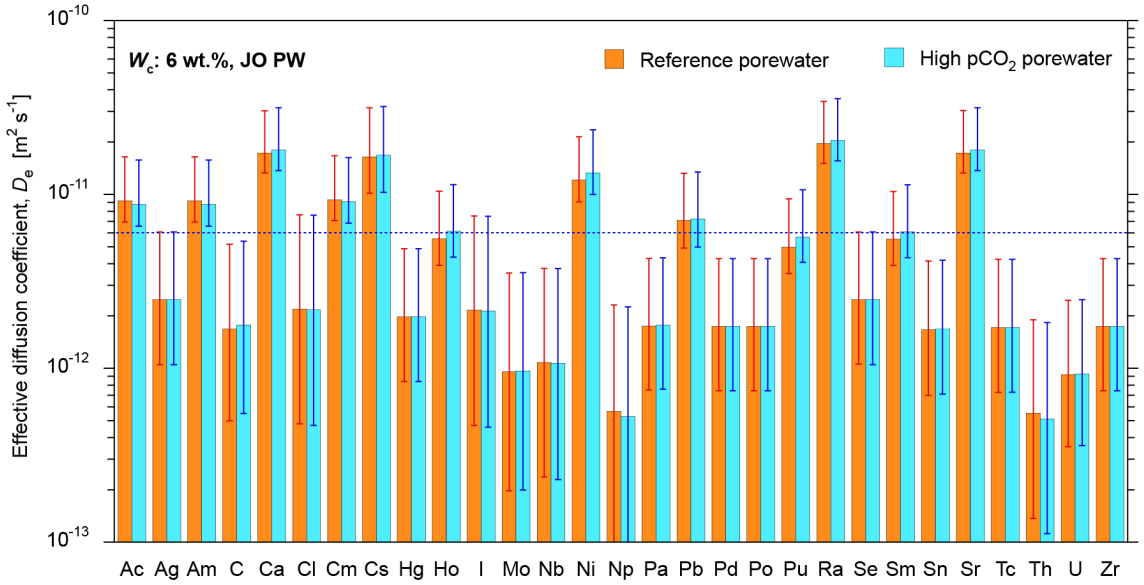

Fig. 3-7: Comparison of the prediction of D_e values for argillaceous rocks with a W_c of 6 wt.% for the JO reference porewater (pH = 7.34, I = 0.168 mol kg^{-1}) and its high-pCO_2 variant (pH = 7.14, I = 0.169 mol kg^{-1})

The dashed line indicates the prediction for the uncharged HTO tracer to give an approximate idea of the effects of surface diffusion or anion exclusion.

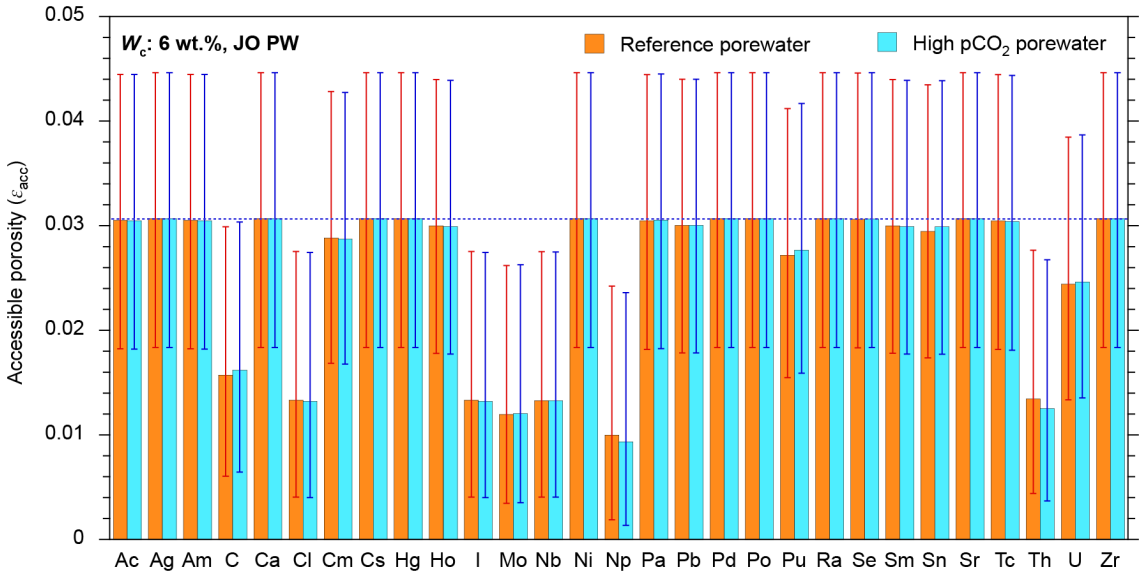

Fig. 3-8: Comparison of the prediction of ε_{acc} values for argillaceous rocks with a W_c of 6 wt.% for the JO reference porewater (pH = 7.34, I = 0.168 mol kg^{-1}) and its high-pCO$_2$ variant (pH = 7.14, I = 0.169 mol kg^{-1})

The dashed line indicates the prediction for the uncharged HTO tracer.

Fig. 3-9 and Fig. 3-10 show the predicted D_e and ε_{acc} values for the bentonite reference case in which a bulk dry density of 1,450 kg m^{-3} is assumed (Curti 2023).

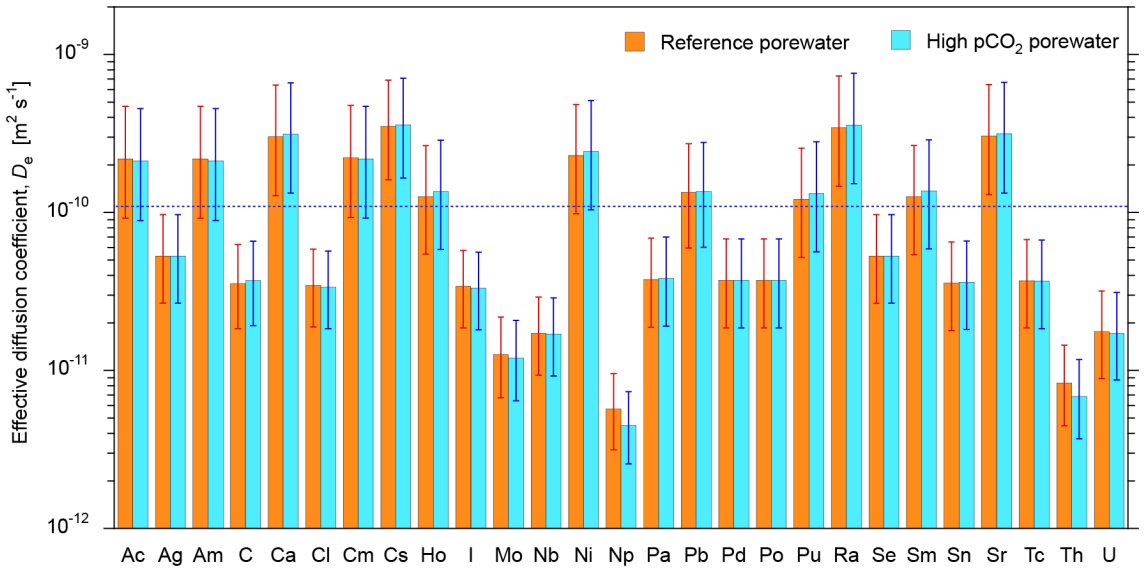

Fig. 3-9: Comparison of the prediction of D_e values for bentonite compacted to the reference bulk dry density of 1,450 kg m^{-3} and bentonite reference porewater (pH = 7.41, I = 0.586 mol kg^{-1}) and its high-pCO$_2$ variant (pH = 7.12, I = 0.578 mol kg^{-1})

The dashed line indicates the prediction for the uncharged HTO tracer to give an approximate idea of the effects of surface diffusion or anion exclusion.

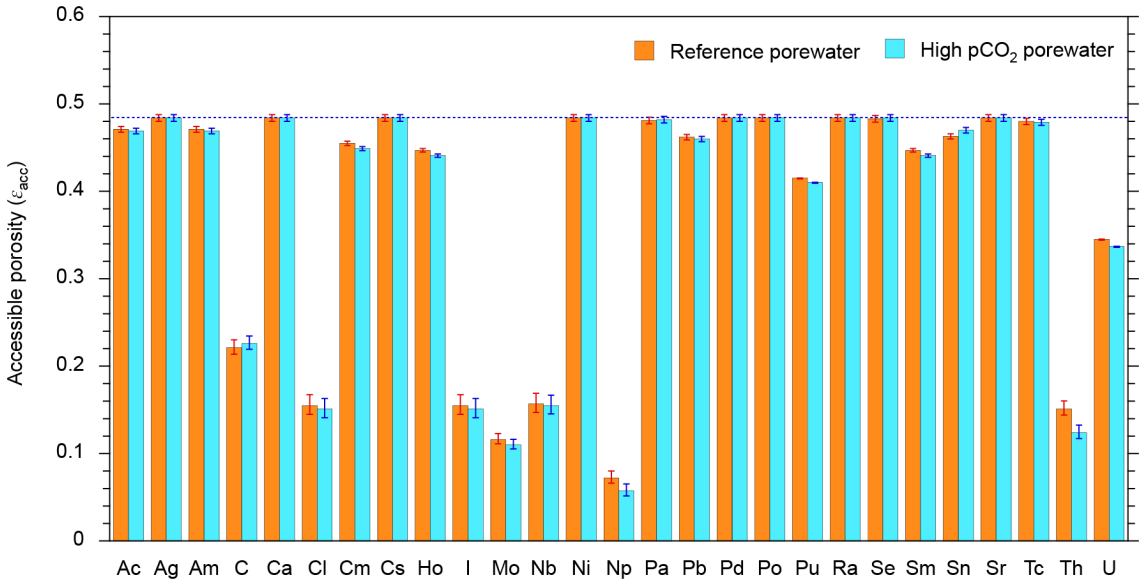

Fig. 3-10: Comparison of the prediction of ε_{acc} values for bentonite compacted to the reference bulk dry density of 1,450 kg m^{-3} and bentonite reference porewater (pH = 7.41, I = 0.586 mol kg^{-1}) and its high-pCO_2 variant (pH = 7.12, I = 0.578 mol kg^{-1})

The dashed line indicates the prediction for the uncharged HTO tracer.

3.2 Effect of temperature on diffusion parameters

The same assumptions as in Van Loon (2014) regarding the temperature dependence of diffusion in the form of the Arrhenius equation are made for both clay rock and bentonite in the present report. In Van Loon et al. (2024), the activation energy for diffusion in porewater of highly compacted clay ($E_{a,wc}$) was assumed to be 22.7 ±2.2 kJ mol^{-1}. The experimental results of the PSI measurements were obtained at 26.7 ± 0.8 °C (Van Loon et al. 2023). For the sake of simplicity, it is assumed here that the values tabulated in Sections 3.1 and 3.2 are valid for a temperature of 25 °C. The temperature dependence of diffusion in the EDL must be regarded as effectively unknown. For this reason, the applicability of the specified activation energy could be questioned. However, the activation energy for the diffusion of cations in bentonite bound by a cation-exchange mechanism (Bestel et al. 2018) does not significantly deviate from the range specified here. The activation energy of cations does not significantly deviate from that of anions (Kozaki et al. 1998a, Kozaki et al. 1998b). Only in the case of Cs^+ were higher values found for $E_{a,wc}$ by Kozaki et al. (1996). There is no obvious reason to assume that the temperature dependence in the EDL would significantly differ from the findings in bentonite in which diffusion occurs predominantly in hydrated interlayers at high degrees of compaction (Glaus et al. 2017). For all these reasons, the same value of $E_{a,wc}$ and the same ranges of uncertainty are recommended here as in Van Loon (2014). Currently, experiments addressing the temperature dependence of Co^{2+} in compacted illite and in Opalinus Clay are ongoing to corroborate the validity of the assumptions made here.

3.3 Effect of clay particle orientation on diffusion parameters

An extensive discussion of the effect of particle orientation on diffusion parameters and the pertinent literature references can be found in Van Loon et al. (2003), Van Loon et al. (2004) and Van Loon (2014). Substantial progress in the understanding of this phenomenon has since been

achieved for pure clay minerals by a research group at the University of Poitiers in France (Asaad et al. 2021, Ferrage et al. 2023). Based on these findings, it can be assumed that diffusion in clay rocks is strongly influenced by the orientation of the clay platelets or, in other words, by so-called anisotropy effects, while diffusion in bentonite only exhibits rather small anisotropy effects owing to the house-of-cards structure of the smectite platelets in compacted bentonite.

For clay rocks, the prediction of anisotropy effects largely relies on empirical knowledge. In agreement with the report by Van Loon (2014), it is recommended here to assume anisotropy factors of four to six, which relate to diffusion coefficients parallel to the bedding and diffusion coefficients perpendicular to the bedding. It is important to note that the D_e values presented in Section 3.1 are derived from measurements for diffusion perpendicular to the bedding. No measurements are available for diffusion parallel to the bedding (Van Loon et al. 2023). Dedicated experiments for this purpose are currently ongoing.

As outlined in the discussion of literature results from other countries in Van Loon (2014), anisotropy factors can differ from the recommended range for sediments with different palaeogeological history. Furthermore, the degree of particle orientation can also differ for rock material with different types of cementation (Van Loon et al. 2023). It is thus reasonable to assume that the effect of particle orientation on diffusion parameters is partly addressed by the empirical relationships used to predict G factors (Eq. (2-14)). Consequently, the application of the recommended anisotropy factors rather overpredicts the real values for parts of the rock formations other than the Opalinus Clay. In this respect, the proposed methodology is comparatively conservative, because the ranges of factors observed for the Opalinus Clay are rather in the upper range compared with other formations (Van Loon 2014).

3.4 Uncertainties of diffusion parameters and limitations of the model

The results of the LUTs are given as best-estimate values with lower and upper bounding ranges. From a statistical point of view, the true parameter values with a given probability (commonly set at a 95% confidence level) lie within the ranges delimited by the bounding values. The bounding values can basically be determined using error propagation or statistical sampling methods. The former case is applied if the result can be represented by an analytical expression, whereas the latter is the preferred procedure if this prerequisite cannot be fulfilled. Neither approach is fully realised for the present case. The algorithms used to calculate D_e values involve iterative procedures (approximation of Ψ_D), for which error propagation methods cannot be applied. It would be beyond the scope of feasibility to apply statistical sampling methods for the evaluation of the experimental diffusion data, as was done for sorption data (Marinich et al. 2024), because the evaluation procedures for these data, in turn, rely on numerical methods (e.g. solving the diffusion equation using Comsol Multiphysics®).

In view of this situation, a pragmatic solution had to be applied here. Arbitrary sensitivity tests showed that the uncertainties involved in the evaluation of the diffusion parameters of an uncharged tracer (cf. Sections 2.2.1 and 2.2.2) are rather dominant compared to other sources of uncertainty like the uncertainties of the underlying thermodynamic equilibrium data. Furthermore, the methods for the evaluation of uncertainties related to the diffusion parameters of an uncharged tracer are based on established statistical procedures (i.e. minimisation of error functions and statistically representative numbers of experimental data allowing for confidence limits to be set). For these reasons, it was decided to use these uncertainties (cf. Tab. 2-1 for clay rock and information and Section 2.2.2 for bentonite) as the basis for estimating the uncertainties of the diffusion data presented in the LUTs.

It is, however, crucial to be aware that the applicability of the "geometrical model" (Van Loon et al. 2023) to uncharged tracers is itself limited to the sedimentary structures used for the calibration of the model. It is certainly best applied on clay-rich rocks, and data also indicate that its validity

is also given for other types of comparatively carbonate-rich and siliciclastic sedimentary formations. However, the applicability may be severely hampered in the cases of rocks with different sedimentary, thermal or diagenetic history (e.g. evaporites or formations without a clear Füchtbauer classification, such as dolomites). Preliminary results of ongoing experiments (not shown) with anhydrite-dominated rock types indicate rather erratic diffusion behaviour for HTO, $^{22}Na^{+}$ and $^{36}Cl^{-}$ in terms of the ClaySorDif model predictions. Also, the comparison of the model predictions with experimental data based on different rock types from those evaluated within the framework of the deep borehole campaign in Northern Switzerland (cf. following Chapter 4) reveals the limitations of applicability.

This arbitrary choice of uncertainty estimation leads to limitations of the predictions which must be specified explicitly. Among these, the most important ones are:

- The predictions of diffusion data for elements for which no experimental data are available involve the same uncertainties as those of the uncharged HTO tracer. The discussion in Van Loon et al. (2023) and Glaus et al. (2024) shows that the scatter of the experimental HTO data is mainly caused by the incomplete knowledge of the variability of geometrical properties (pore network orientation, pore connectivity) within the entire sedimentary rock sequence. It is reasonable to assume that this uncertainty also propagates to other elements. It is an inherent assumption of the model that the *G* factors are identical for all aqueous solutes. However, this could be an inadequate assumption for, e.g., negatively charged species.
- It is not fully clear whether the "geometrical" uncertainties are larger than the uncertainties related to thermodynamic properties (aqueous and surface speciation, DL distribution, surface mobility (q_η) of unknown elements). Rather, the opposite could be the case.
- The Donnan approach chosen for the ClaySorDif model is based on a homogenised (average or mean-field) calculation of pore diameter and DL thickness, which certainly does not fully comply with the reality of the complex pore structures of sedimentary rocks. The resulting uncertainties are <u>not</u> included in the variability of the uncharged HTO tracer and in the related uncertainty bands. They are expected to be expressed in the variability of diffusion data for the charged $^{22}Na^{+}$ and $^{36}Cl^{-}$ tracers. Uncertainty analysis (Glaus et al. 2024) has demonstrated that the dominant sources of uncertainty of these data are indeed found in "geometrical" properties rather than in "chemical" properties. Whether such a conclusion based on diffusion data of $^{22}Na^{+}$ and $^{36}Cl^{-}$ tracers can be transferred to ionic species of other elements cannot be comprehensively explored. However, there is selective evidence restricted to clay-rich rocks for the feasibility of such a conclusion, see Glaus et al. (2021) and Van Loon et al. (2025), for example. For rock types with a low clay content, there is no valid basis for such a conclusion.

The chemical equilibrium distribution between the DL and the free aqueous phase is based on the choice of a best-estimate value for FCC calibrated on experimental data measured at "room temperature" (mostly between ~20 and ~28 °C). The functional dependence of FCC on temperature is completely unexplored. Extrapolation of diffusion data to *in-situ* temperatures of rocks is solely based on an Arrhenius-type relationship (cf. Section 3.3). Uncertainties related to such effects are also not included in the uncertainties specified for the look-up tables. In this sense, the ongoing activities in international projects to extend the applicability of thermodynamic data related to surface-controlled processes (sorption, solid-solution formation, etc.) to different ranges of temperature and pressure compared to those under typical laboratory conditions should also include the data related to surface diffusion of counter-ionic species and exclusion of co-ionic species in charged media such as clay and cement minerals.

Finally, it should be noted that the parametrisation of the ClaySorDif model is valid for Volclay KWK bentonite. It has been shown elsewhere (Delavernhe et al. 2025 *in prep.*) that this bentonite shows somewhat different diffusion behaviour to other reference bentonites (e.g. Calcigel, Bavaria, Germany, or Cabo de Gata, Almería, Spain). If the ClaySorDif model is to be applied to different types of bentonites in the future, the model might need to be re-calibrated.

3.5 Comparison between ClaySorDif and PHREEQC calculations

The implementation in ClaySorDif of the MPDL model is described in Section 2.3, the implementation in PHREEQC in Glaus et al. (2024). For the comparison, the same synthetic porewater systems were applied in both codes, and calculations of porewater equilibria were checked using the same thermodynamic database and input porewater compositions. The PHREEQC results for a range of clay contents from 1% to 99% were collected into CSV files, along with the ClaySorDif results. A Python code and a Jupyter notebook were written to read these CSV files along with the experimental data (also provided in CSV files), plot them together, and export the plots into PNG or PDF graphical files.

MPDL models in PHREEQC and in ClaySorDif differ in the implementation of ion-exchange and in the treatment of clay charge acting on the DL. The former uses the "free" planar-site charge species as part of the balance defined by the CEC to provide the DL charge, the density of which can be set by adjusting the cation-binding reaction constants (see Tab. 2-5). The latter uses the charge-neutral site-binding cation-exchange model from the ClaySor model, with the CBC parameter set equal to the CEC as given in ClaySor; the illite permanent charge density acting on the DL is defined by an adjustable FCC parameter for illite, which is treated independently of CBC or CEC.

Keeping in mind these differences between Donnan model implementations before any comparison or verification, a calibration was performed using the experimental data and the PHREEQC results for $D_{\mathrm{e,HTO}}$, $D_{\mathrm{e,Cl}}$, $D_{\mathrm{e,Na}}$ for each of the four boreholes concerned. The calibration consisted of calculating the ClaySorDif curves for these properties while adjusting the FCC parameter in the range of $0.1 < \mathrm{FCC} < 0.225$ eq (kg illite)$^{-1}$ (upper bound = CEC of illite in the ClaySor model) until a perfect match with the PHREEQC curve was achieved. This process for datasets from each of the four cases (BUL, TRU, STA, BOZ) has led to an adjusted FCC of 0.17 ± 0.01 eq (kg illite)$^{-1}$, i.e. practically identical for all four cases in the three siting regions. This value appears reasonable, comprising 76% of the CEC = 0.225 eq (kg illite)$^{-1}$ used in ClaySor for illite ion-exchange; in turn, this is similar to the fraction of Su- species relative to CEC in PHREEQC calculations.

The graphical comparison of ClaySorDif and PHREEQC calculations obtained at the verification stage can be seen in Fig. 3-11 to Fig. 3-13. Starting with $D_{\mathrm{e,HTO}}$, the match is (almost) perfect in all cases, and describes the experimental data well. ClaySorDif provides the same quality of fit for experimental α_{Cl} (anion-accessible porosity) values as the PHREEQC model, but a significantly better fit (without any additional adjustment) for experimental α_{Na} rock-capacity factor values than those provided by the PHREEQC model. As explained in Glaus et al. (2024), the α_{Na} factors were systematically overestimated by the PHREEQC model, likely due to an unsuitable choice of selectivity coefficients for the cation-exchange reactions between Na^+, K^+, Ca^{2+} and Mg^{2+}, which were then used as the basis to derive the formation constants of Stern-layer surface complexes. It was indeed found that the α_{Na} factors were in some disagreement with the cation loading derived from the cation composition obtained after replacing all cations with Cs^+ (Marques Fernandes et al. 2024c). In this context, it must also be noted that the *in-situ* cation occupancy of the clay-rock samples reflects the composition of the *in-situ* equilibrium porewater, whereas a synthetic porewater was used for the diffusion experiments. For this reason, some ambiguity about the α_{Na} values will always remain.

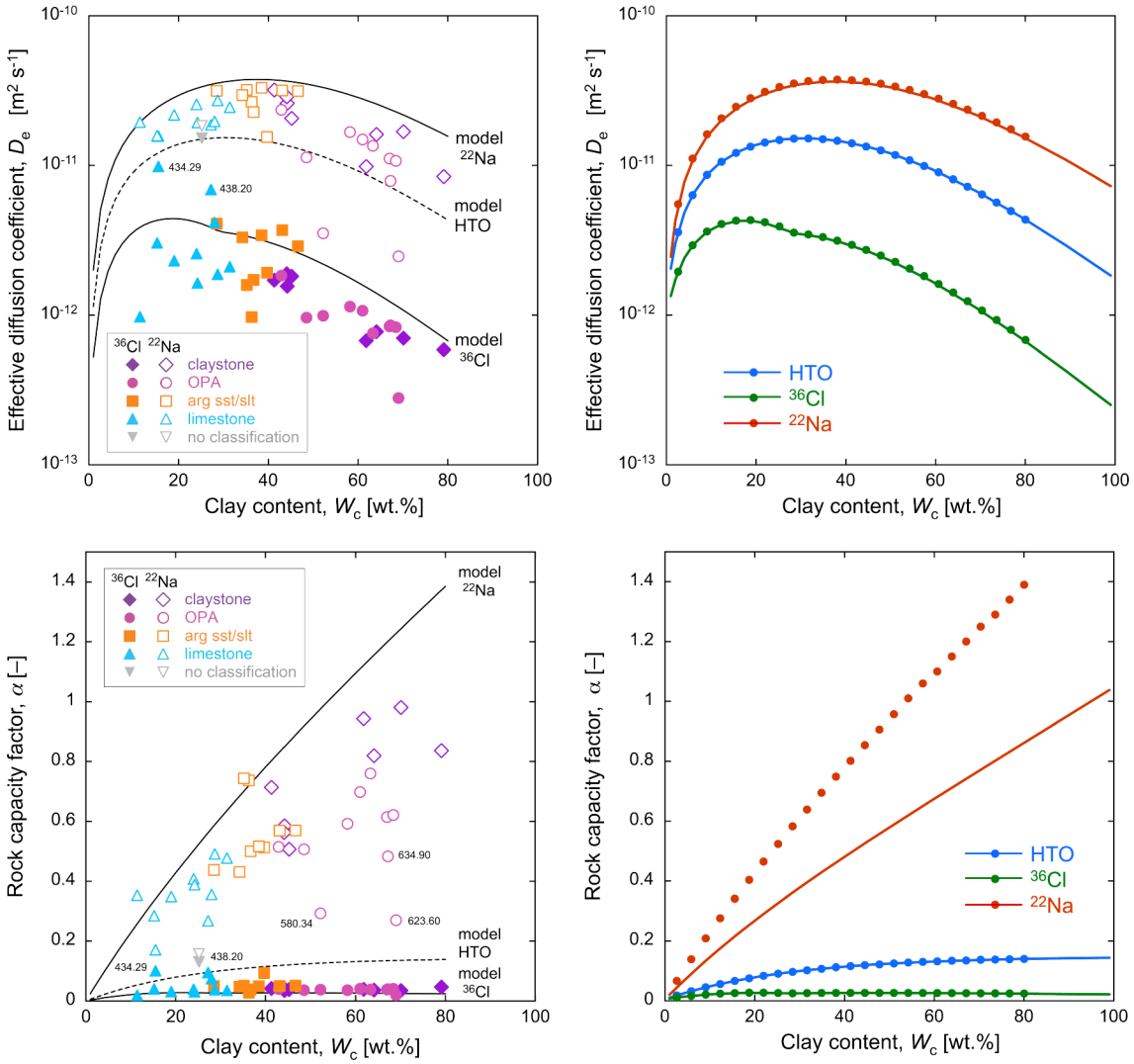

Fig. 3-11: Comparison between the experimental data and the EDL simulations involving samples from the JO siting region (Bözberg boreholes; BOZ 1-1 and BOZ 2-1) using SPW-BOZ data

The left-hand plots show the experimental data along with the simulations obtained by PHREEQC (plots taken from Glaus et al. (2024)) and the right-hand plots compare the PHREEQC modelling results (dots) with those obtained from ClaySorDif (lines). Note that α equals the ε_{AN} for the $^{36}Cl^-$ tracer (Eq. (2-45)); R_d values can be derived from α in the case of the $^{22}Na^+$ tracer according to Eq. (1-4).

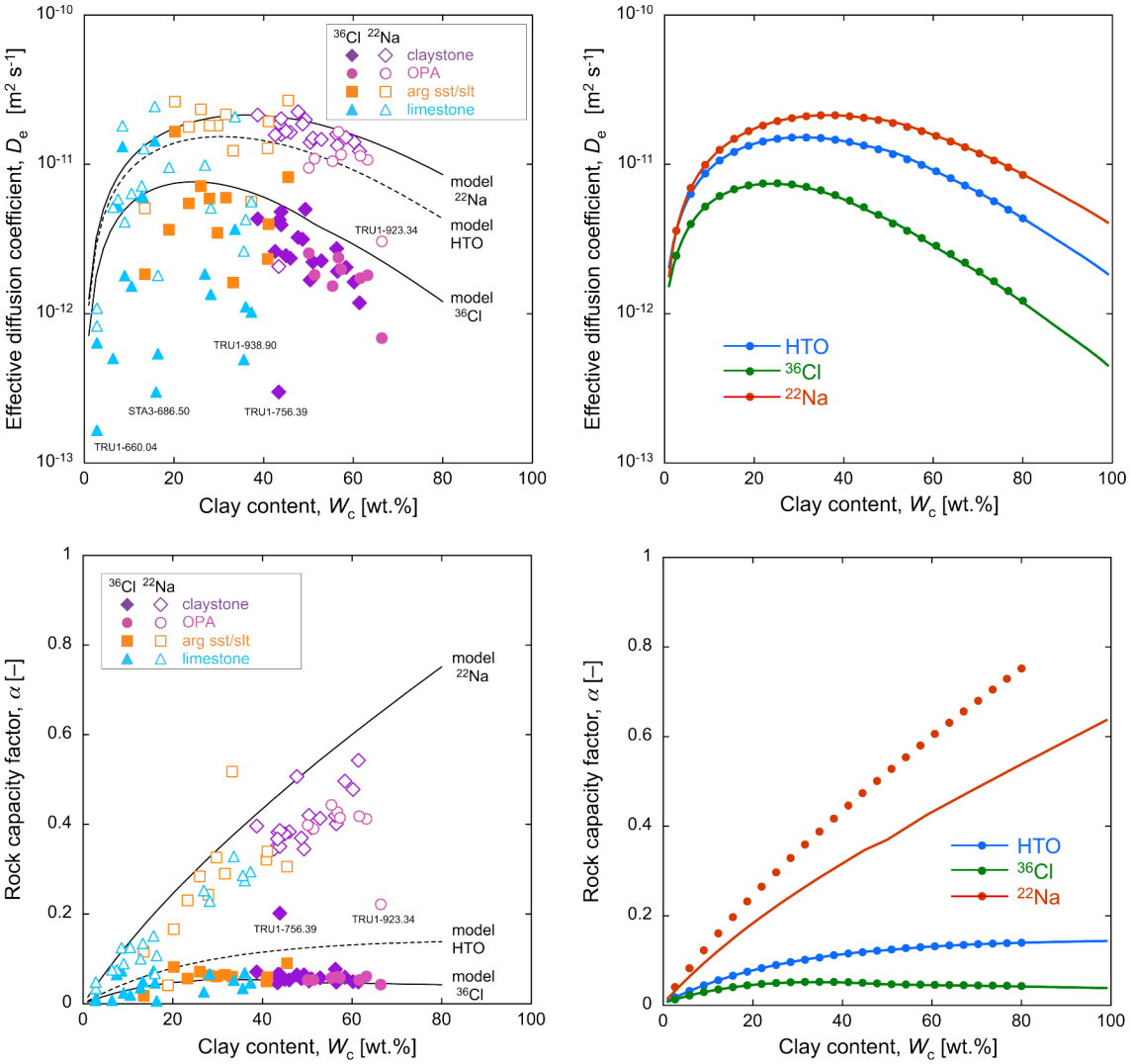

Fig. 3-12: Comparison between the experimental data and the EDL simulations involving samples from the NL (Stadel boreholes; STA2-1 and STA 3-1) and ZNO siting regions (Trüllikon and Marthalen boreholes; TRU 1-1 and MAR 1-1) using SPW-STA and SPW-TRU data, respectively

The left-hand plots show the experimental data along with the simulations obtained by PHREEQC (plots taken from Glaus et al. (2024)) and the right-hand plots compare the PHREEQC modelling results (dots) with those obtained by ClaySorDif (lines). Note that α equals the ε_{AN} for the $^{36}Cl^-$ tracer (Eq. (2-45); R_d values can be derived from α in the case of the $^{22}Na^+$ tracer according to Eq. (1-4).

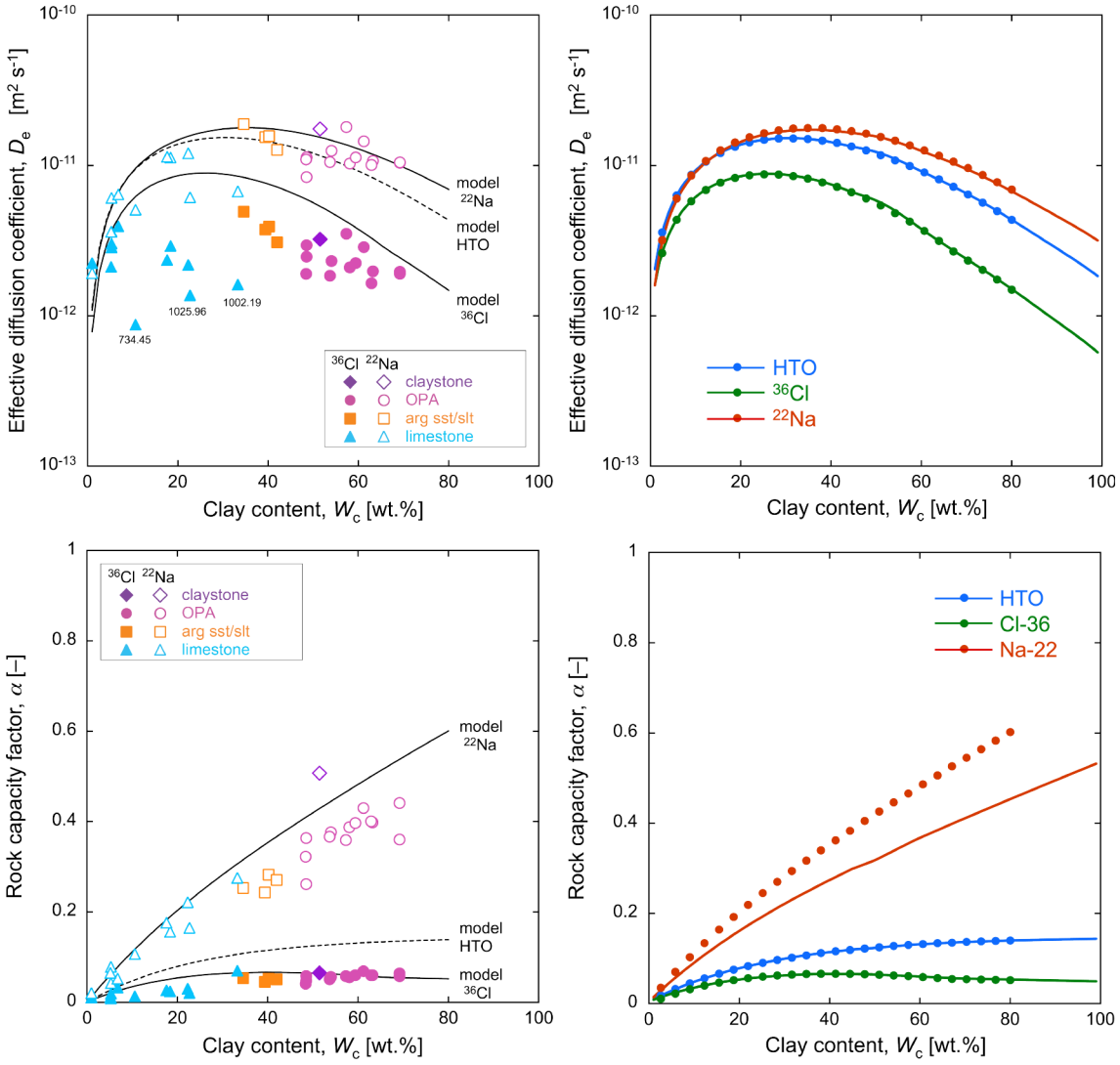

Fig. 3-13: Comparison between the experimental data and the EDL simulations involving samples from the NL siting region (Bülach borehole; BUL 1-1) using SPW-BUL data

The left-hand plots show the experimental data along with the simulations obtained by PHREEQC (plots taken from Glaus et al. (2024)) and the right-hand plots compare the PHREEQC modelling results (dots) with those obtained by ClaySorDif (lines). Note that α equals the ε_{AN} for the $^{36}Cl^-$ tracer (Eq. (2-45)); R_d values can be derived from α in the case of the $^{22}Na^+$ tracer according to Eq. (1-4).

Verification of the ClaySorDif performance for the calculation of D_e in bentonite was possible, albeit with less detail than that for the clay rock (see above). No established PHREEQC diffusion model for bentonite or montmorillonite is available so far, therefore no direct comparison between GEMS and PHREEQC calculations for bentonite could be performed. However, a limited comparison was possible between the calculated D_e values for HTO, Cl, S, Na, Sr and Cs (from ClaySorDif) and the experimental data on compacted Volclay KWK bentonite at dry densities between 1,300 kg m^{-3} and 1,900 kg m^{-3} (Glaus et al. 2017). This bentonite contains ca. 70 wt.% smectite (assumed to be montmorillonite), with a CEC of between 0.76 eq kg^{-1} and 1.2 eq kg^{-1} and a total porosity of ~0.54 (at 1,300 kg m^{-3}) or ~0.32 (at 1,900 kg m^{-3}) (Van Loon et al. 2007). The composition of bentonite porewater used in experiments, taken from Tab. 1 in Van Loon & Glaus (2008), was reproduced well in scoping GEMS calculations using the ClaySor model (Marinich et al. 2024), yielding a pH of 8.0, an ionic strength of 0.28 M to 0.30 M, and a log(pCO_2) of approximately -3.4. The redox potential was controlled by the pyrite-magnetite buffer. The CEC in this system was determined to be 0.822 eq kg^{-1} bentonite by extraction with 0.5 M $CsNO_3$ (Van Loon & Glaus (2008), Tab. 2). At 70% montmorillonite in bentonite, this leads to CEC = 1.174 eq kg^{-1} for montmorillonite. Note that in the ClaySor model, a much lower CBC = CEC = 0.8 eq kg^{-1} is used for montmorillonite in sorption R_d calculations. These differences between measured CEC values and those used in sorption models only underscore the advantage of using FCC as a separate adjustable parameter for the MPDL model calculations of D_e values, as it allows the CEC (CBC) parameter to be consistently used in a sorption model of choice for R_d calculations.

As in the case of clay rock, the calibration of the ClaySorDif model for bentonite mainly consisted of varying the FCC parameter for montmorillonite and checking how well the calculated elemental D_e values described the experimentally measured ones. The upper limit of FCC variation was set to the maximum known value of the CEC (1.3 eq kg^{-1}), with the lower limit at 0.65 eq kg^{-1} (one half of the maximum CEC). GEMS ClaySorDif scoping calculations revealed that adjustment of the FCC parameter moderately affects the calculated D_e values for Cl, S, Na, Sr and Cs values, although the scarce experimental D_e data do not allow the precise fitting of all mentioned elements when considered simultaneously. Rather, there is a broad range of FCC values from 0.8 eq kg^{-1} to 1.3 eq kg^{-1} where the computed D_e values are not too different from the experimental ones. The best overall fit is achieved at FCC = 1.05 eq kg^{-1}, a value in the middle of the above interval. At a dry density of 1,300 kg m^{-3}, this FCC value leads to reproduction of experimental values within 10% for Na, Sr and S (sulphate), 15% for Cs and 25% for Cl. At a dry density of 1,600 kg m^{-3}, the same FCC value results in deviations within 10% for Sr and Cs, 20% for Na, 50% for Cl and 180% for S (sulphate). These different deviations at different dry densities demonstrate that more experimental diffusion data for bentonites are still needed to obtain more statistically relevant fits of the FCC parameter of montmorillonite.

Based on these considerations, the FCC of 1.05 ± 0.25 eq kg^{-1} for montmorillonite is set as a provisional value for bentonites. This value has been used in ClaySorDif calculations of diffusion properties for MX-80 bentonite in bentonite porewaters, such as those presented in Fig. 3-9 and Fig. 3-10.

A relatively broad range of feasible FCC values should not be a surprise, considering the significant variability of CEC values measured in experiments of different duration and porewater composition (Herbert et al. 2008).

3.6 Influence of aqueous speciation on the calculation of weighted diffusion parameters: a comparison between ClaySorDif and PHREEQC calculations

The ClaySorDif model provides full access to the equilibrium speciation in both "free" porewater (i.e. model porewater) and in Donnan layer porewater at a given clay content. Along with the D_wDB database of bulk diffusion coefficients for ca. 60 elements (compiled as part of the ClaySorDif development), this allows the effect of speciation to be plotted and analysed in detail. This is only indirectly possible in PHREEQC. The default output data of PHREEQC only comprise the "total element concentration" in the Donnan layer. The concentration of individual species can, however, be assessed using the Coulomb factor in Eq. (2-20). It has been verified in various cases that the sum of species in the Donnan layer calculated in this way is in perfect agreement with the values specified for "total element concentration" in the output file.

The following examples show how the presence of species with different charge numbers affects the effective diffusion parameters. Speciation in porewater layers can be directly extracted from the ClaySorDif output. The respective D_e value for the element, calculated using Eq. (2-32) or Eq. (2-33), is then compared with the respective output from PHREEQC calculations. As examples, Fig. 3-14 to Fig. 3-16 show the results for sodium, sulphur and strontium for the SPW in the BOZ case, as calculated by the ClaySorDif model. The respective PHREEQC calculation results for the effective element-diffusion coefficient ("Dee") are also shown in these plots.

In the case of sodium, almost no difference between the "Dee" and the dominant effective ion-diffusion coefficient ("Dei") can be seen (Fig. 3-14, blue versus green curves). This is explained by the fact that the aqueous speciation fraction of the Na^+ cation is >99%, whereas the contributions of the $NaSO_4^-$ complex and the uncharged NaOH ion pair are almost negligible.

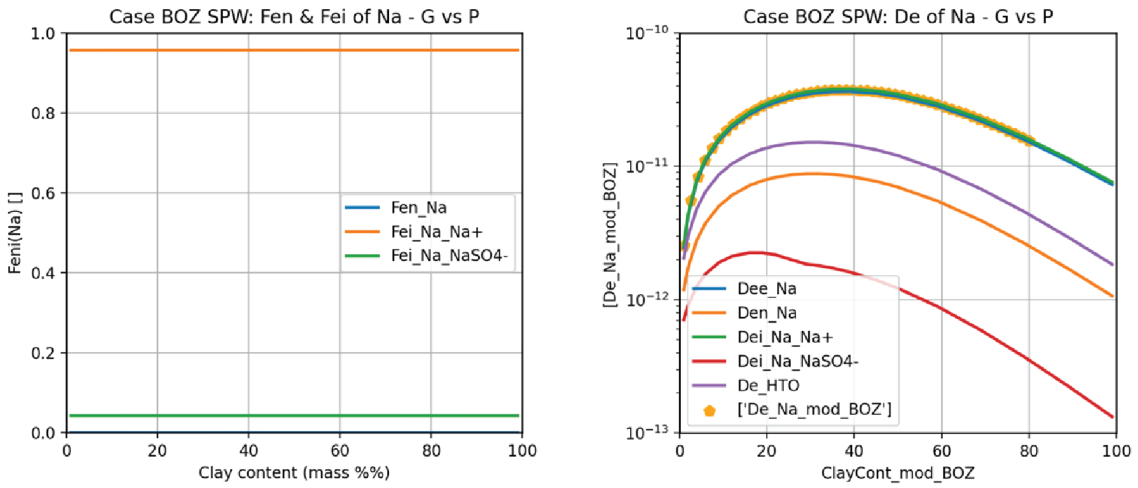

Fig. 3-14: Contributions of neutral (Fen_) and charged (Fei_) speciation fractions in porewater (left-hand plot) to the effective element-diffusion coefficient (Dee_Na) of sodium (right-hand plot) for the SPW conditions in BOZ 1-1 and BOZ 2-1 as function of clay content

In these ClaySorDif images, the abscissa is W_c (in wt.%); the ordinate on the left-hand plot is the aqueous speciation fraction; the ordinate on the right-hand plot is the effective diffusion coefficient [m^2 s^{-1}]; the orange hexagons show the results for Dee from the respective PHREEQC calculations; the smooth curves originate from the ClaySorDif model. The "De_HTO" curve for the D_e of water is shown as a guidance. Blue and green curves overlap.

In the case of sulphur (Fig. 3-15), the porewater speciation is largely dominated by the divalent SO_4^{2-} anion (~75%). The remaining part is predominantly made up of neutral complexes of SO_4^{2-} with Ca^{2+} and Mg^{2+} and, to a much lower extent, of the anionic $NaSO_4^-$ complex. The presence of such complexes is the reason why the effective element-diffusion coefficient of sulphur does not scale proportionally with the square of the double negative charge of SO_4^{2-} compared to the effective diffusion coefficient of chloride, for example.

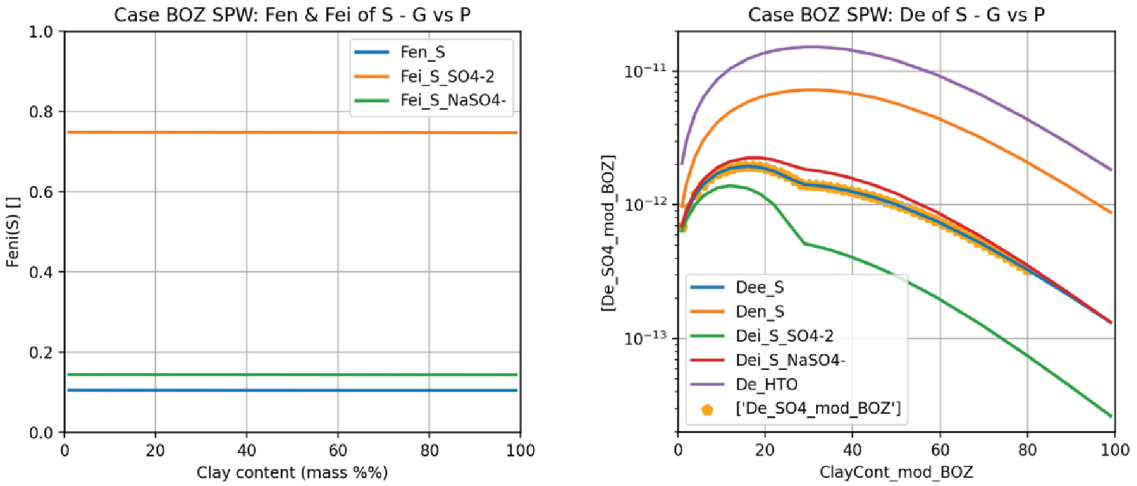

Fig. 3-15: Contributions of neutral (Fen_) and charged (Fei_) speciation fractions in porewater (left-hand plot) to the effective element-diffusion coefficient (Dee_S) of sulphur (right-hand plot) for the SPW conditions in the BOZ boreholes as function of clay content

In these ClaySorDif images, the abscissa is W_c (in wt.%); the ordinate on the left-hand plot is the aqueous speciation fraction; the ordinate on the right-hand plot is the effective diffusion coefficient [m^2 s^{-1}]; the orange hexagons show the results for Dee from the respective PHREEQC calculations; the smooth curves originate from the ClaySorDif model. The "De_HTO" curve for the D_e of water is shown as a guidance.

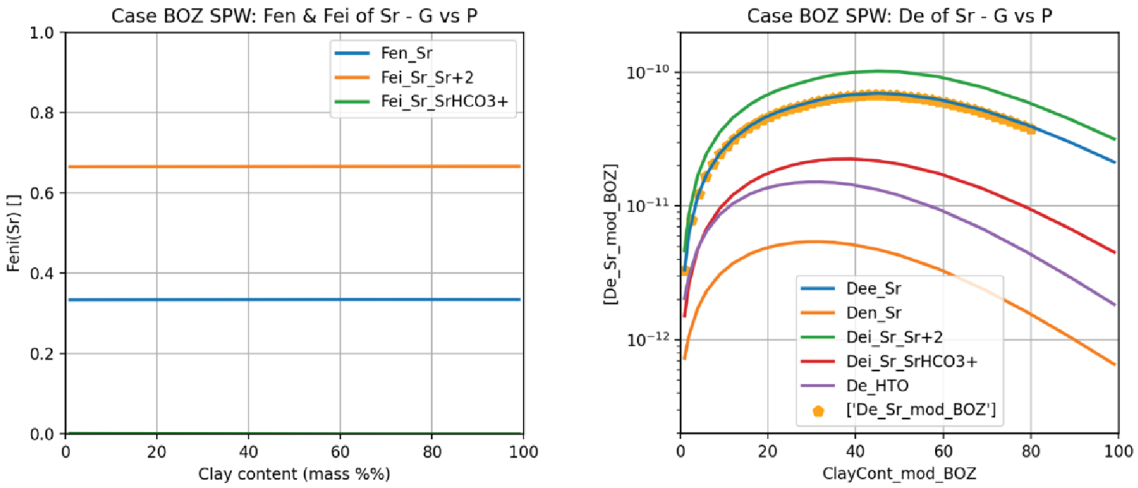

Fig. 3-16: Contributions of neutral (Fen_) and charged (Fei_) speciation fractions in porewater (left-hand plot) to the effective element-diffusion coefficient (Dee_Sr) of strontium (right-hand plot) for the SPW conditions in the BOZ boreholes as function of clay content

In these ClaySorDif images, the abscissa is W_c (in wt.%); the ordinate on the left-hand plot is the aqueous speciation fraction; the ordinate on the right-hand plot is the effective diffusion coefficient [m^2 s^{-1}]; the orange hexagons show the results for Dee from the respective PHREEQC calculations; the smooth curves originate from the ClaySorDif model. The "De_HTO" curve for the D_e of water is shown as a guidance.

Fig. 3-16 shows the case of strontium. The Sr^{2+} aqua ion dominates the speciation of charged species, while the contribution of $SrHCO_3^+$ is almost negligible (<1%). However, there is a significant contribution from neutral species dominated by the $SrSO_4$ complex with a minor (<1%) fraction of the $SrCO_3$ complex. Similar to the case of sulphur, the contribution of these neutral complexes explains why there is no direct correlation of effective element-diffusion coefficients between sodium and strontium simply based on the different charge numbers of the aqua ions. Rather, the effective element-diffusion coefficient of strontium is closer to that of sodium than would be predicted by the charge numbers.

To fully demonstrate the comparability of ClaySorDif and PHREEQC calculations in terms of species contribution, Fig. 3-17 shows the species contributions to the element-specific effective diffusion coefficient of strontium as calculated by PHREEQC (shown as dashed lines in order to be clear that these curves are not identical with the solid lines computed in ClaySorDif in Fig. 3-16). Note that the comparison between ClaySorDif and PHREEQC in Figs. 3-14 to 3-16 is only done for the element-specific D_e, but not for the individual charged and uncharged species. The agreement (cf. Fig. 3-16) with the ClaySorDif calculations shown in Fig. 3-17 is perfect on a visual basis.

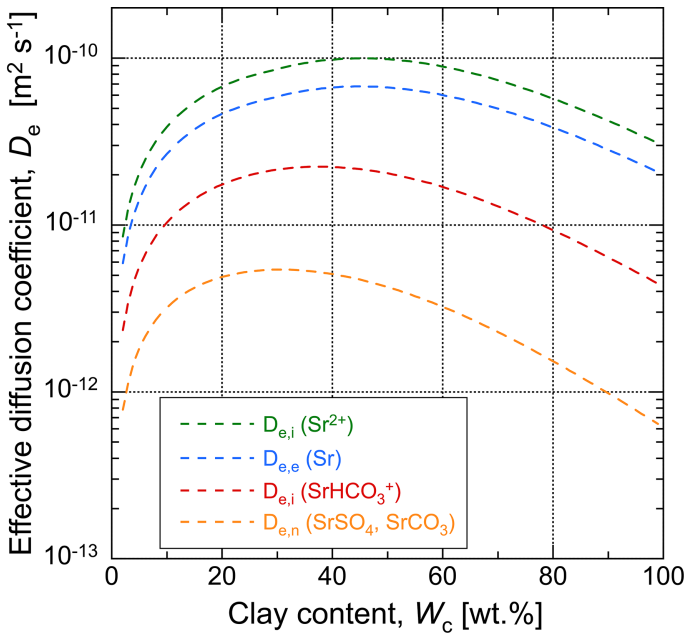

Fig. 3-17: Contributions of neutral and charged species to the effective element-diffusion coefficient ($D_{e,e}$) of strontium for the SPW conditions in the BOZ boreholes as calculated by PHREEQC (dashed curves)

4 Comparison between methods for clay rocks and bentonite in the past and in the present work

Diffusion data recommended for clay rocks and bentonite are proposed in the present report for different scenarios regarding clay content and porewater composition. The methods previously applied for the respective calculations for SGT-E2 are extended here by the use of an electrostatic model to calculate effective diffusion coefficients and accessible porosities for all elements under evaluation based on aqueous speciation data. The present section summarises the most important differences in the procedures and in the data available for setting up the methods between the present compilations (referred to in the following sections as "current" procedures) and those applied in SGT-E2 (referred to as "previous" procedures).

Both procedures are based on the general experience that the effective diffusion coefficients (D_e) for anionic species are lower compared to the respective D_e values of an uncharged reference tracer (after normalisation for the respective diffusion coefficients in bulk water) owing to anion exclusion effects, while those for cationic species are larger owing to surface-diffusion effects. Similarly, both procedures assume that the total water porosity is accessible for neutral and positively charged species, while negatively charged species are partly excluded from this porosity. As a key difference, the current procedure uses the full aqueous speciation of a radionuclide under consideration as the basis for considering these effects, while in the previous procedures these were taken into account for the dominant species only. Many radionuclides are present in significant proportions as cationic and anionic aqueous species, and their behaviour can cancel each other out in these forms. For these reasons, the current approach is more comprehensive.

Despite the numerous similarities, the results obtained using the current procedures differ also in other respects from the calculation results obtained in Van Loon (2014):

- The previous calculations (Van Loon 2014) were based on the porosity of the argillaceous medium as a primary input variable. The reference D_e values for an uncharged tracer were calculated using an extended Archie's relationship. The current calculations rely on the total clay content as a primary input variable. The current calculation of the D_e value of an uncharged tracer is based on empirical relationships of porosity and the so-called geometrical factor with total clay content (cf. Section 2.2.1). These relationships were derived using an extensive series of diffusion measurements of tritiated water (HTO) in ~130 rock samples obtained from Nagra's deep borehole campaign (Mazurek et al. 2023). These measurements are much more comprehensive than the data material available for the previous study.
- A classical diffusivity-porosity relationship is, however, applied here for the case of bentonite. Bentonite has a random house-of-cards structure of clay platelets that is not comparable with the oriented clay-particle structure in consolidated sedimentary rocks. For this reason, the empirical relationships for sedimentary rocks cannot be applied to compacted bentonite. Furthermore, the clay-to-liquid mass ratio in compacted bentonite is a fixed value according to the target bulk dry density of the backfill material. The D_e value of an uncharged reference tracer is directly available from pertinent diffusion measurements. No extrapolation to unknown conditions, as is the case for sedimentary clay rock, has to be applied for bentonite.

- The calculation of the increased D_e values for cationic species in the previous calculations was based on the "Gimmi-Kosakowski" approach (Gimmi & Kosakowski 2011), involving R_d values for a single sorption site. This approach, although applicable for multi-site sorption (Gimmi & Kosakowski 2011), was restricted to cations undergoing cation-exchange with the clay surface owing to the lack of pertinent diffusion data for other elements, such as representatives of the transition metal, lanthanide or actinide series. In the past years, such data have become available and it was shown that surface-diffusion effects of these elements could be successfully described by an electrical double-layer (EDL) approach (Glaus et al. 2015, Glaus et al. 2020, Glaus et al. 2021). This approach can be regarded as a permissible simplification of more complex diffusion models, such as described in Krejci et al. (2021), and has turned out to be a valuable method for the generic derivation of diffusion data.

  The EDL approach also produces valuable diffusion data for anionic species. All diffusion estimates for anionic species in Van Loon (2014) were adjusted to those of chloride in the previous procedures, irrespective of the charge number of the species. The current EDL approach now considers such effects.

- Only two values for the diffusion coefficients in bulk water (D_w) were used for all elements in the previous procedures. In the current approach, species-specific D_w values were applied according to data obtained from literature and used by Andra (2022). In view of the rather narrow range of D_w values and the many gaps in knowledge for species-specific D_w values, the new procedure should be seen as an elaboration rather than a considerable improvement.

- The diffusivity-porosity relationship for bentonite was based on diffusion data for chloride. These data fulfilled the same extended Archie's relationship as used for neutral species for clay rock data. The assumed porosities for neutral species ($\varepsilon_{tot} = 0.36$) were rather different from the value used here because the target bulk dry density was higher (1,750 kg m^{-3}). Furthermore, the anion-accessible porosity was previously assumed to be 0.05, which may also result in systematic differences compared to the present approach.

The differences in the predictions of D_e values for the dose-relevant elements between the current and the previous procedures are illustrated in Fig. 4-1 to Fig. 4-8 for the conditions of SGT-E2, as described in Van Loon (2014) and Baeyens et al. (2014a). It is important to pay close attention to the individual sources of information. The predictions are mainly based on:

- Generic values of ε_{tot} and ε_{AN} (cf. Tables. 20 to 28 in Van Loon 2014) for the predictions according to the previous procedures.
- Composition of reference porewaters given in Baeyens et al. (2014a) for the predictions according to the previous procedures.
- Total clay contents from the reference mineralogical compositions given in Baeyens et al. (2014a) for the predictions according to the current procedures with fixed porewater conditions (see below).

As can be seen from the figures, the predictions of the two procedures are not fully equivalent. While different porewater compositions were considered in the previous approach, a single type of porewater composition is applied for the entire sedimentary rock sequence in the current approach. For the following comparison, the reference NL-ZNO porewater (cf. Section 3.1) was chosen for that purpose. It would be theoretically possible to transform the predicted values of the current approach to the conditions of the reference porewaters used in Van Loon (2014), but this would require a redefinition of the chemical systems in the GEMS software, which is a comparatively laborious task. Such adapted values would, nevertheless, remain within the specified uncertainties and, for this reason, such an exercise is omitted here. The discrepancies between the chemical conditions are shown in the figure legends.

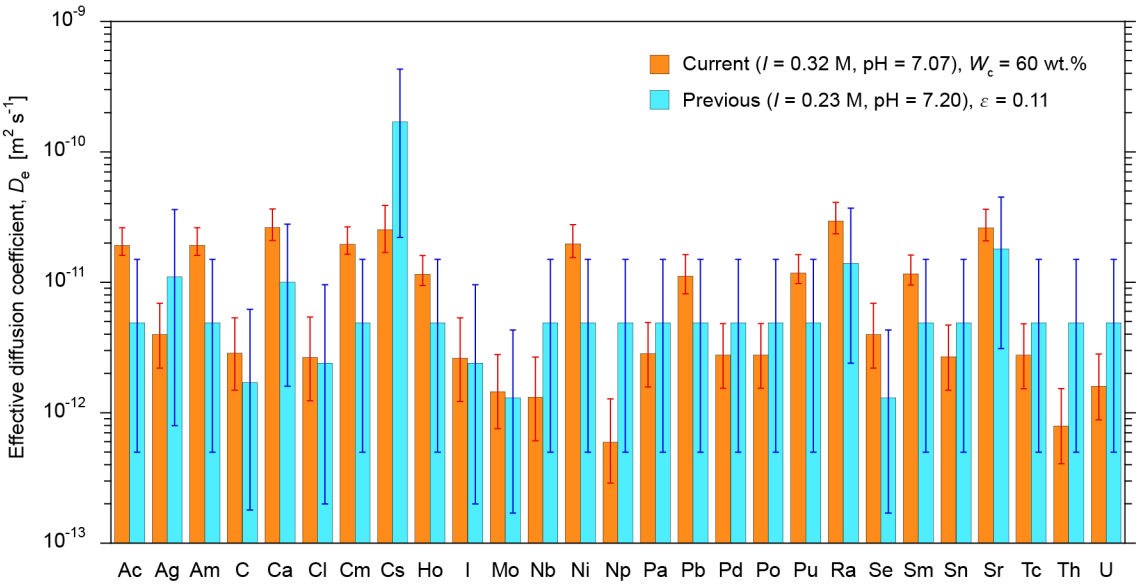

Fig. 4-1: Comparison of the prediction of D_e values for Opalinus Clay according to the previous procedures in Van Loon (2014) based on a porosity of 11% with the current predictions (ClaySorDif) for the conditions of the NL-ZNO reference porewater and a W_c of 60 wt.%

The differences in porewater composition are given in the legend.

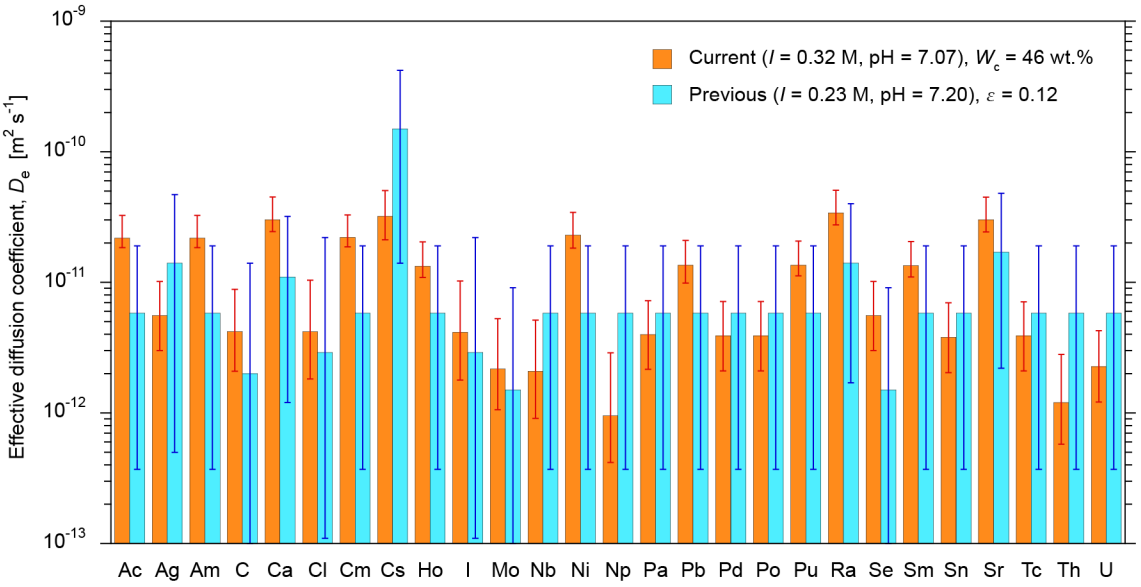

Fig. 4-2: Comparison of the prediction of D_e values for Brauner Dogger (clay-rich and sandy clay-rich sequences) according to the previous procedures in Van Loon (2014), based on a porosity of 12% with the current predictions (ClaySorDif) for the conditions of the NL-ZNO reference porewater and a W_c of 46 wt.%

The differences in porewater composition are given in the legend.

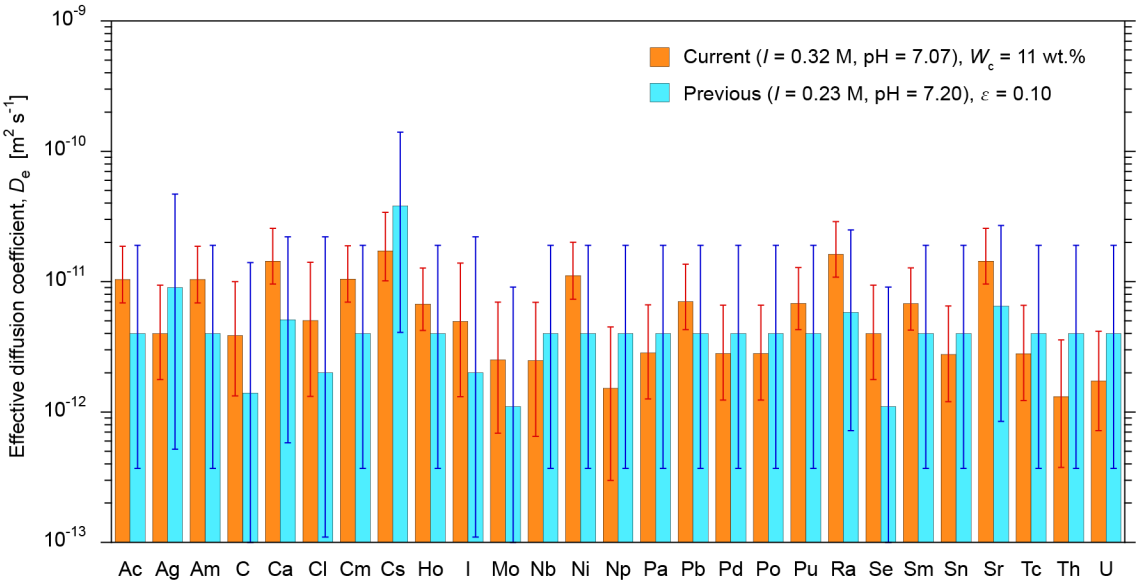

Fig. 4-3: Comparison of the prediction of D_e values for Brauner Dogger (sandy limestone sequences) according to the previous procedure in Van Loon (2014), based on a porosity of 10% with the current predictions (ClaySorDif) for the conditions of the NL-ZNO reference porewater and a W_c of 11 wt.%

The differences in porewater composition are given in the legend.

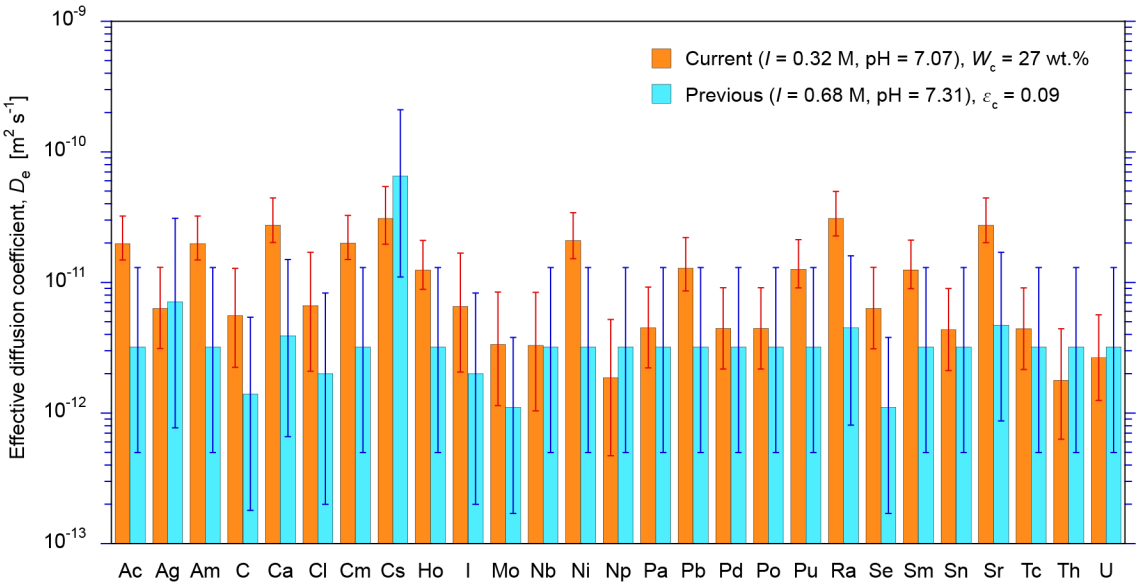

Fig. 4-4: Comparison of the prediction of D_e values for the Effingen Member (calcareous marl sequences) according to the previous procedure in Van Loon (2014), based on a porosity of 9% with the current predictions (ClaySorDif) for the conditions of the NL-ZNO reference porewater and a W_c of 27 wt.%

The differences in porewater composition are given in the legend.

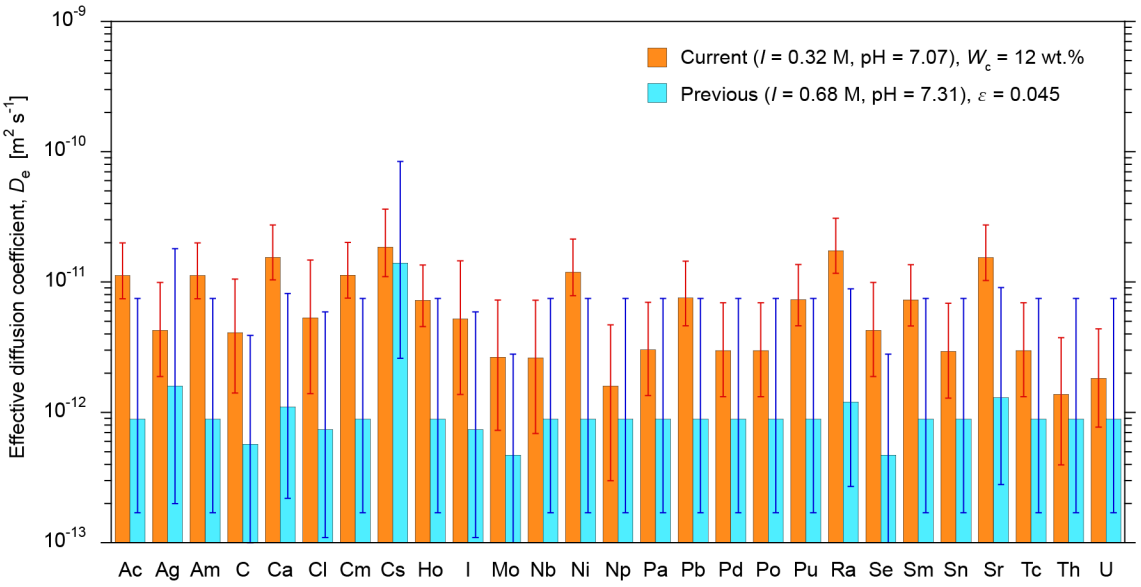

Fig. 4-5: Comparison of the prediction of D_e values for the Effingen Member (limestone sequences) according to the previous procedure in Van Loon (2014), based on a porosity of 4.5% with the current predictions (ClaySorDif) for the conditions of the NL-ZNO reference porewater and a W_c of 12 wt.%

The differences in porewater composition are given in the legend.

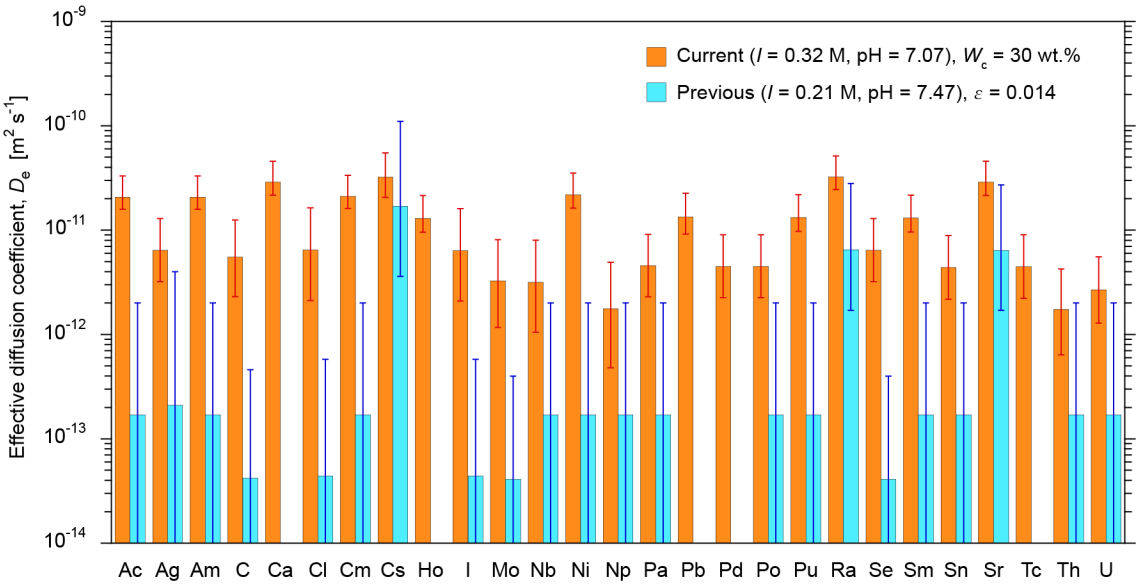

Fig. 4-6: Comparison of the prediction of D_e values for the Helvetic Marls (calcareous marls) according to the previous procedure in Van Loon (2014), based on a porosity of 1.4% with the current predictions (ClaySorDif) for the conditions of the NL-ZNO reference porewater and a W_c of 30 wt.%

The differences in porewater composition are given in the legend.

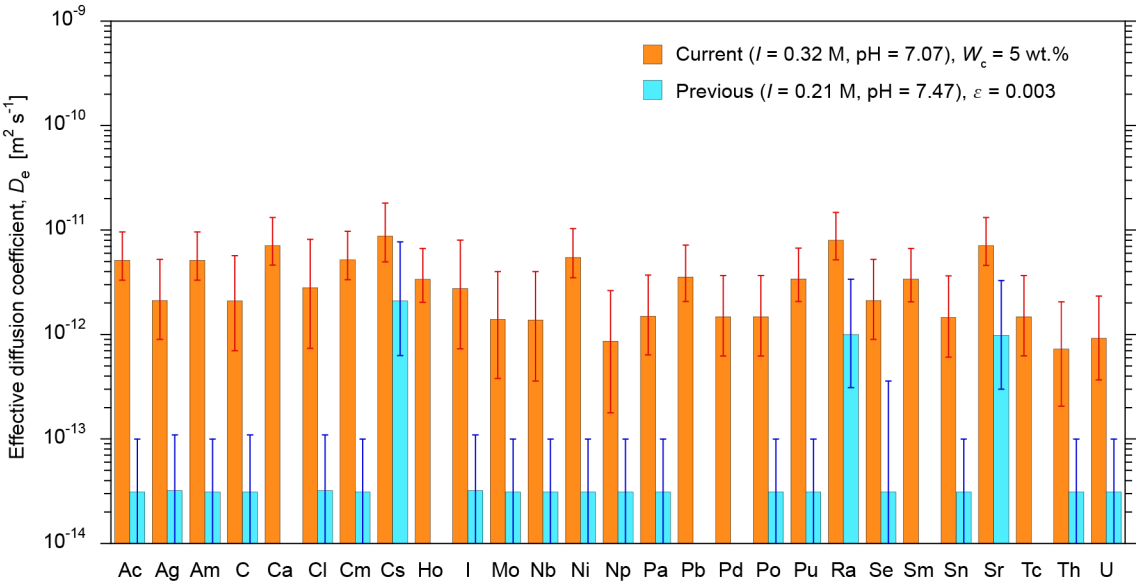

Fig. 4-7: Comparison of the prediction of D_e values for the Helvetic Marls (limestone sequences) according to the previous procedure in Van Loon (2014), based on a porosity of 0.3% with the current predictions (ClaySorDif) for the conditions of the NL-ZNO reference porewater and a W_c of 5 wt.%

The differences in porewater composition are given in the legend.

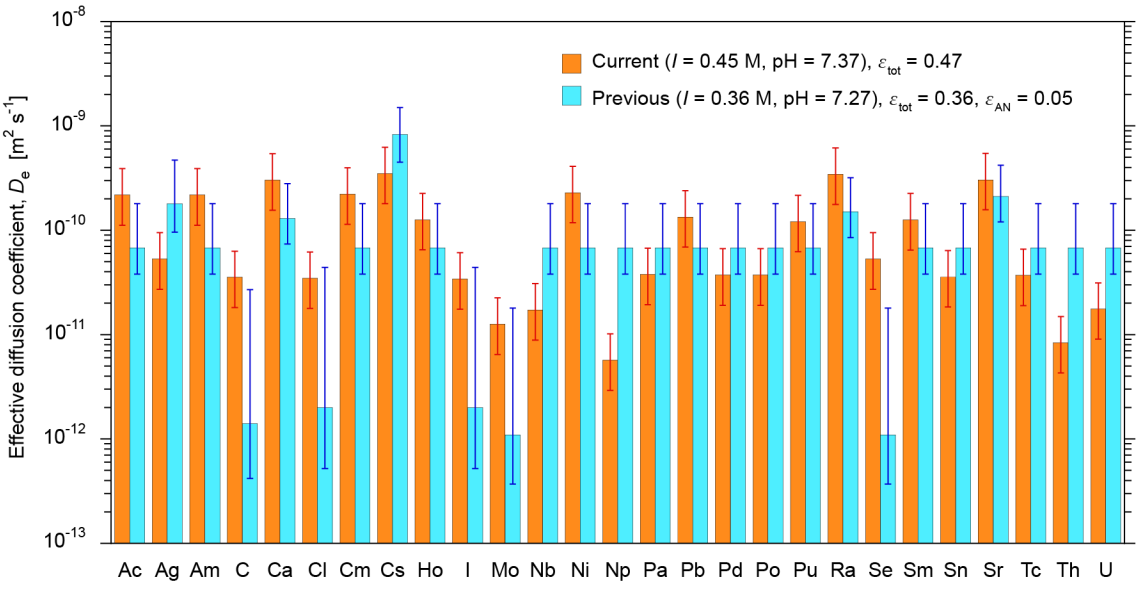

Fig. 4-8: Comparison of the prediction of D_e values for bentonite according to the previous procedure in Van Loon (2014), based on a porosity of 36% with the current predictions (ClaySorDif) for the conditions of the bentonite reference porewater and a W_c of 81 wt.%.

The differences in porewater composition are given in the legend.

In most of the cases, the two approaches result in equivalent predictions in terms of the uncertainty ranges. Obviously, these ranges are clearly larger in the previous approach compared to the current one, which demonstrates that the purpose of reducing the modelling uncertainties in the ClaySorDif model has been achieved. Some systematic differences can be identified in those cases for which no detailed electrostatic effects were considered in the previous approach. Such cases can be found, for example, in the case of the transition metals, lanthanides and bivalent anions. In the case of clay-rich sedimentary rocks, the current estimates for the elements that undergo surface diffusion tend to be somewhat larger than those made previously. The inverse observation can be made in single cases for elements that are mainly considered as anionic species in the current approach (e.g. Np), but which were considered as neutral species in the previous approach. Further differences can be noted for those elements treated as uncharged elementary species in the current approach (e.g. Ag), but which were previously treated as cations.

Large discrepancies are found only for the limestone sequences of the Effingen Member and Helvetic Marls. These discrepancies are primarily related to intrinsic differences in the prediction of the pore-diffusion properties of these elements. As can be seen from Fig. 6 in Van Loon et al. (2023), the extended Archie's relationship shows increasing discrepancies with the results obtained in the diffusion measurements on the drill core samples for low porosities. Fig. 4-9 shows the porosity to clay-content relationships for the reference cases given in Fig. 4-1 to Fig. 4-7. Most of the datasets fulfil the empirical relationship established in Van Loon et al. (2023) comparatively well. However, the data for Helvetic Marls are clearly incongruous, which largely explains the discrepancies shown in Fig. 4-6 and Fig. 4-7.

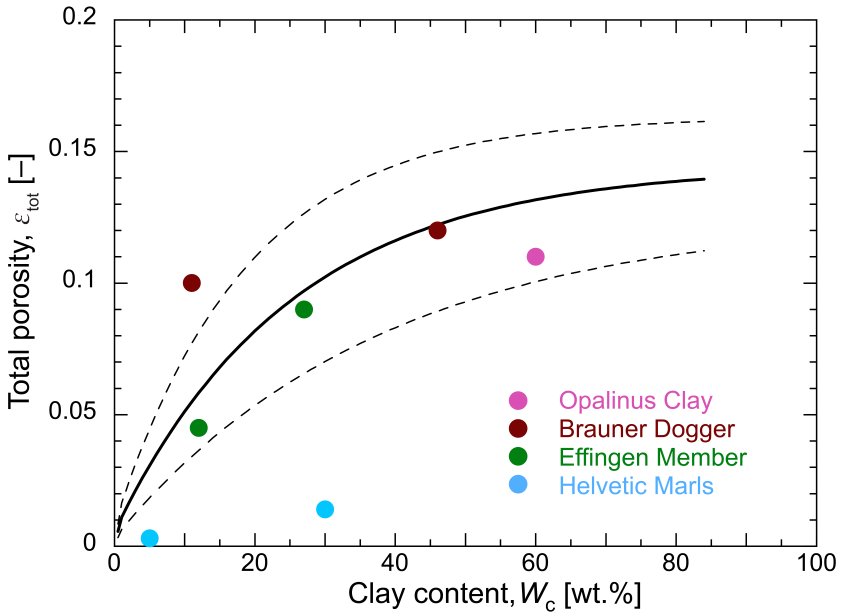

Fig. 4-9: Comparison of the clay content-porosity relationships of the basic data for Fig. 4-1 to Fig. 4-7 with the empirical model given in Eq. (2-15)

Both model predictions for the D_e values of HTO are represented in Fig. 4-10, which shows the predicted dependence on ε. For this purpose, Eq. (2-15) is solved for W_c, from which G can be calculated. With both information for ε and G, the D_e value of HTO can be calculated according to Eq. (2-16).

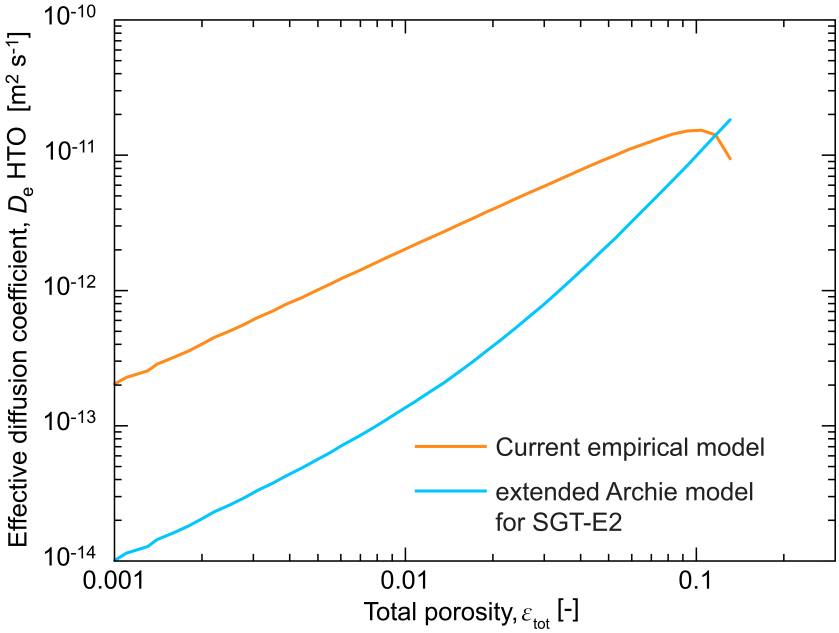

Fig. 4-10: Comparison of the previous and the current model prediction for the D_e value of the uncharged HTO

Note that the maximum value in the current model predictions strongly depends on the limiting value of porosity which is given by the a_3 parameter (cf. Tab. 2-1).

Fig. 4-10 shows that the two model predictions for the pore-diffusion behaviour are more or less equivalent at the typical porosity of clay-rich sediments (e.g. $0.05 < \varepsilon < 0.14$). However, for lower porosity values, the current predictions are clearly higher than those of the previous model. In the case of sandy limestone sequences of Brauner Dogger, this effect is partly compensated by the underprediction of porosity (Fig. 4-9), which again leads to a comparatively consistent picture for the two predictions shown in Fig. 4-3.

5 Quality control

The results produced in this work are available as LUTs containing predicted D_e and ε_{acc} values calculated for each combination of W_c value and dose-relevant radionuclide. Each value is the result of an iterative calculation implemented in rather complex programming environments. Although the structure and the use of the numerous variables in these scripts are readily traceable, it is an almost impossible task to individually check the accuracy of all the results produced therein. It is also not possible to verify the validity of results using analytical expressions, nor does it make sense to check all calculations for erratic lapses.

The most promising strategy in such a situation is to check the results with respect to plausibility. Using such an approach, errors exceeding one or several orders of magnitude can be prevented. The comparison of the results for each radionuclide with the respective predictions for the uncharged HTO tracer is probably one of the most elegant plausibility checks and has been implemented in all plots shown in Sections 3.1 and 3.2. The calculation of the D_e and ε_{acc} values for HTO is based on analytical equations (Eqs. (2-15) and (2-16) and can readily be checked using a pocket calculator or an Excel sheet. Again, it should be mentioned that a comparison of the HTO reference D_e values with those of the dose-relevant radionuclides would involve a normalisation step for the different D_w values of HTO and the respective elements. Since the D_e values for the latter are averaged over the fractional contribution of species, such a normalisation step cannot be done in a straightforward calculation. For this reason, the HTO reference values are used only for a qualitative comparison.

Another useful plausibility check can be achieved by cross-comparison of the results obtained for different porewater conditions. The following plots (Fig. 5-1 to Fig. 5-4) show the ratios of D_e and ε_{acc} values predicted for JO porewater conditions divided by those of the NL-ZNO conditions.

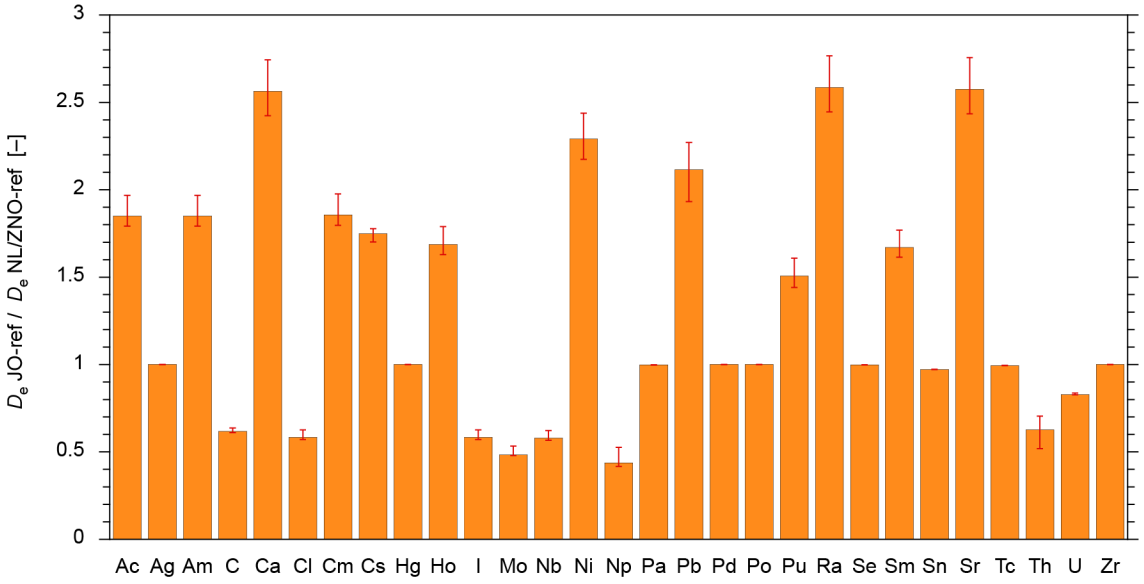

Fig. 5-1: Ratio of D_e values calculated for reference conditions of JO porewater (pH = 7.34, I = 0.168 mol kg^{-1}) and a total clay content of 56 wt.% divided by those for the NL-ZNO porewater (pH = 7.07, I = 0.33 mol kg^{-1})

The most important property of the porewater composition in this comparison is the difference in ionic strength (or more generally, in cation composition), while the differences in pH do not have a significant effect. Accordingly, ratios of $D_e > 1$ are expected for those elements that are predominantly present in cationic form, and ratios of $D_e < 1$ for those predominantly present in anionic form. In contrast, the ratio of D_e values of those elements that are expected to be neutral species is exactly 1. This expectation is perfectly reflected by the data shown in Fig. 5-1. Similar expectations can be made for ε_{acc}. The elements present in neutral or cationic form exhibit a ratio of 1 because they are accessible to the entire porosity. Only those elements present as anionic species exhibit ratios other than 1. As the accessibility is less at low ionic strength compared to high ionic strength, the ratios are <1. Again, this expectation is supported by the data shown in Fig. 5-2.

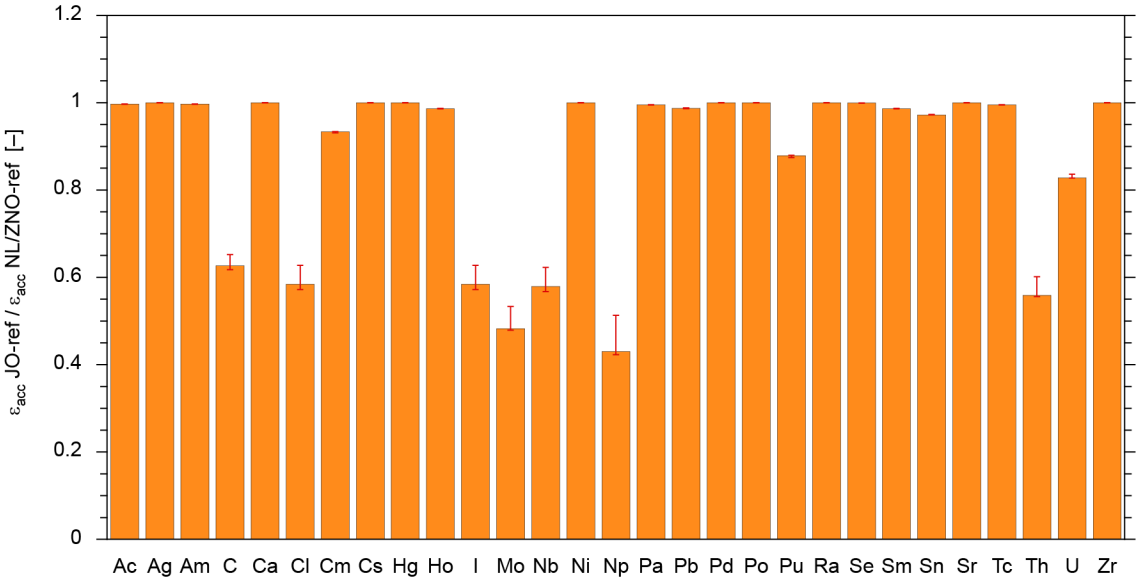

Fig. 5-2: Ratio of ε_{acc} values calculated for reference conditions of JO porewater (pH = 7.34, I = 0.168 mol kg^{-1}) and a total clay content of 56 wt.% divided by those for the NL-ZNO porewater (pH = 7.07, I = 0.33 mol kg^{-1})

The respective plots for the high-pCO_2 variants of the reference porewaters are shown in Fig. 5-3 and Fig. 5-4. As can be expected, no significant differences exist between these plots and those shown for the reference porewaters.

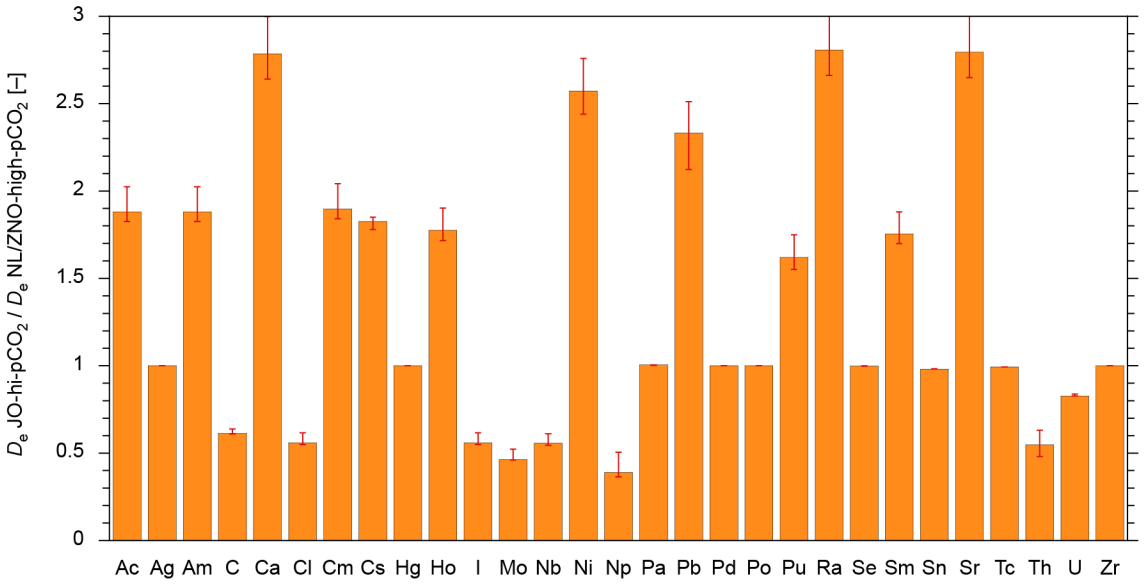

Fig. 5-3: Ratio of D_e values calculated for the high-pCO$_2$ variant of JO porewater (pH = 7.14, I = 0.169 mol kg^{-1}) and a total clay content of 56 wt.% divided by those for the high-pCO$_2$ NL-ZNO porewater (pH = 6.87, I = 0.34 mol kg^{-1})

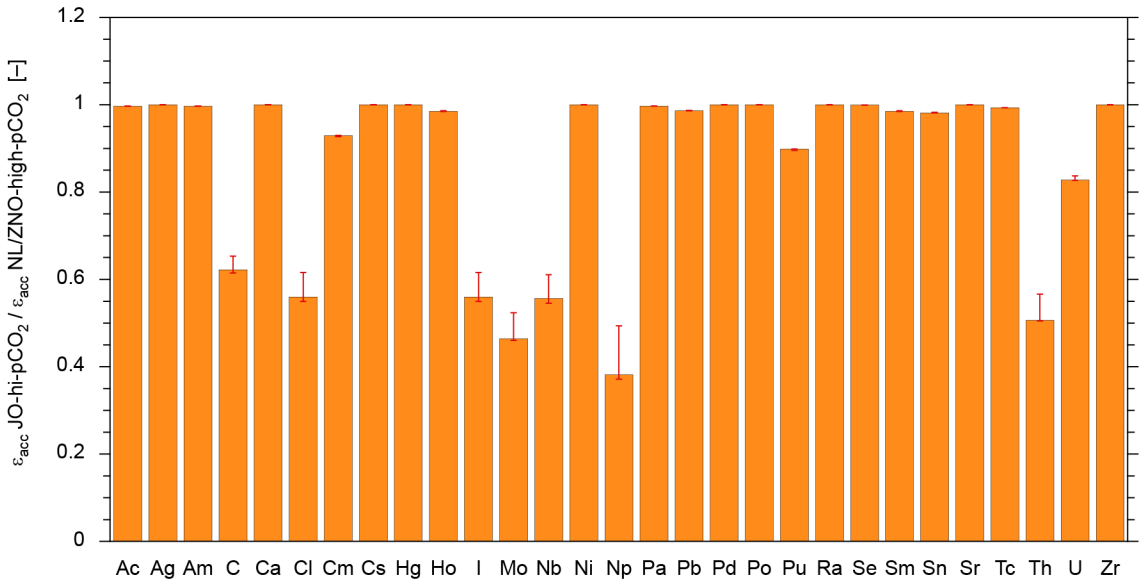

Fig. 5-4: Ratio of ε_{acc} values calculated for the high-pCO$_2$ variant of JO porewater (pH = 7.14, I = 0.169 mol kg^{-1}) and a total clay content of 56 wt.% divided by those for the high-pCO$_2$ NL-ZNO porewater (pH = 6.87, I = 0.34 mol kg^{-1})

6 Application of the look-up tables for the safety analysis

6.1 Introduction

The newly established correlations between the total clay content and the diffusion and sorption behaviour from the previous sections and in NTB 23-06 (Marques Fernandes et al. 2024b), respectively, provide the basis for an innovative approach to calculate continuous profiles of diffusion and sorption properties along any borehole or stratigraphic column with known mineralogical compositions (for given porewater compositions and elements). As these D_e, ε_{acc} and R_d LUTs are directly derived from rocks in Northern Switzerland of varying rock compositions, i.e. total clay contents, they can be systematically combined with the available high-resolution geological data (Nagra 2024a). This approach transforms downhole logs (of total clay content and porosity) into detailed data plots for D_e and ε_{acc} (this report), and R_d (Marques Fernandes et al. 2024b), which then can be statistically evaluated or upscaled to specific output coefficients. This increased data resolution reduces uncertainties across the entire dataset. Consequently, reference, upper and lower bounding data of the parameters for every abstracted unit are identified and compiled for use in transport model calculations.

This approach is far superior to that applied in Nagra's previous DDB where diffusion properties for only few selected units, mostly on very few samples, were determined and tabulated (Van Loon 2014). Specifically, for the SGT-E2 diffusion database, the methodology for estimating D_e for radionuclide diffusion in argillaceous rocks used literature data, primarily for the Opalinus Clay, in combination with D_e measured in diffusion experiments (involving HTO, $^{36}Cl^-$ and $^{22}Na^+$) on few samples from Opalinus Clay, Helvetic Marls, Brauner Dogger, and the Effingen Member. From the literature and measured data, a relationship between diffusion properties and total porosity was derived (see Chapter 2). The results were used for the calibration of the extended Archie relationship (cf. Eq (2-12)). This relationship was subsequently used to derive, along with considerations of sorption properties of cationic elements (Baeyens et al. 2014b, Baeyens et al. 2014a) the diffusion properties of the dose-relevant radioelements and their method-related uncertainties (Van Loon 2014).

The new approach, developed for the current report, is based on an extensive investigation during Nagra's latest drilling campaign where thousands of metres of new core material from the Opalinus Clay and the confining geological rock units were recovered (Nagra 2024b). For the determination of diffusion properties and the necessary method development, over 130 core samples were analysed (Van Loon et al. 2024, Van Loon et al. 2023, Glaus et al. 2024). The resulting DDB provides a much-improved statistical scope due to the integration of high-resolution mineralogical and petrophysical data (from MultiMin analyses, see Becker & Marnat (2024)), which increases flexibility and comprehensiveness of the applications.

6.2 Abstraction of lithostratigraphic units for implementations in transport models for PA and SA

The first step in preparing the data for the computational transport models was an abstraction and subsequent simplification of the lithostratigraphic units determined from boreholes. This resulted in abstracted units with properties that closely represent the physical properties of the respective lithostratigraphic units. For this purpose, the detailed and complex Mesozoic lithologies were combined into manageable abstracted units. For this first lithostratigraphic abstraction, the unit delineation processes and the representative geological (Nagra 2024b) and petrophysical (Becker & Marnat 2024) rock properties were considered. Fig. 6-1 gives an overview of the simplification of the lithostratigraphic units into abstracted units.

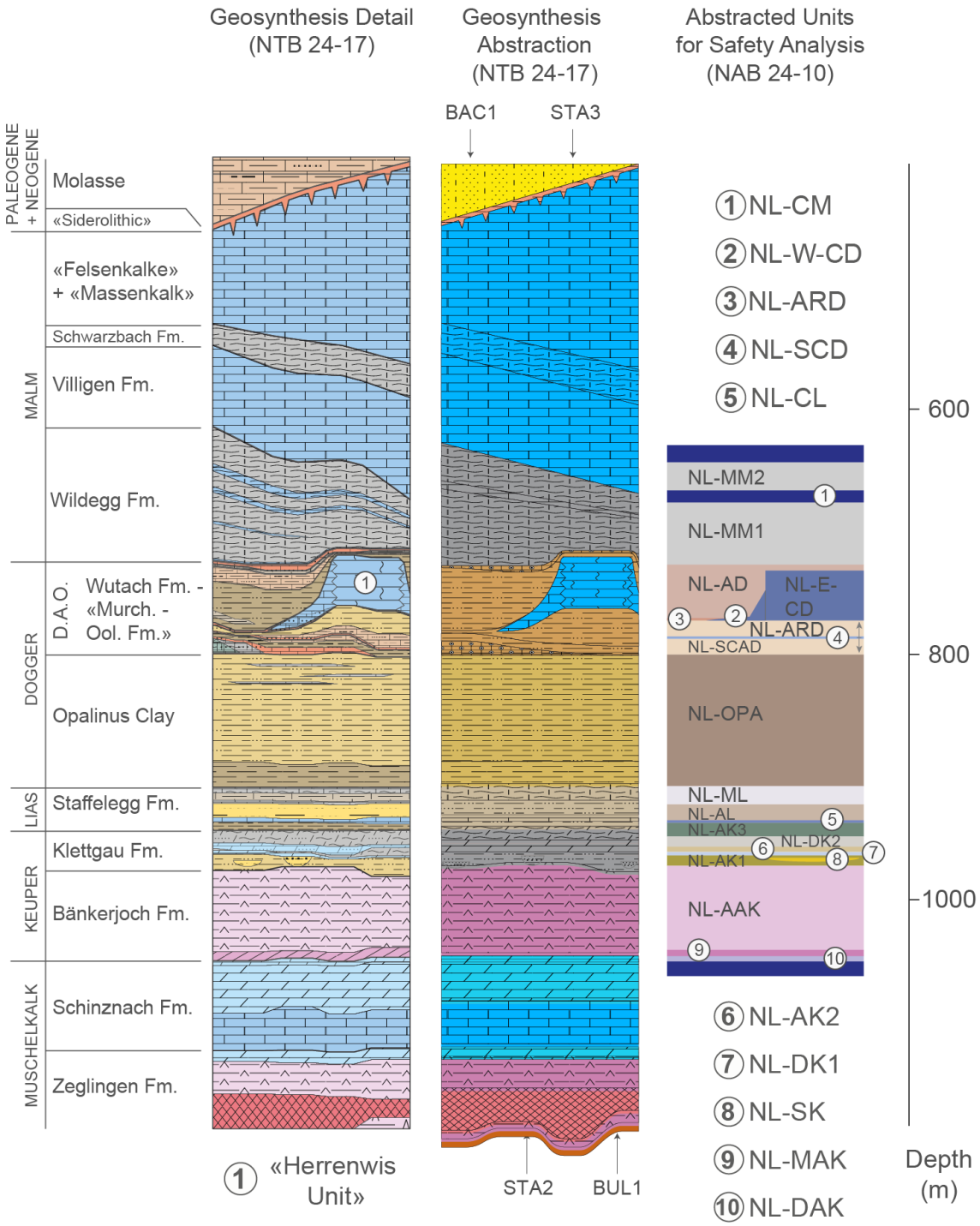

Fig. 6-1: Example of the abstraction of the sedimentary Mesozoic sequence (Nagra 2024b) of the NL siting region into abstracted units (Nagra 2024a). The abstracted units include the overall confining rock sequence considered for transport models

For the transport models used for performance and safety analyses, several of the thin abstracted units (Fig. 6-1) were further combined for the following reasons:

- The lowermost confining units DAK and MAK (argillaceous Keuper) (Fig. 6-2), overlying the Muschelkalk, are thin and have minimal impact on the overall transport of radionuclides compared to AAK (similar in composition) or the other confining units. These two thin units have very similar geological and petrophysical properties. Combining them into a single unit (KAK) (see abstracted units) simplifies the model without compromising accuracy (individual contributions are negligible).
- The units DK and AK1/SK may contain water-bearing sedimentary subunits in the form of lenses or channels (Fig. 6-2). Combining these units into a single unit (KAL) acknowledges their hydrogeological similarity and encompasses the uncertainties associated with the location of such features within the lithostratigraphic section. This facilitates a coherent representation of possible groundwater flow and transport pathways and allows for conservative model setups and calculations.
- Some units are particularly thin (*e.g.* CL, DK) and often contain no lab data and limited MultiMin data and have been amalgamated despite the different geological properties. In NL, AK2 is combined with DK2 (Fig. 6-2) to form the unit KAU; likewise, for AK2 and DSK in ZNO. The thin carbonate-rich CL unit (Beggingen Member) is combined together with AK2/3 (JO) or AK3 (NL and ZNO) to form the KEU model unit (Fig. 6-2). From a modelling perspective, this process expands the stratigraphic continuity and ensures a consistent stratigraphic framework across different regions.

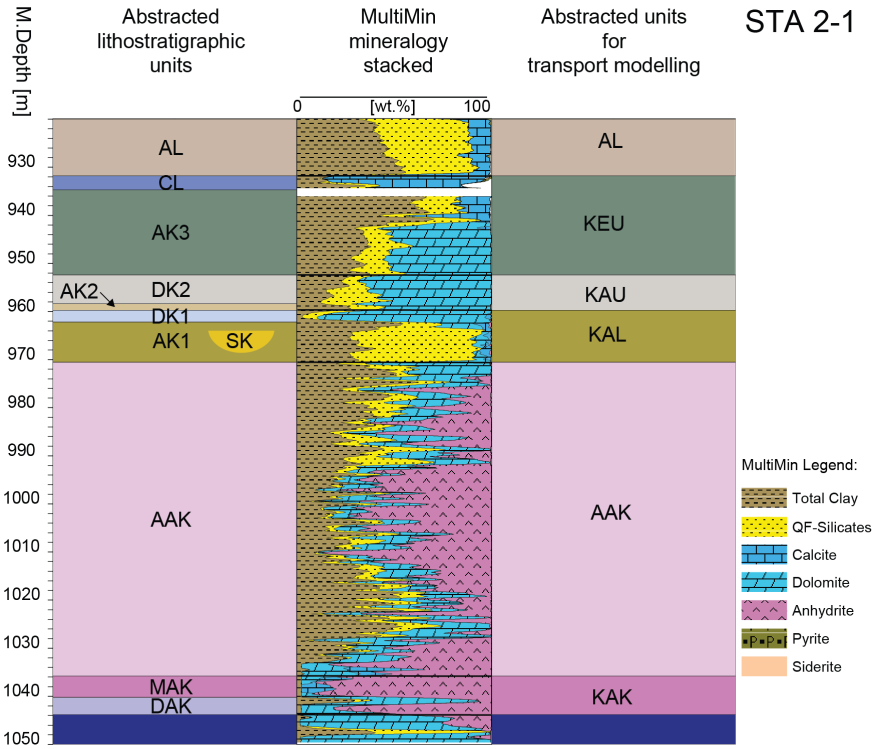

Fig. 6-2: Amalgamation of lithostratigraphic units below the Opalinus Clay into abstracted units for transport modelling using the example of the STA2-1 borehole, NL

QF-Silicates is the combined quartz and feldspar content.

- The units SCAD and SCD (Fig. 6-3) are combined to streamline the modelling process. This simplification reduces complexity (of the variable number and thickness of the carbonate beds within the argillaceous layers), while still capturing the essential geological and hydro-geological characteristics necessary for accurate modelling and the development of robust safety and performance assessments. Details of these highly heterogeneous units across all siting regions are provided in Nagra (2024a).

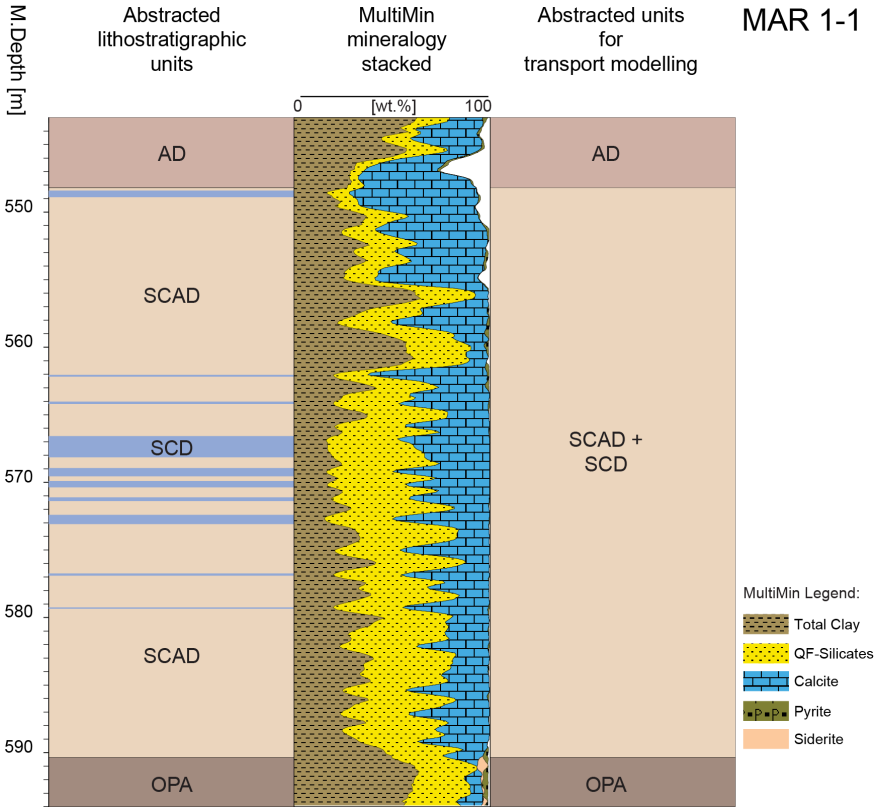

Fig. 6-3: Amalgamation of lithostratigraphic units above the Opalinus Clay (SCAD and SCD) into abstracted units for transport modelling using the example from the MAR 1-1 borehole in the ZNO siting region

QF-Silicates is the combined quartz and feldspar content.

In summary, the amalgamation of these units across the siting regions improved the clarity and efficiency of the geological and hydrogeological models used for the radionuclide transport analysis in the performance and safety analyses without losing information. The abstraction for transport model applications represents a minimal deviation from the abstracted lithostratigraphic units (see App. A) and ensures that the models are both scientifically sound and practically applicable to the post-closure performance and safety analysis of the deep geological repository. Fig. A-1 gives an overview of the lithostratigraphic units and their abstraction for input into transport models using the example of NL and ZNO.

The resulting high-resolution datasets of each of the aforementioned simplified geological units were analysed to determine representative transport parameter ranges and parameter best-estimate values. This procedure also allowed for detailed numerical and statistical analysis critical for a cohesive transport model setup and ensured that the most accurate and reliable data were used for subsequent modelling (comparing best estimates with upper and lower boundary values). Examples of such detailed analyses are given in Section 6.4.

6.3 Downhole properties of diffusion properties

All Nagra's exploratory boreholes in the siting regions (Fig. 1-1) have established precise and continuous downhole profiles of total clay content. These were determined from combining petrophysical logs, mineralogical (X-ray diffraction) data from laboratory analyses, and results from a Multi Sensor Core Logger (MSCL). Each high-resolution profile represents an individual stochastic multimineral interpretation on a per-borehole basis (see Becker & Marnat 2024). This multimineral interpretation method relies on the principle that downhole petrophysical measurement data (from petrophysical logs or core scans) are largely determined by the mineralogy and pore fluid. Therefore, the petrophysical measurement results can be used to determine mineralogy and porosity, amongst other parameters. Conversely, if the mineralogical content, pore fluid and porosity are known, a theoretical petrophysical measurement response can be predicted. By using known mineralogical compositions, porosity values and pore fluid compositions (in this case a slightly saline water) from laboratory analyses, continuous profiles of mineralogical composition and porosity can be predicted. This approach allowed the determination of high-resolution total clay content profiles for all boreholes. In a following step, these high-resolution profiles from the MultiMin interpretations were integrated with the established LUTs of the sorption and diffusion data linked to total clay contents detailed in this report and Marques Fernandes et al. (2024b) to generate high-resolution datasets of transport properties for every borehole across all siting regions (see Fig. 6-4).

For this integration, the total clay content of the MultiMin data was first rounded to whole numbers to be compatible with the total clay content values in the LUT. Values below 0.5 wt.% were set to 1 wt.%. If rounded correctly, these values would obviously result in a total clay content of 0 wt.%. However, with the current diffusion correlation model (Van Loon et al. 2024), such values would result in null values, prohibiting diffusion along a 1D profile. The current approach ensures that continuous vertical profiles of effective diffusion coefficients $D_e > 0$ are obtained (see Fig. 6-4 for an example from the STA2-1 borehole). Importantly, effective diffusion coefficients for rocks with clay contents <5 wt.% need to be treated carefully as the uncertainties may be significant (Van Loon et al. 2024).

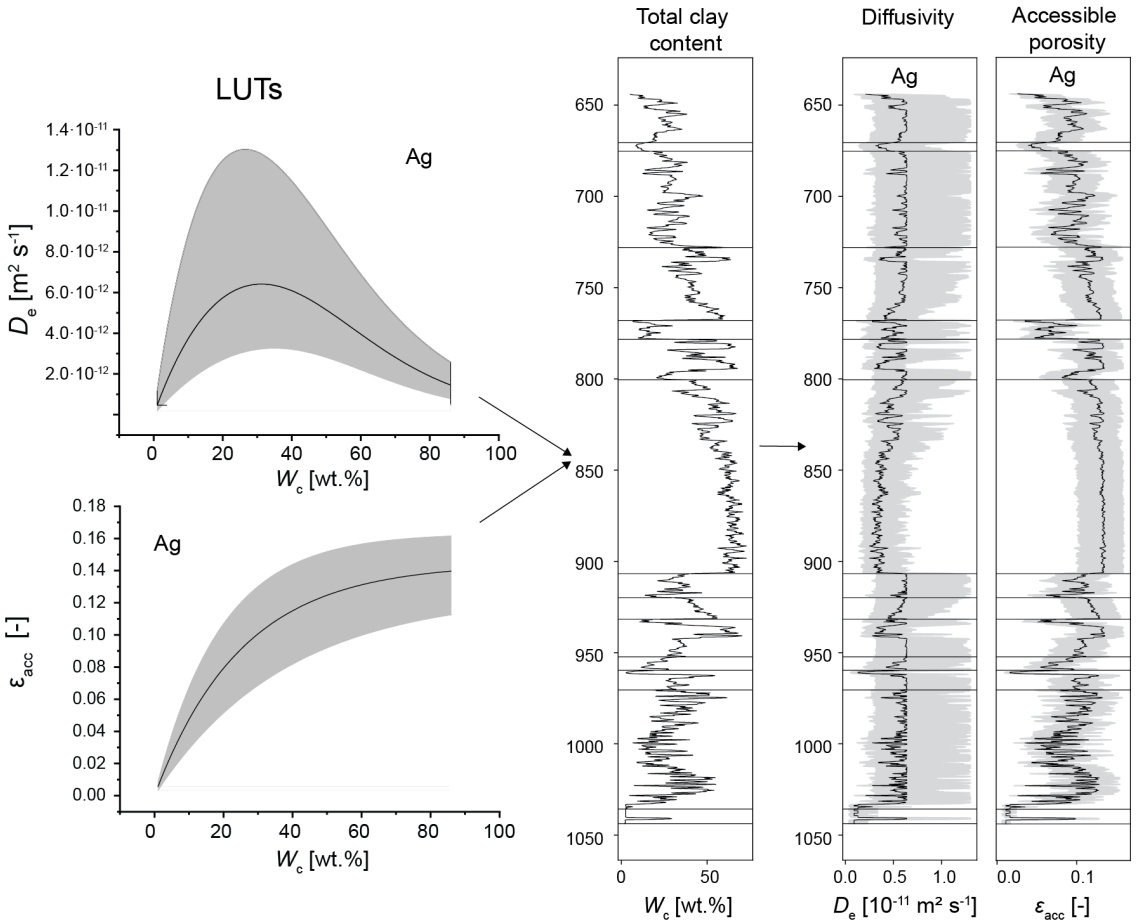

Fig. 6-4: Schematic processes showing how diffusivity transport properties (using the element Ag) are derived from total clay mineral content relationships

The LUTs (left side) show the spectrum of the total clay content with corresponding ε_{acc} and D_e, where reference values (solid line) and upper and lower values are given. By combining the LUT data with the MultiMin total clay content data (central display), high-resolution D_e and ε_{acc} profiles can be calculated. In this illustration of the borehole STA2-1, the data for Ag considering the NL-ZNO reference porewater are used as an example.

The numerical processing described above was implemented in computer scripts (using Python). This has the advantage that, if new data becomes available in the future, the generation of continuous downhole profiles of transport properties based on the LUTs and total clay content (or, in fact, any other mineralogy if such data become available) can easily be repeated.

Fig. 6-5 shows downhole plots of the effective diffusion coefficients (D_e), derived from total clay content for representative elements with various charges. These downhole profiles provide a high-resolution representation of the variable D_e values within, and across, the geological units, allowing for precise identification of transport properties at different depths.

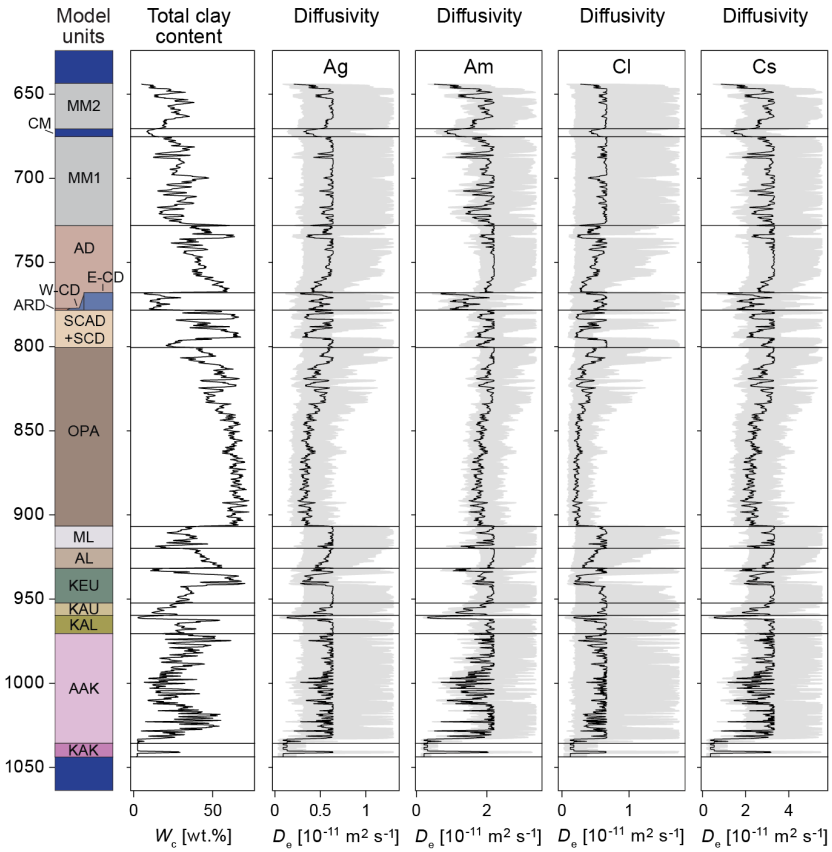

Fig. 6-5: Illustration of downhole high-resolution D_e values of the elements Ag, Am, Cl, and Cs, as determined from the LUTs of STA2-1 using the NL-ZNO reference porewater

The D_e profiles are generated by combining the LUT data with the MultiMin total clay content profile shown in the second column.

Each of the abstracted units have unique, variable patterns of the D_e and ε_{acc} data (in alignment with W_c). The curves of the selected elements Ag, Am, Cl and Cs in the profile of STA2-1 in Fig. 6-5 serve as a visual example of these variations, illustrating the compositional heterogeneity downhole throughout the entire profile (from the basal Muschelkalk to Malm at the top, see Fig. 1-2) as well as variability within abstracted units (e.g. AD). This detailed illustration enhances the understanding of the unit's specific composition and how the diffusive transport characteristics are influenced by the mineralogical composition (i.e. total clay content). This, therefore, provides support for the development of more accurate models for radionuclide transport behaviour at a high resolution.

In view of the basic dependence of D_e values on W_c, the patterns of the profiles look similar with differences due to element-specific diffusion behaviour. The magnitude of the individual profiles nicely reflects the concept shown in Fig. 1-3. As expected, Am and Cs show the highest D_e values because they are present in cationic form, while the lowest values are found for Cl which is present almost entirely in anionic form. The discrepancy between these species is strongest in the case of clay-rich sediments according to the expected dependence of Ψ_D on W_c. The D_e values for Ag, as a neutral element, are expected to be in between the charged elements. This is the case for clay-rich sediments. For sediments with low W_c values, the D_e values of Ag and Cl are, however, rather similar. Cl has a significantly higher D_w value than Ag. This makes the "chemical" difference between Ag and Cl almost disappear in clay-poor sediments.

In Fig. 6-6, the ε_{acc} determined from the effective diffusion calculations and the correlation with the total clay content are plotted downhole and illustrate their relationship with the total clay content. These downhole profiles provide a high-resolution representation of the variable ε_{acc} values within, and across, abstracted units, allowing for precise identification of transport properties at different depths.

In the case of ε_{acc}, the individual values of the elements are basically governed by the dependence of ε_{tot} on W_c (cf. Eq. 2-15). On top of this behaviour, the anion exclusion effect also influences ε_{acc} according to the dependence on W_c. Because Ag, Am and Cs do not comprise negatively charged solution species, the ε_{acc} values for these elements are identical ($\varepsilon_{acc} = \varepsilon_{tot}$). A different behaviour is seen for Cl. For this element, anion exclusion is also effective and leads to decreasing accessibility with increasing W_c. On the other hand, ε_{tot} increases with increasing W_c. These trends of ε_{tot} and anion exclusion compensate each other to some extent. This is the reason why the ε_{acc} data for Cl change only slightly in the comparison between clay-rich and clay-poor sediments.

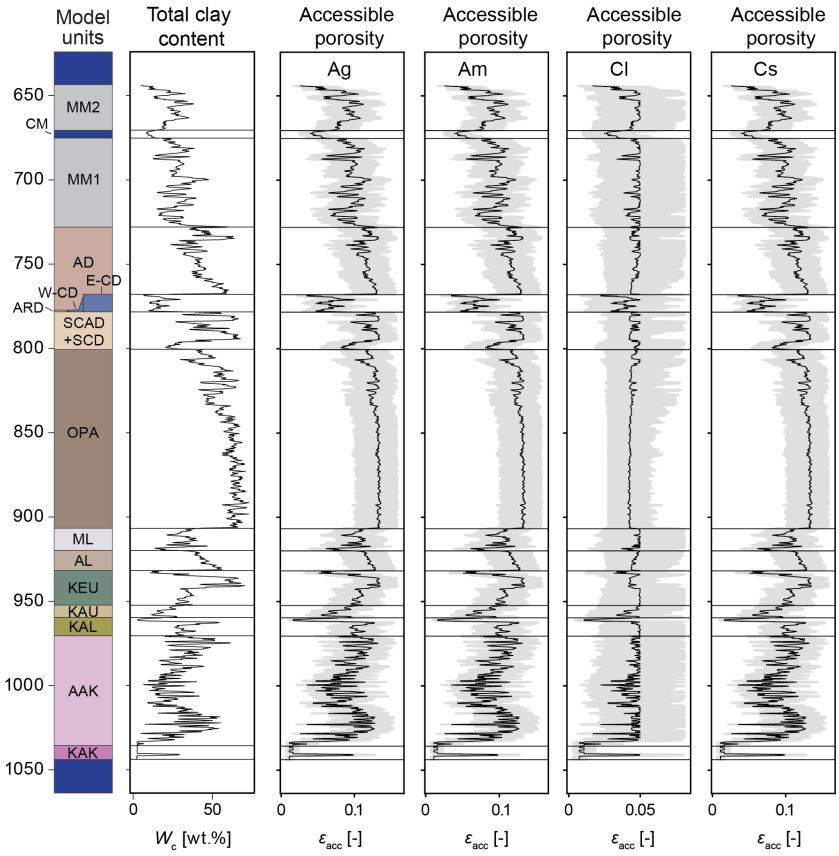

Fig. 6-6: Illustration of downhole high-resolution profiles of ε_{acc} values as determined from the LUTs of STA2-1 using the NL-ZNO reference porewater

The ε_{acc} values profiles are generated by combining the LUT data with the MultiMin total clay content profile shown in the second column.

Fig. 6-7 gives a more detailed account of the effective diffusion coefficients (D_e) derived from total clay contents across four units (SCAD+SCD, Opalinus Clay, argillaceous Lias (AL), and marly Lias (ML)). Note that the scale differs across all units due to their varying thicknesses. Similar to the figures above, the selected unit profiles exhibit distinctive curves, reflecting

variations in total clay content and thus rock properties. Plotting the data for the high-pCO_2 porewater (blue lines) leads to its superimposition on the reference porewater data (dark grey lines), clearly illustrating the limited impact of porewater composition on the effective diffusion coefficients.

The high-resolution representation of the upper and lower bounding values, as well as the reference values illustrates the overall variability of the diffusivity that can be determined based on the method of the LUTs. This detailed depiction helps visually with the understanding of the effective diffusion coefficient variability across each unit.

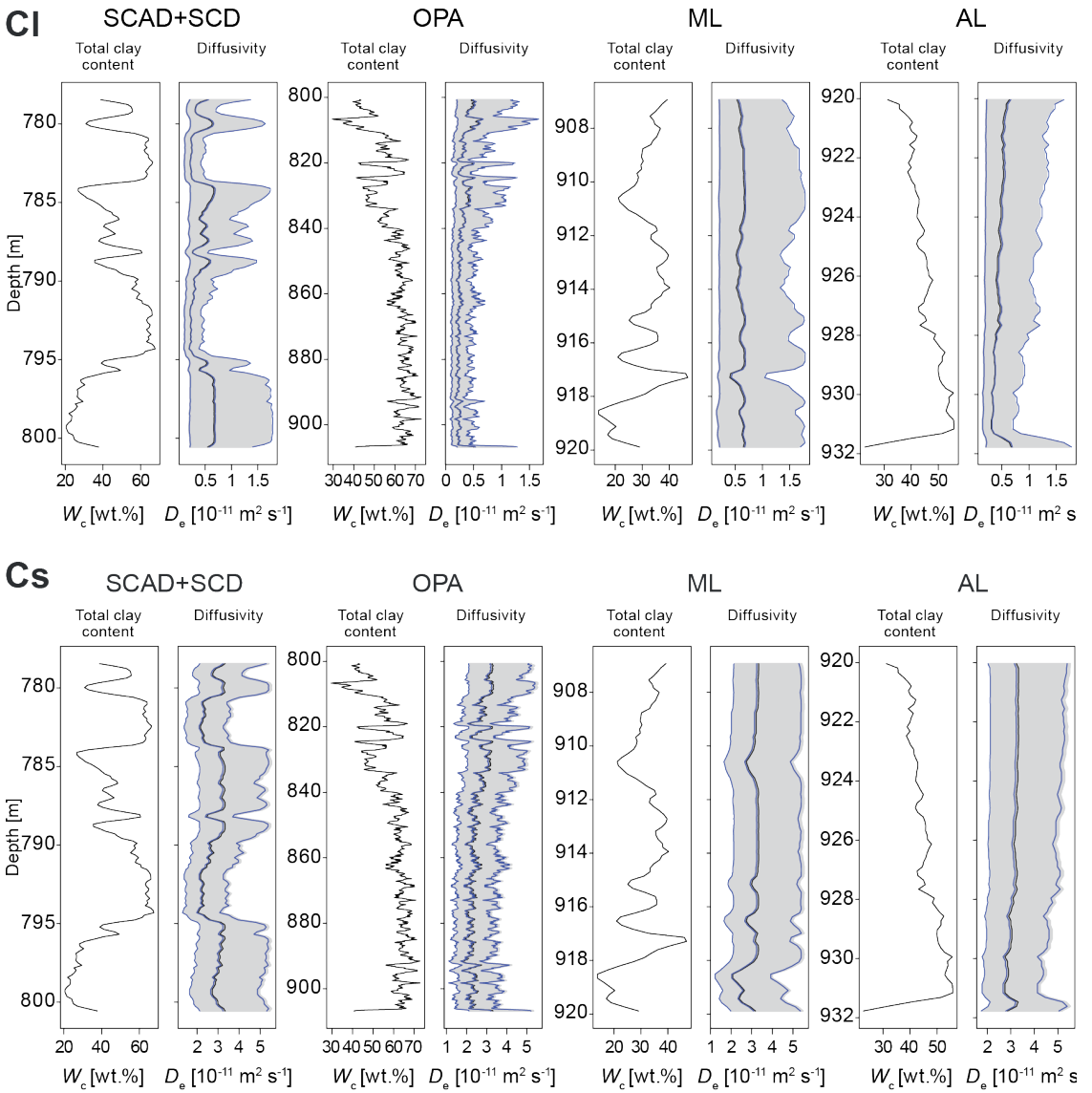

Fig. 6-7: Examples of D_e for Cl and Cs derived from W_c across four selected units (SCAD+SCD, Opalinus Clay, ML and AL)

The figures show values for both reference (dark grey) and high-pCO_2 (blue lines) values of STA2-1, indicating that the diffusivity shows little difference between these porewater compositions.

Similar to Fig. 6-7 above showcasing the D_e of selected elements, variability of the accessible porosity can also be visually displayed. Fig. 6-8 illustrates the same units (SCAD+SCD, OPA, ML, AL) and the variability in ε_{acc} of upper, reference and lower bounding values. Again, the blue line represents the data of the high-pCO_2 porewater and illustrates minimal deviations from the data of the reference porewater (dark grey lines).

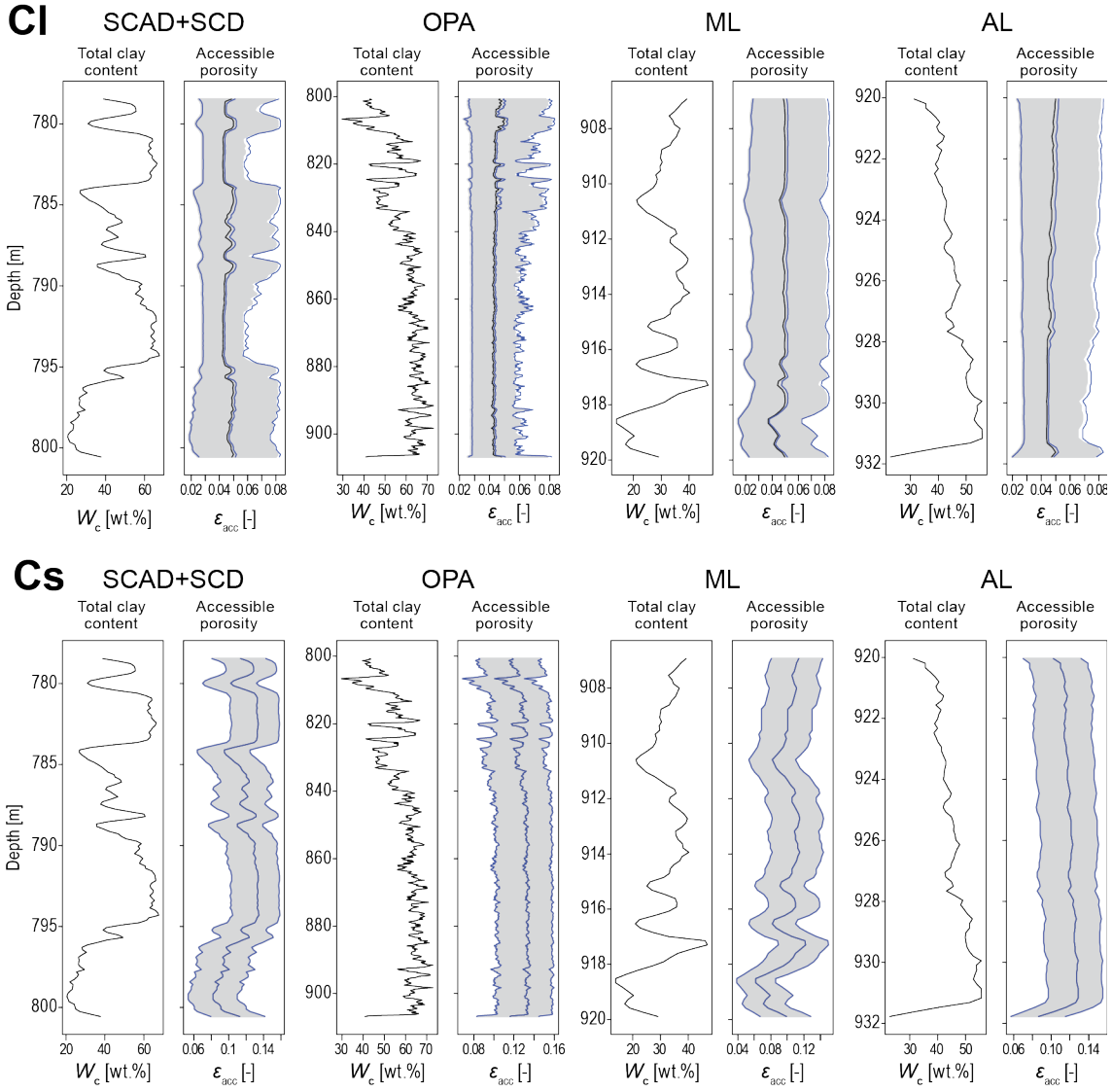

Fig. 6-8: Examples of calculated ε_{acc} derived from W_c across four selected units (SCAD+SCD, Opalinus Clay, ML and AL)

The figures show values for both reference (dark grey) and high-pCO_2 (blue lines) values of the STA2-1 borehole.

6.4 Statistical data analysis of effective diffusion and accessible porosity

The compilation of all data for the individual units used for transport modelling also allows for a statistical investigation of the distribution of each parameter (see Fig. 6-9).

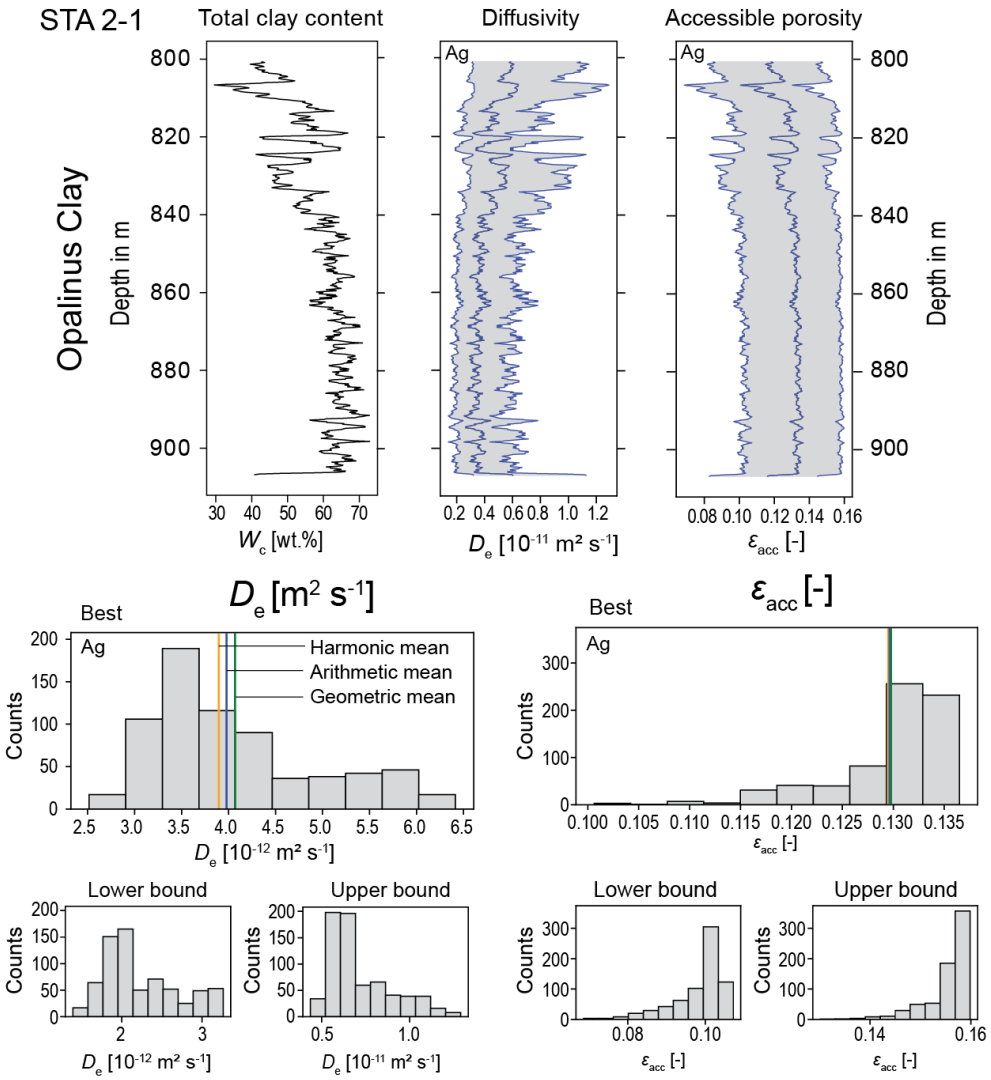

Fig. 6-9: Data from individual units can be further analysed in terms of parameter distributions and descriptive statistics

Shown is an example of STA2-1 for D_e and ε_{acc} of Ag in the Opalinus Clay.

Illustrated as histograms, D_e for two elements (Cl, Cs) have been plotted (Fig. 6-10), showing their distribution across the four selected model units (SCD+SCAD, OPA, ML, AL). For example, the data distribution for the element Cl within the Opalinus Clay shows that the majority of values range between 2×10^{-12} m^2 s^{-1} and 3×10^{-12} m^2 s^{-1}. The harmonic mean of D_e_best_Cl is 2.69×10^{-12} m^2 s^{-1}. The data distribution shows a unimodal pattern, and the spread of data is relatively narrow, within a factor of 3.

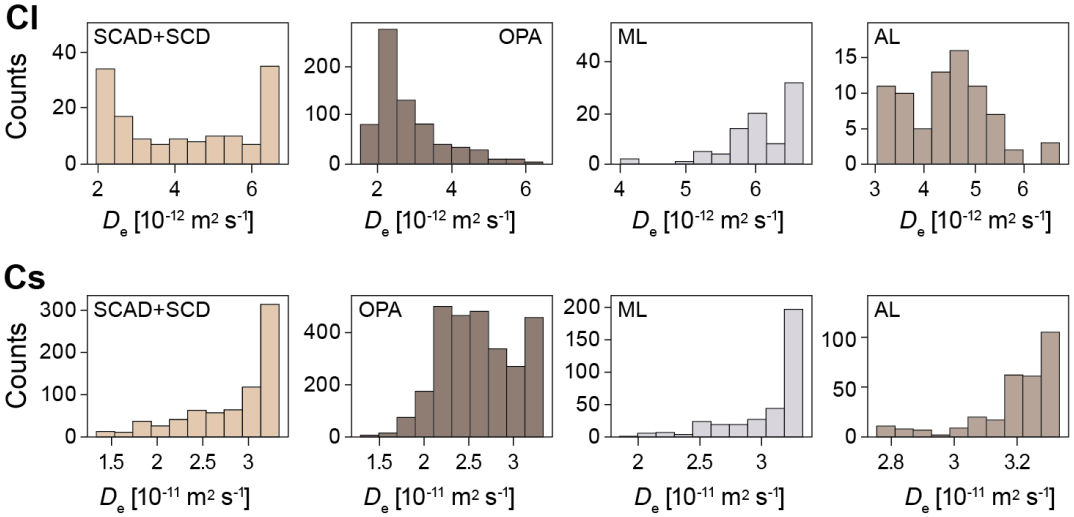

Fig. 6-10: Histograms of the harmonic mean D_e data for Cl and Cs from all boreholes investigated in the NL siting region showing data characteristic for each unit (reflecting composition variabilities)

Similarly, all other data, including the ε_{acc}, can be plotted and analysed. Such visual plots allow the illustration of variability and outlier detection. Most importantly though, they provide the basis for the simplification of the large datasets generated with the aid of the LUTs. In Fig. 6-11, the ε_{acc} histograms show different visual variabilities to the diffusion coefficients (Fig. 6-10). The figure illustrates, for example, that the ε_{acc} based on the diffusion measurements of the Opalinus Clay have a range of 0.04 – 0.05, with the majority between 0.042 – 0.044, while the calculated values are determined at 0.042 – 0.052 (Nagra 2024b).

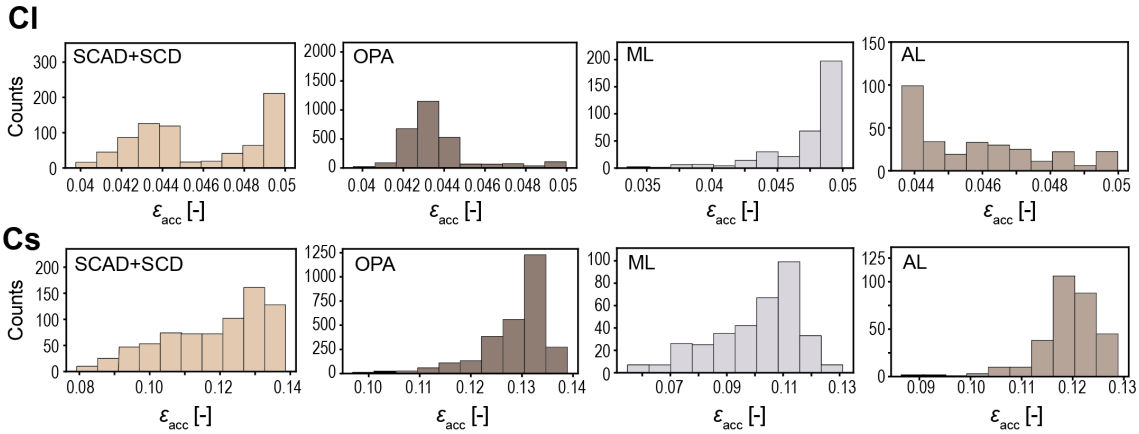

Fig. 6-11: Histograms of the harmonic mean ε_{acc} data for Cl and Cs from all boreholes in the NL siting region showing data characteristic for each unit

Following statistical analysis of the diffusion and sorption parameters of each abstracted unit in each borehole of all three siting regions, the datasets can be presented depending on the context of use. This implies that the data spread of the systematic statistical analysis can be displayed depending on the purpose of the data, including the:

- harmonic mean (used for RN transport modelling for safety analysis (Nagra 2024c));
- geometric mean (used for some of the 3D transport models of the performance assessment (Nagra 2024d)); and
- arithmetic mean and P50 values for each unit.

Among the different averaging methods, the harmonic mean generally produces the lowest values because it adds more weight to lower values. With respect to diffusive transport calculations, the choice of the harmonic mean may be considered as non-conservative, i.e. lower effective diffusion coefficients result in longer breakthrough times and thus lower doses at the surface. However, the choice of the harmonic mean prevents overweighting of single outliers that exhibit large parameter values. It can further be noted that the differences between the choices of the three options are in general much lower than the associated parameter uncertainties. For all these reasons, a non-conservative choice of averaging may be considered permissible.

For all these means, details of reference and deviatory values for each radionuclide (i.e. upper and lower bounds, e.g. Tab. 6-1) can be displayed and determined. The subsequent applications of these robust datasets in the different transport models are the basis of performance and safety analysis.

In general, a quality check of these detailed characterisations of transport parameters, including the different types of means, needs to consider the following:

1. variability of the rock composition (large or narrow);
2. number of datapoints; and
3. data comparison with samples analysed in the laboratory (comparison of LUT data and laboratory data).

The complete datasets and statistical information are part of Nagra's data management system and can be obtained upon request from Nagra.

Tab. 6-1: Example of tabulated harmonic mean values of D_e for Cl and Cs of the SCAD+SCD, Opalinus Clay, ML and AL units

The values represent the mean value of all samples of each unit for the NL siting region. The data are based on the reference porewater chemistry and 25 ºC.

Model unit	D_e_low_Cl [m^2 s^{-1}]	D_e_best_Cl [m^2 s^{-1}]	D_e_up_Cl [m^2 s^{-1}]	D_e_low_Cs [m^2 s^{-1}]	D_e_best_Cs [m^2 s^{-1}]	D_e_up_Cs [m^2 s^{-1}]
SCAD+SCD	1.45E-12	3.40E-12	7.36E-12	1.80E-11	2.74E-11	4.39E-11
OPA	1.24E-12	2.69E-12	5.56E-12	1.68E-11	2.53E-11	3.93E-11
ML	1.98E-12	5.84E-12	1.47E-11	1.94E-11	3.04E-11	5.23E-11
AL	1.83E-12	4.35E-12	1.06E-11	2.11E-11	3.19E-11	5.07E-11

The statistical data can also be visually displayed for ease of comparison of ranges or means. In Fig. 6-12, a few selected elements and their D_e are illustrated as box plots. These plots easily summarise the data and outline the data range, inform about the skewness (box), and provide a cross-unit comparison. For example, the dotted lines provide the harmonic mean values of the Opalinus Clay.

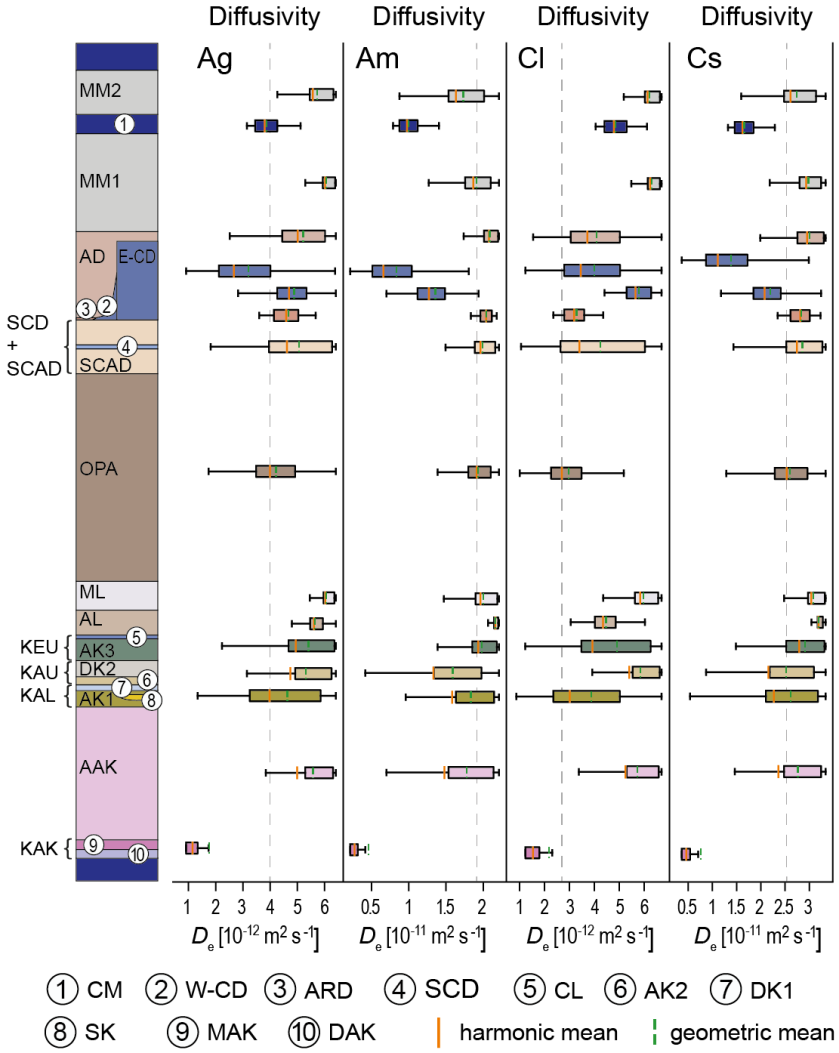

Fig. 6-12: Box plots showing the data distribution of D_e of selected elements across abstracted units for NL

Grey dotted lines indicate the harmonic mean value of the Opalinus Clay.

Box and whisker plots are informative tools to visually summarise the data including the illustration of the data median, the quartiles and the potential outliers (whiskers). The shape of the box and the length of the whiskers indicate the skewness. Additional means (harmonic and geometric) are also included.

The same approach can be used for all other data and each element. Tab. 6-2 and Fig. 6-13 provide examples of tables and figures displaying the ε_{acc}. These can be generated instantly from the data tables using the scripts developed for this purpose.

Tab. 6-2: Example of tabulated harmonic mean values of ε_{acc} for Cl and Cs of the SCAD+SCD, Opalinus Clay, ML and AL units

The values represent the mean value of all samples of the four units for the NL siting region. The data shown considers the reference porewater at 25 ºC.

SR	Unit	ε_{acc}_low_Cl [-]	ε_{acc} _best_Cl [-]	ε_{acc} _up_Cl [-]	ε_{acc} _low_Cs [-]	ε_{acc} _best_Cs [-]	ε_{acc} _up_Cs [-]
NL	SCAD+SCD	0.025	0.046	0.069	0.084	0.117	0.145
NL	OPA	0.027	0.044	0.063	0.097	0.128	0.154
NL	ML	0.022	0.047	0.078	0.066	0.097	0.126
NL	AL	0.026	0.046	0.075	0.086	0.119	0.147

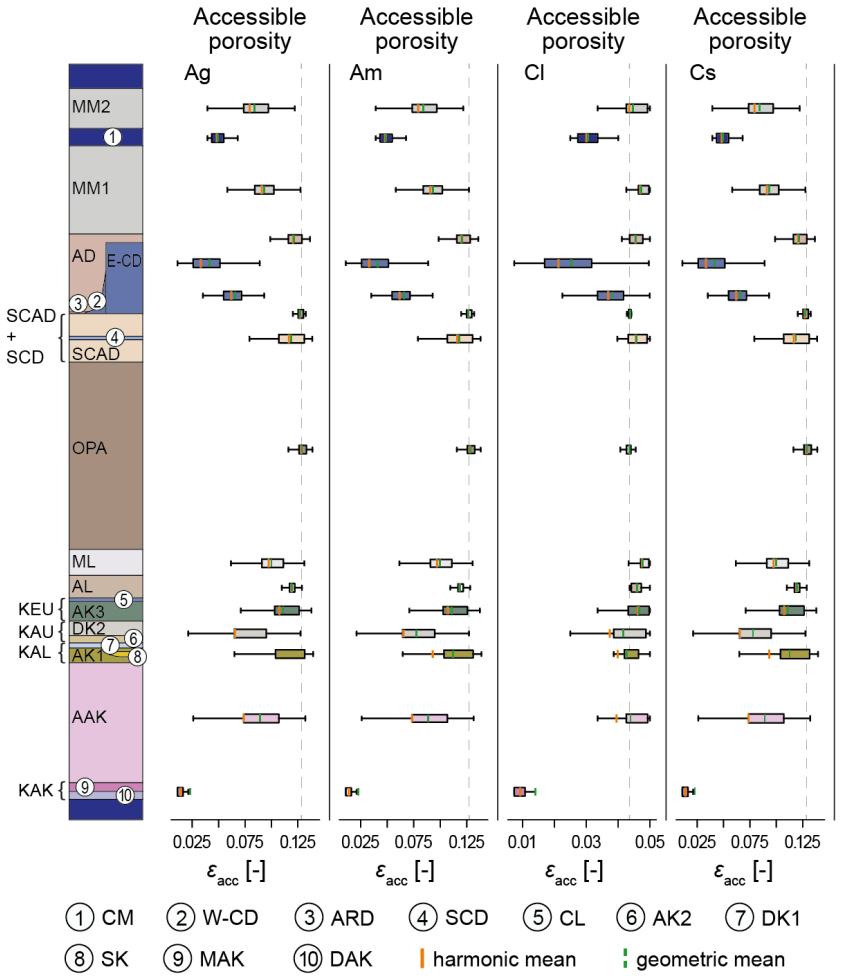

Fig. 6-13: Box plots showing the data distribution of ε_{acc} (HM) values of selected elements of abstracted units of NL

Grey dotted lines indicate the harmonic mean value of the Opalinus Clay.

Similarly, following the methodology used to determine D_e and R_d, the same statistical analysis can also be performed to analyse the statistical distribution of other properties. An example of the table with the harmonic mean data of the units for NL is provided below (Tab. 6-3).

Tab. 6-3: Harmonic mean (HM), geometric mean (GM), arithmetic mean (AM) data of clay content, MultiMin porosity and grain density of all borehole data for Nördlich Lägern

Note that values have been rounded to the second decimal place and hence are often very similar.

Unit	**Total clay content** [wt.%]			**Porosity** [-]			**Grain density** [g cm^{-3}]		
	HM	GM	AM	HM	GM	AM	HM	GM	AM
SCAD+SCD	42.4	44.9	47.3	0.11	0.12	0.12	2.73	2.73	2.73
OPA	56.0	56.9	57.6	0.11	0.11	0.11	2.70	2.70	2.70
ML	28.5	29.9	31.1	0.07	0.08	0.08	2.66	2.66	2.66
AL	43.8	44.2	44.6	0.08	0.08	0.08	2.68	2.68	2.68

6.5 Probabilistic data analysis

For statistical evaluation, selected data were probabilistically analysed for applications in PA and SA. To achieve this, a distribution fitting process was executed to determine the theoretical statistical distributions based on the calculated dataset.

Given that most clays have predominantly negatively charged surfaces, they exhibit high retention for cations, which in turn affects radionuclide transport. In an environment like the Opalinus Clay, only a few elements are important when considering transport and radiological consequences. Consequently, a short list of seven elements (Ag, Ca, C, Cl, I, Se, Hg) was selected (Nagra 2024c) for probabilistic analysis[3] of the data derived from the LUTs.

In the probabilistic radiological consequence analysis in Nagra (2024c), the abovementioned seven radionuclides are taken into account. Based on the histogram shown in Fig. 6-14, the statistical distribution of D_e and ε_{acc} can be assumed as a log-normal distribution (theoretical distribution). The expected mean value and standard deviation of the fitted theoretical distribution are estimated using the Matlab function “fitdist()”.

Additionally, to achieve a more representative sampling in the probabilistic analysis, the randomly generated values are truncated based on the specified boundary values for each individual element and rock formation. The resulting theoretical distribution types and their corresponding distribution parameters are documented separately for each siting region dataset (see example below in Fig. 6-14).

[3] Radionuclide screening for inclusion in probabilistic assessments relies on their transport properties and inventory. The inventory is typically well-established with minor uncertainties. However, the evolving chemical environment surrounding the waste can significantly influence radionuclide mobility. To account for uncertainties in this evolving environment, a conservative approach assumes the chemical form with higher mobility. In the future stages of the project, scientific advances may lead to a reduction in the list of considered radionuclides.

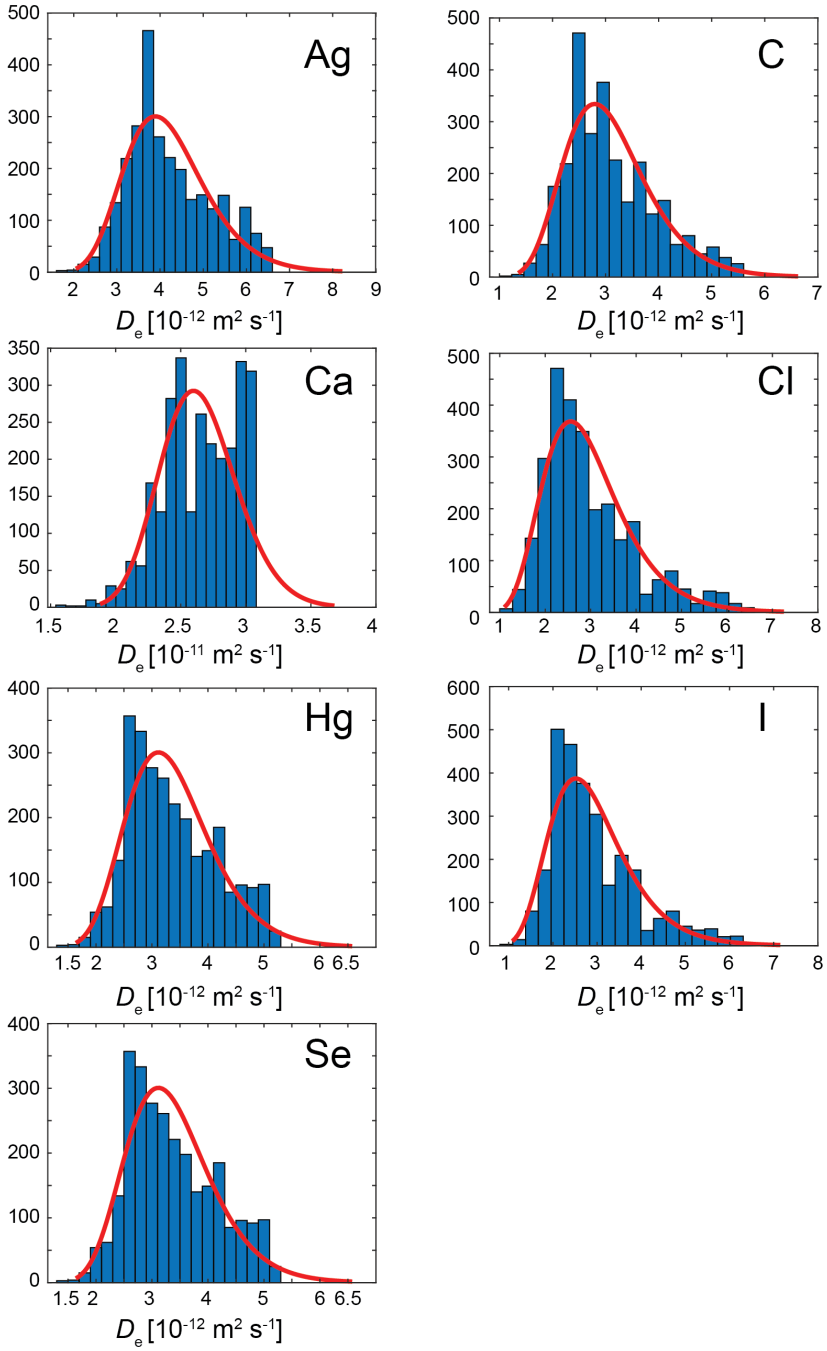

Fig. 6-14: D_e dataset of the NL reference values for the Opalinus Clay of selected elements for probabilistic analysis used in the modelling of the safety analysis

Extrapolation of the D_e data to different temperatures may be performed according to the methods described in Van Loon (2014).

7 Conclusions

This report describes the methods applied to derive diffusion parameter values (effective diffusion coefficients and accessible porosities, D_e and ε_{acc}) of all dose-relevant radioelements in clay rock of the sedimentary lithologies of the Jura Ost, Nördlich Lägern and Zürich Nordost siting regions involving the pertinent porewater composition, as well as for compacted bentonite. The proposed methods use the so-called Mean-Potential Donnan Layer (MPDL) approach to account for the electrostatic enrichment/depletion phenomena near the charged clay surfaces of charged solution species of all chemical elements under consideration. These effects, as well as the geometrical properties of diffusion in porous argillaceous media, are basically described as a function of the total clay content in the rock and the composition of the reference porewaters in the bulk aqueous phase.

Compared with previous methods applied to derive diffusion data in safety analysis, the present methods are applicable in a broader sense with regard to the mineralogical and lithological properties of the clay rock and the chemical behaviour of the radioelements in the various types of reference porewaters. Furthermore, they are based on a much broader set of experimental data (Van Loon et al. 2023). The broader scope of applicability therefore allows for a significant reduction of the uncertainties associated with the predicted parameter values. It is further shown in dedicated sections of this report that the proposed methods are fully in line with the recently proposed experimental data (Van Loon et al. 2023) and model schemes (Glaus et al. 2024) for the diffusion of tritiated water, $^{36}Cl^-$ and $^{22}Na^+$ tracers in more than 100 rock samples gained from the deep drilling campaign of Nagra. Owing to the programmed (Python, Jupyter notebook) implementation of the present method (named ClaySorDif), look-up tables for the diffusion parameter values can be compiled for any constellation of radioelements, lithostratigraphy and reference porewater. This represents an important advancement compared to the methods previously applied as it does not rely on subjective decisions. The comparison between the diffusion data from previous safety analyses and the present data compilation shows that the discrepancies are largely within the specified parameter uncertainties for clay-rich lithologies, while some notable discrepancies exist for rather clay-poor rocks. These differences can be readily explained by the different assumptions made in the approaches to predicting the pore diffusion properties ("geometrical properties") of the clay pore network. With regard to the broader data support, the present data appear to be preferable compared with the former predictions despite the fact that they may result in higher D_e values.

Parameter uncertainties in the current model predictions are globally defined according to best available knowledge and vary across the prediction range and elements considered. While uncertainties for average clay rocks and well-studied elements are tightly constrained, predictions extrapolated beyond the ranges of available experimental data, may be associated with larger uncertainties. Examples are clay rocks with very low total clay contents or radioelements like Ac, Ag, Cm, Hg, Mo, Pa, Pd, or Po.

The compilation of look-up tables for the effective diffusion coefficients and accessible porosities as a function of the total clay content in rock and the reference porewaters allows for statistical processing of the huge amount of data created in the look-up tables in order to produce a reduced set of average values along with their statistical variances for dedicated model lithostratigraphic units used in performance assessment.

8 References

Aldaba, D., Glaus, M.A., Leupin, O.X., Van Loon, L.R., Vidal, M. & Rigol, A. (2014): Suitability of various materials for porous filters in diffusion experiments. Radiochimica Acta 102/8, 723-730.

Andra (2022): Le comportement des radionucléides et des toxiques chimiques. Le socle de connaissances scientifiques et techniques du centre de stockage Cigéo - Les référentiels de connaissances CG-TE-D-NTE-AMOA-SR2-0000-20-0022. Andra.

Appelo, C.A.J. & Postma, D. (2005): Geochemistry, groundwater and pollution. 2nd edition. CRC Press, London.

Appelo, C.A.J., Van Loon, L.R. & Wersin, P. (2010): Multicomponent diffusion of a suite of tracers (HTO, Cl, Br, I, Na, Sr, Cs) in a single sample of Opalinus Clay. Geochimica et Cosmochimica Acta 74, 1201-1219.

Appelo, C.A.J. & Wersin, P. (2007): Multicomponent diffusion modeling in clay systems with application to the diffusion of tritium, iodide, and sodium in Opalinus Clay. Environmental Science & Technology 41/14, 5002-5007.

Asaad, A., Hubert, F., Ferrage, E., Dabat, T., Paineau, E., Porion, P., Savoye, S., Gregoire, B., Dazas, B., Delville, A. & Tertre, E. (2021): Role of interlayer porosity and particle organization in the diffusion of water in swelling clays. Applied Clay Science 207, 106089. DOI: 10.1016/j.clay.2021.106089.

Baeyens, B., Marques Fernandes, M. & Bradbury, M.H. (2014a): Comparison of sorption measurements on argillaceous rocks and bentonite with predictions using the SGT-E2 approach to derive sorption data bases. Nagra Technical Report NTB 12-05.

Baeyens, B., Thoenen, T., Bradbury, M.H. & Marques Fernandes, M. (2014b): Sorption data bases for argillaceous rocks and bentonite for the provisional safety analyses for SGT-E2. Nagra Technical Report NTB 12-04.

Becker, J. & Marnat, S. (2024): Petrophysical data and core-calibrated multimineral interpretation. Nagra Arbeitsbericht NAB 24-17.

Bestel, M., Glaus, M.A., Frick, S., Gimmi, T., Juranyi, F., Van Loon, L.R. & Diamond, L.W. (2018): Combined tracer through-diffusion of HTO and ^{22}Na through Na-montmorillonite with different bulk dry densities. Applied Geochemistry 93, 158-166. DOI: 10.1016/j.apgeochem.2018.04.008.

BFE (2008): Sachplan Geologische Tiefenlager: Konzeptteil. BFE 2. April 2008 (Revision vom 30. November 2011). Departement für Umwelt, Verkehr, Energie und Kommunikation UVEK, Bern.

Birgersson, M. & Karnland, O. (2009): Ion equilibrium between montmorillonite interlayer space and an external solution — Consequences for diffusional transport. Geochimica et Cosmochimica Acta 73/7, 1908-1923.

Bradbury, M.H. & Baeyens, B. (1997): A mechanistic description of Ni and Zn sorption on Na-montmorillonite Part II: Modelling. Journal of Contaminant Hydrology 27, 223-248.

Bradbury, M.H. & Baeyens, B. (2009): Sorption modelling on illite Part I: Titration measurements and the sorption of Ni, Co, Eu and Sn. Geochimica et Cosmochimica Acta 73, 990–1003.

Chagneau, A., Tournassat, C., Steefel, C.I., Bourg, I.C., Gaboreau, S., Esteve, I., Kupcik, T., Claret, F. & Schäfer, T. (2015): Complete restriction of $^{36}Cl^-$ diffusion by celestite precipitation in densely compacted illite. Environmental Science and Technology Letters 2/5, 139-143.

Curti, E. (2021): Bentonite pore waters (BPW) for the Sectoral Plan, Phase SGT-3: model development, testing and final calculations. PSI Internal Technical Report TM-44-21-02. Paul Scherrer Institut PSI, Villigen.

Curti, E. (2023): Bentonite pore waters (BPW) for SGT-E3: Model development, testing and final calculations. Nagra Arbeitsbericht NAB 22-43.

Davis, S.N., Whittemore, D.O. & Fabryka-Martin, J. (1998): Uses of chloride/bromide ratios in studies of potable water. Groundwater 36/2, 338-350. DOI: 10.1111/j.1745-6584.1998.tb01099.x.

Delavernhe, L., Joseph, C., Kupcik, T., Montoya, V., Moisei-Rabund, S., Glaus, M.A., Schäfer, T. & Emmerich, K. (2025) (*in prep.*): Multitracer (HTO, $^{36}Cl^-$, $^{85}Sr^{2+}$) diffusion in compacted natural and reduced-charge dioctahedral smectites.

Delavernhe, L., Steudel, A., Darbha, G.K., Schäfer, T., Schuhmann, R., Wöll, C., Geckeis, H. & Emmerich, K. (2015): Influence of mineralogical and morphological properties on the cation exchange behavior of dioctahedral smectites. Colloids and Surfaces A: Physico-chemical and Engineering Aspects 481, 591-599. DOI: 10.1016/j.colsurfa.2015.05.031.

Ferrage, E., Hubert, F., Dabat, T., Asaad, A., Dazas, B., Grégoire, B., Savoye, S. & Tertre, E. (2023): Anisotropy in particle orientation controls water diffusion in clay materials. Applied Clay Science 244, 107117. DOI: 10.1016/j.clay.2023.107117.

Fox, P.M., Tournassat, C., Steefel, C. & Nico, P.S. (2024): HTO and selenate diffusion through compacted Na-, Na–Ca-, and Ca-montmorillonite. Applied Geochemistry 170, 106090. DOI: 10.1016/j.apgeochem.2024.106090.

Gimmi, T. & Alt-Epping, P. (2018): Simulating Donnan equilibria based on the Nernst-Planck equation. Geochimica et Cosmochimica Acta 232, 1-13. DOI: 10.1016/j.gca.2018.04.003.

Gimmi, T. & Kosakowski, G. (2011): How mobile are sorbed cations in clays and clay rocks? Environmental Science & Technology 45/4, 1443-1449. DOI: 10.1021/es1027794.

Glaus, M.A., Aertsens, M., Appelo, C., Kupcik, T., Maes, N., Van Laer, L. & Van Loon, L.R. (2015): Cation diffusion in the electrical double layer enhances the mass transfer rates for Sr^{2+}, Co^{2+} and Zn^{2+} in compacted illite. Geochimica et Cosmochimica Acta 165, 376-388. DOI: 10.1016/j.gca.2015.06.014.

Glaus, M.A., Frick, S., Rossé, R. & Van Loon, L.R. (2010): Comparative study of tracer diffusion of HTO, $^{22}Na^+$ and $^{36}Cl^-$ in compacted kaolinite, illite and montmorillonite. Geochimica et Cosmochimica Acta 74/7, 1999-2010. DOI: 10.1016/j.gca.2010.01.010.

Glaus, M.A., Frick, S. & Van Loon, L.R. (2017): Diffusion of selected cations and anions in compacted montmorillonite and bentonite. PSI Bericht Nr. 17-08. PSI, Villigen.

Glaus, M.A., Frick, S. & Van Loon, L.R. (2020): A coherent approach for cation surface diffusion in clay minerals and cation sorption models: Diffusion of Cs^+ and Eu^{3+} in compacted illite as case examples. Geochimica et Cosmochimica Acta 274, 79-96. DOI: 10.1016/j.gca.2020.01.054.

Glaus, M.A., Frick, S. & Van Loon, L.R. (2021): Competitive effects of cations on the diffusion properties of strongly sorbing trace cations in compacted illite and Opalinus Clay. ACS Earth and Space Chemistry 5/10, 2621-2625. DOI: 10.1021/acsearthspacechem.1c00250.

Glaus, M.A., Van Loon, L.R. & Wüst, R.A.J. (2024): Diffusion of HTO, $^{36}Cl^-$ and $^{22}Na^+$ in the Mesozoic rocks of northern Switzerland. II: Data interpretation in terms of an electrical double layer model. Applied Geochemistry 162, 105842. DOI: 10.1016/j.apgeochem.2023.105842.

González Sánchez, F., Van Loon, L.R., Gimmi, T., Jakob, A., Glaus, M.A. & Diamond, L.W. (2008): Self-diffusion of water and its dependence on temperature and ionic strength in highly compacted montmorillonite, illite and kaolinite. Applied Geochemistry 23/12, 3840-3851. DOI: 10.1016/j.apgeochem.2008.08.008.

Herbert, H.J., Kasbohm, J., Sprenger, H., Fernandez, A.M. & Reichelt, C. (2008): Short and long-term behavior of compacted bentonites in contact with solutions of different salinities: a safety issue for the long-term closure of repositories for radioactive waste? EUROSAFE 2008 Proceedings, 1-26.

Hummel, W., Kulik, D.A. & Miron, G.D. (2023): Solubility limits for bentonite near field (update of NTB 14-06). Nagra Technical Report NTB 23-04.

Hummel, W. & Thoenen, T. (2023): The PSI chemical thermodynamic database 2020. Nagra Technical Report NTB 21-03.

Jenni, A., Meeussen, J.C., Pakkanen, T.A., Hirvi, J.T., Akinwunmi, B., Yustres, Á., Navarro, V., López-Vizcaíno, R., Muuri, E., Niskanen, M., Wersin, P. & Mäder, U. (2021): Coupling of chemical and hydromechanical properties in bentonite: A new reactive transport model. Applied Clay Science 214, 106274. DOI: 10.1016/j.clay.2021.106274.

Jordan, P. & Deplazes, G. (2019): Lithostratigraphy of consolidated rocks expected in the Jura Ost, Nördlich Lägern and Zürich Nordost Regions. Nagra Arbeitsbericht NAB 19-14.

Karnland, O., Olsson, S. & Nilsson, U. (2006): Mineralogy and sealing properties of various bentonites and smectite-rich clay materials. Technical Report TR-06-30. Swedish Nuclear Fuel and Waste Management SKB, Stockholm.

KEG (2003): Kernenergiegesetz (KEG) of March 21, 2003, status as of January 1, 2024. Systematische Sammlung des Bundesrechts SR 732.1, Schweiz.

Keller, L.M., Holzer, L., Wepf, R. & Gasser, P. (2011): 3D geometry and topology of pore pathways in Opalinus clay: Implications for mass transport. Applied Clay Science 52/1-2, 85-95. DOI: 10.1016/j.clay.2011.02.003.

KEV (2004): Kernenergieverordnung (KEV) of December 10, 2004, status as of January 1, 2024. Systematische Sammlung des Bundesrechts SR 732.11, Schweiz.

Kozaki, T., Fujishima, A., Sato, S. & Ohashi, H. (1998a): Self-diffusion of sodium ions in compacted sodium montmorillonite. Nuclear Technology 121/1, 63-69. DOI: 10.13182/NT98-A2819.

Kozaki, T., Saito, N., Fujishima, A., Sato, S. & Ohashi, H. (1998b): Activation energy for diffusion of chloride ions in compacted sodium montmorillonite. Migration '97 : 26-31 October, 1997, Sendai, Japan : Sixth International Conference on the Chemistry and Migration Behavior of Actinides and Fission Products in the Geosphere. Special Issue: Journal of Contaminant Hydrology 35, 67-75.

Kozaki, T., Sato, H., Fujishima, A., Sato, S. & Ohashi, H. (1996): Activation energy for diffusion of cesium in compacted sodium montmorillonite. Journal of Nuclear Science and Technology 33/6, 522-524.

Krejci, P., Gimmi, T. & Van Loon, L.R. (2021): On the concentration-dependent diffusion of sorbed cesium in Opalinus Clay. Geochimica et Cosmochimica Acta 298, 149-166. DOI: 10.1016/j.gca.2021.01.012.

Krejci, P., Gimmi, T., Van Loon, L.R. & Glaus, M. (2023): Relevance of diffuse-layer, Stern-layer and interlayers for diffusion in clays: A new model and its application to Na, Sr, and Cs data in bentonite. Applied Clay Science 244, 107086. DOI: 10.1016/ j.clay.2023.107086.

Kulik, D.A., Glaus, M.A., Gimmi, T., Van Loon, L.R. & Wüst, R.A.J. (2023): ClaySorDif: A new model for radionuclide sorption and diffusion in argillaceous media (GEMS implementation and verification against Phreeqc results and experimental data). Abstract C2-2 of the 18th International Conference on Chemistry and Migration Behaviour of Actinides and Fission Products in the Geosphere, Nantes, France.

Kulik, D.A. & Miron, G.D. (2024): Solubility limits for model Opalinus Clay porewaters as input for sorption (SDB) and diffusion (DDB) databases. Nagra Arbeitsbericht NAB 23-07.

Kulik, D.A., Wagner, T., Dmytrieva, S.V., Kosakowski, G., Hingerl, F.F., Chudnenko, K.V. & Berner, U.R. (2013): GEM-Selektor geochemical modeling package: revised algorithm and GEMS3K numerical kernel for coupled simulation codes. Computational Geosciences 17, 1-24. DOI: 10.1007/s10596-012-9310-6.

Li, Y.-H. & Gregory, S. (1974): Diffusion of ions in sea water and in deep-sea sediments. Geochimica et Cosmochimica Acta 38/5, 703-714.

Mäder, U. & Wersin, P. (2023): Reference porewaters for SGT Stage 3 of the Opalinus Clay for the siting regions Jura Ost (JO), Nördlich Lägern (NL) and Zürich Nordost (ZNO). Nagra Arbeitsbericht NAB 22-47.

Maes, N., Glaus, M., Baeyens, B., Marques Fernandes, M., Churakov, S., Dähn, R., Grangeon, S., Tournassat, C., Geckeis, H., Charlet, L., Brandt, F., Poonoosamy, J., Hoving, A., Havlova, V., Scheinost, A., Fischer, C., Noseck, U., Britz, S., Siitari-Kauppi, M. & Missana, T. (2021): State-of-the-art report on the understanding of radionuclide retention and transport in clay and crystalline rocks. Final version as of 30.04.2021 of deliverable D5.1 of the HORIZON 2020 project EURAD. European Joint Programme on Radioactive Waste Management EURAD.

Marinich, O., Marques Fernandes, M., Miron, G.D. & Kulik, D.A. (2024): ClaySor 2023: Update of 2SPNE SC/CE Sorption Model for Illite and Montmorillonite in GEMS Implementation. Nagra Technical Report NTB 23-05.

Marques Fernandes, M., Marinich, O., Miron, G.D. & Baeyens, B. (2024a): Sorption of Cs, Ni, Eu, Th and U on drill core samples of Opalinus Clay and confining geological units from deep boreholes in the potential siting regions Nördlich Lägern, Zürich Nordost and Jura Ost: Measurements and predictive sorption modelling. Nagra Technischer Bericht NTB 23-01.

Marques Fernandes, M., Marinich, O., Miron, G.D., Kulik, D.A., Baeyens, B., Wüst, R.A.J., Becker, J. & Li, X. (2024b): Sorption databases for Opalinus Clay, confining geological units, and bentonite: Methods, concepts, and upscaling of data. Nagra Technical Report NTB 23-06.

Marques Fernandes, M., Mazurek, M., Wersin, P., Wüst, R.A.J. & Baeyens, B. (2024c): Cation-exchange properties of the Mesozoic sedimentary sequence of Northern Switzerland and modelling of the Opalinus Clay porewater. Applied Geochemistry. DOI: 10.1016/ j.apgeochem.2023.105852.

Mazurek, M., Gimmi, T., Zwahlen, C., Aschwanden, L., Gaucher, E.C., Kiczka, M., Rufer, D., Wersin, P., Fernandes, M.M., Glaus, M.A., Van Loon, L.R., Traber, D., Schnellmann, M. & Vietor, T. (2023): Swiss deep drilling campaign 2019–2022: Geological overview and rock properties with focus on porosity and pore-space architecture. Applied Geochemistry 159, 105839. DOI: 10.1016/j.apgeochem.2023.105839.

Naef, H., Büchi, M., Bläsi, H.R., Deplazes, G. & Gysi, M. (2019): Lithology Manual: Lithological description of drill cores and cuttings in Northern Switzerland. Nagra Arbeitsbericht NAB 19-11.

Nagra (1985): Project Gewähr 1985: Nuclear waste management in Switzerland: Feasibility studies and safety analyses. Nagra Project Report NGB 85-09.

Nagra (2002): Project Opalinus Clay: Safety report: Demonstration of disposal feasibility for spent fuel, vitrified high-level waste and long-lived intermediate-level waste (Entsorgungsnachweis). Nagra Technical Report NTB 02-05.

Nagra (2024a): Geological properties of the Jura Ost, Nördlich Lägern and Zürich Nordost siting regions for safety assessment. Nagra Arbeitsbericht NAB 24-10.

Nagra (2024b): Geosynthesis of Northern Switzerland. Nagra Technical Report NTB 24-17.

Nagra (2024c): Radiological consequence analysis for a deep geological repository in Northern Switzerland. Nagra Technical Report NTB 24-18.

Nagra (2024d): Synthesis of the performance assessment for a deep geological repository for radioactive waste. Nagra Technical Report NTB 24-22.

Ochs, M., Lothenbach, B., Wanner, H., Sato, H. & Yui, M. (2001): An integrated sorption-diffusion model for the calculation of consistent distribution and diffusion coefficients in compacted bentonite. Journal of Contaminant Hydrology (Migration '99) 47/43923, 283-296.

Oscarson, D.W. (1994): Surface diffusion: Is it an important transport mechanism in compacted clays? Clays and Clay Minerals 42/5, 534-543. DOI: 10.1346/CCMN.1994.0420504.

Parkhurst, D.L. & Appelo, C.A.J. (2013): Description of input and examples for PHREEQC Version 3—A computer program for speciation, batch-reaction, one-dimensional transport, and inverse geochemical calculations. (U.S. Geological Survey Techniques and Methods, book 6, Chap. A43). USGS, available online at https://pubs.usgs.gov/tm/06/a43/.

Shackelford, C.D. & Daniel, D.E. (1991): Diffusion in saturated soil. I: Background. Journal of Geotechnical Engineering 117/3, 467-484. DOI: 10.1061/(ASCE)0733-9410(1991) 117:3(467).

Tinnacher, R.M., Holmboe, M., Tournassat, C., Bourg, I.C. & Davis, J.A. (2016): Ion adsorption and diffusion in smectite: Molecular, pore, and continuum scale views. Geochimica et Cosmochimica Acta 177, 130-149. DOI: 10.1016/j.gca.2015.12.010.

Tournassat, C. & Steefel, C.I. (2015): 9. Ionic transport in nano-porous clays with consideration of electrostatic effects. *In:* Steefel, C.I., Emmanuel, S. & Anovitz, L. (eds.): Pore scale geochemical processes. De Gruyter, 287-330.

Tournassat, C. & Steefel, C.I. (2021): Modeling diffusion processes in the presence of a diffuse layer at charged mineral surfaces: a benchmark exercise. Computational Geosciences 25/4, 1319-1336. DOI: 10.1007/s10596-019-09845-4.

Van Loon, L.R. (2014): Effective diffusion coefficients and porosity values for argillaceous rocks and bentonite: Measured and estimated values for the provisional safety analyses for SGT-E2. Nagra Technical Report NTB 12-03.

Van Loon, L.R., Brandt, F., Glaus, M.A. & Klinkenberg, M. (2025) (*in prep.*): Laboratory diffusion experiments with HTO, D_2O, $H_2{}^{18}O$, $^{36}Cl^-$, Br^-, I^-, $^{79}SeO_4^{2-}$, $^{22}Na^+$, $^{85}Sr^{2+}$, $^{133}Ba^{2+}$ and $^{226}Ra^{2+}$ in Opalinus Clay parallel to the bedding plane: experimental results and modelling. Applied Geochemistry.

Van Loon, L.R., Bunic, P., Frick, S., Glaus, M.A. & Wüst, R.A.J. (2023): Diffusion of HTO, ^{36}Cl and ^{22}Na in the Mesozoic rocks of northern Switzerland: I. Effective diffusion coefficients and capacity factors across the heterogeneous sediment sequences. Applied Geochemistry 159, 105843. DOI: 10.1016/j.apgeochem.2023.105843.

Van Loon, L.R. & Glaus, M.A. (2008): Mechanical compaction of smectite clays increases ion exchange selectivity for cesium. Environmental Science & Technology 42/5, 1600-1604. DOI: 10.1021/es702487m.

Van Loon, L.R., Glaus, M.A., Bunic, P., Frick, S. & Wüst, R.A.J. (2024): Diffusion measurements of HTO, $^{36}Cl^-$ and $^{22}Na^+$ on rock samples of Opalinus Clay and confining geological units from deep boreholes of Northern Switzerland: Jura Ost, Nördlich Lägern and Zürich Nordost. Nagra Arbeitsbericht NAB 23-26.

Van Loon, L.R., Glaus, M.A. & Müller, W. (2007): Anion exclusion effects in compacted bentonites: Towards a better understanding of anion diffusion. Applied Geochemistry 22/11, 2536-2552. DOI: 10.1016/j.apgeochem.2007.07.008.

Van Loon, L.R. & Mibus, J. (2015): A modified version of Archie's law to estimate effective diffusion coefficients of radionuclides in argillaceous rocks and its application in safety analysis studies. Applied Geochemistry 59, 85-94. DOI: 10.1016/ j.apgeochem.2015.04.002.

Van Loon, L.R., Soler, J.M. & Bradbury, M.H. (2003): Diffusion of HTO, $^{36}Cl^-$ and $^{125}I^-$ in Opalinus Clay samples from Mont Terri: Effect of confining pressure. Journal of Contaminant Hydrology 61, 73-83.

Van Loon, L.R., Soler, J.M., Müller, W. & Bradbury, M.H. (2004): Anisotropic diffusion in layered argillaceous rocks: A case study with Opalinus Clay. Environmental Science & Technology 38/21, 5721-5728. DOI: 10.1021/es049937g.

Zwahlen, C., Gimmi, T., Jenni, A., Kiczka, M., Mazurek, M., Van Loon, L.R., Mäder, U. & Traber, D. (2024): Chloride accessible porosity fractions across the Jurassic sedimentary rocks of Northern Switzerland. Applied Geochemistry 162, 105841. DOI: 10.1016/ j.apgeochem.2023.105841.

App. A Abstraction supplements

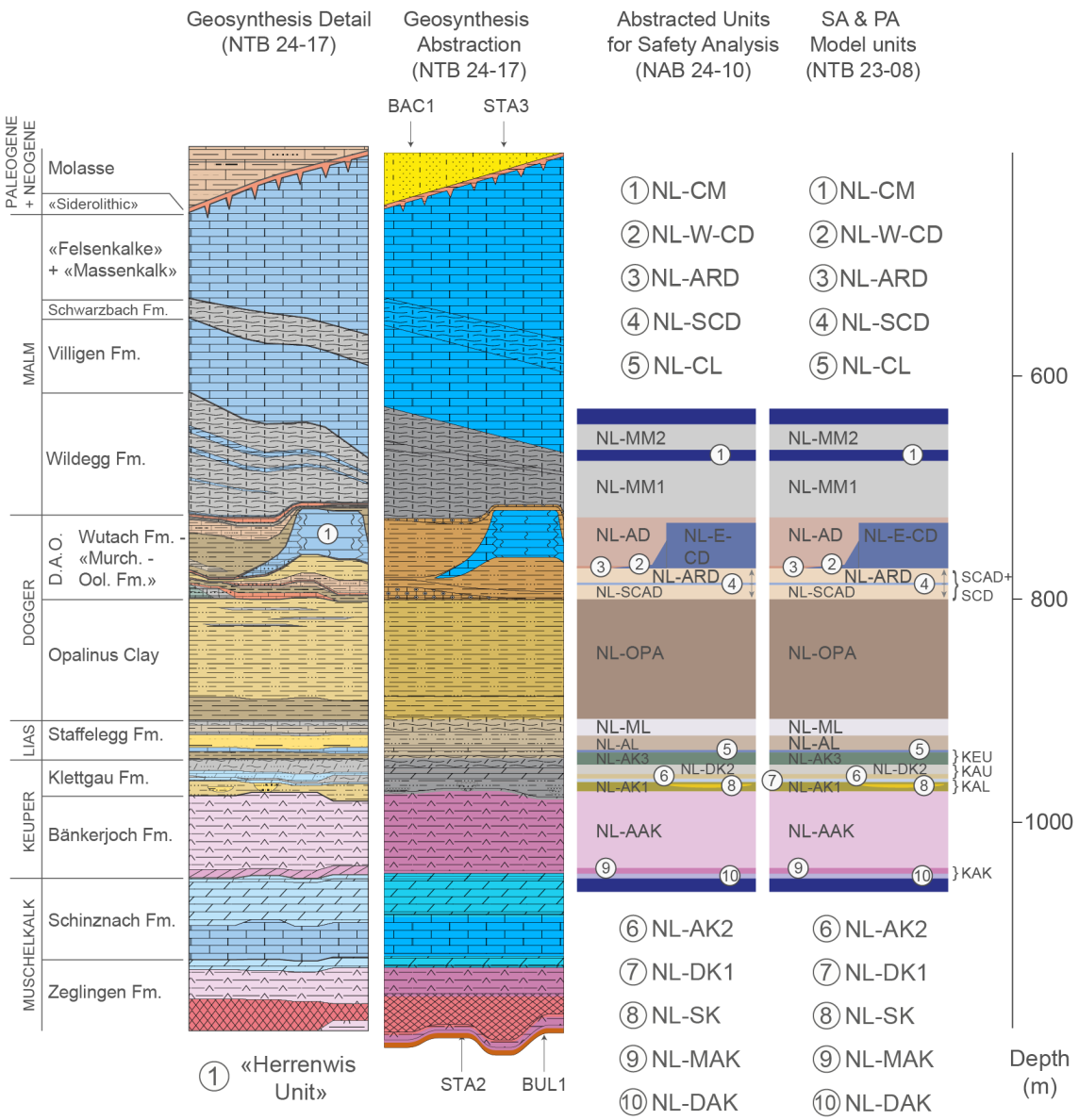

Fig. A-1: Example of the abstraction of the sedimentary Mesozoic sequence (Nagra 2024b) of the NL siting region into modelling units

Some of the abstracted units (Nagra 2024a) were further simplified to form abstracted units used for transport model calculations for safety and performance analysis

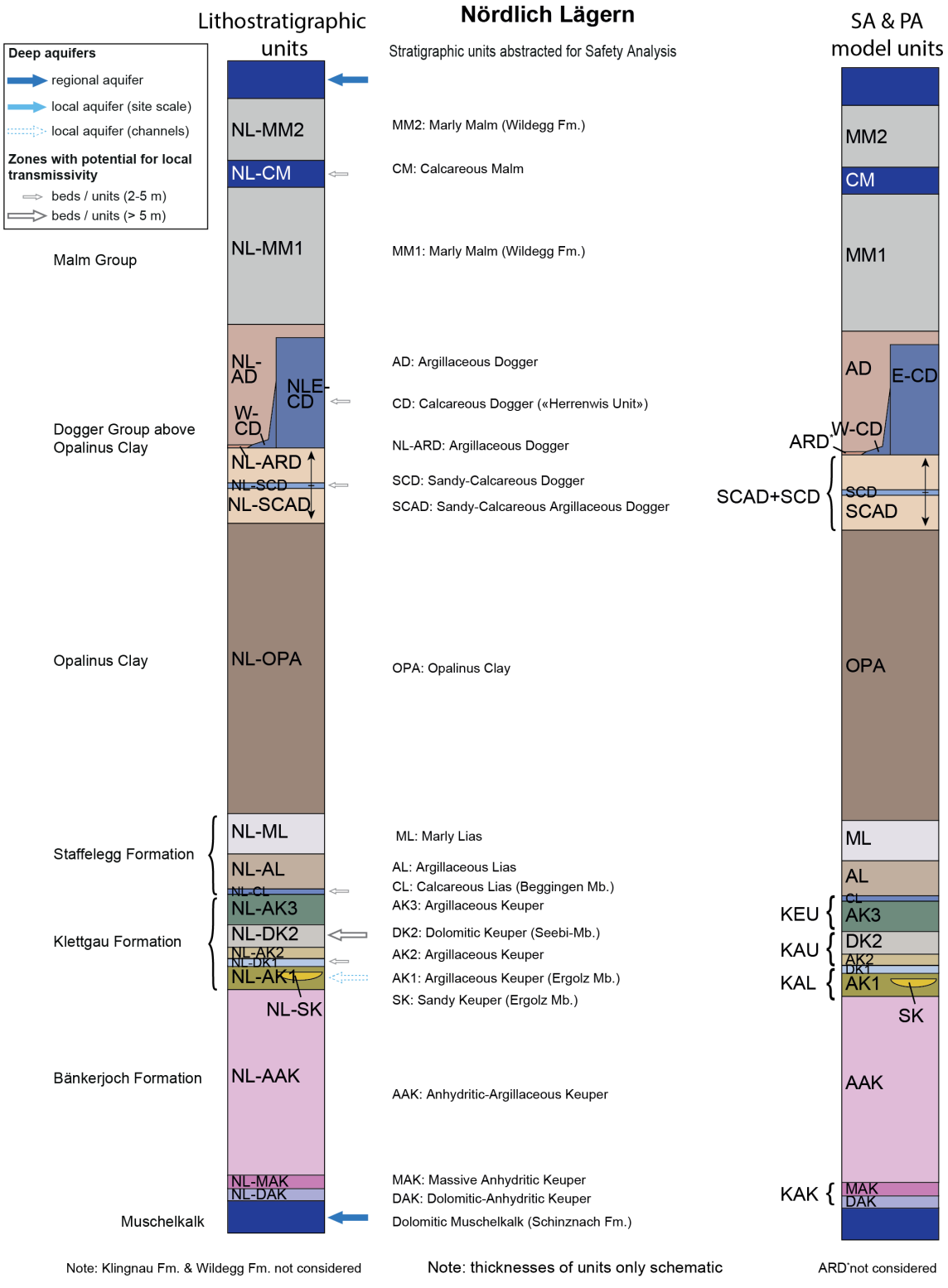

Fig. A-2: Illustration of the abstracted units for transport modelling applications for the NL siting region

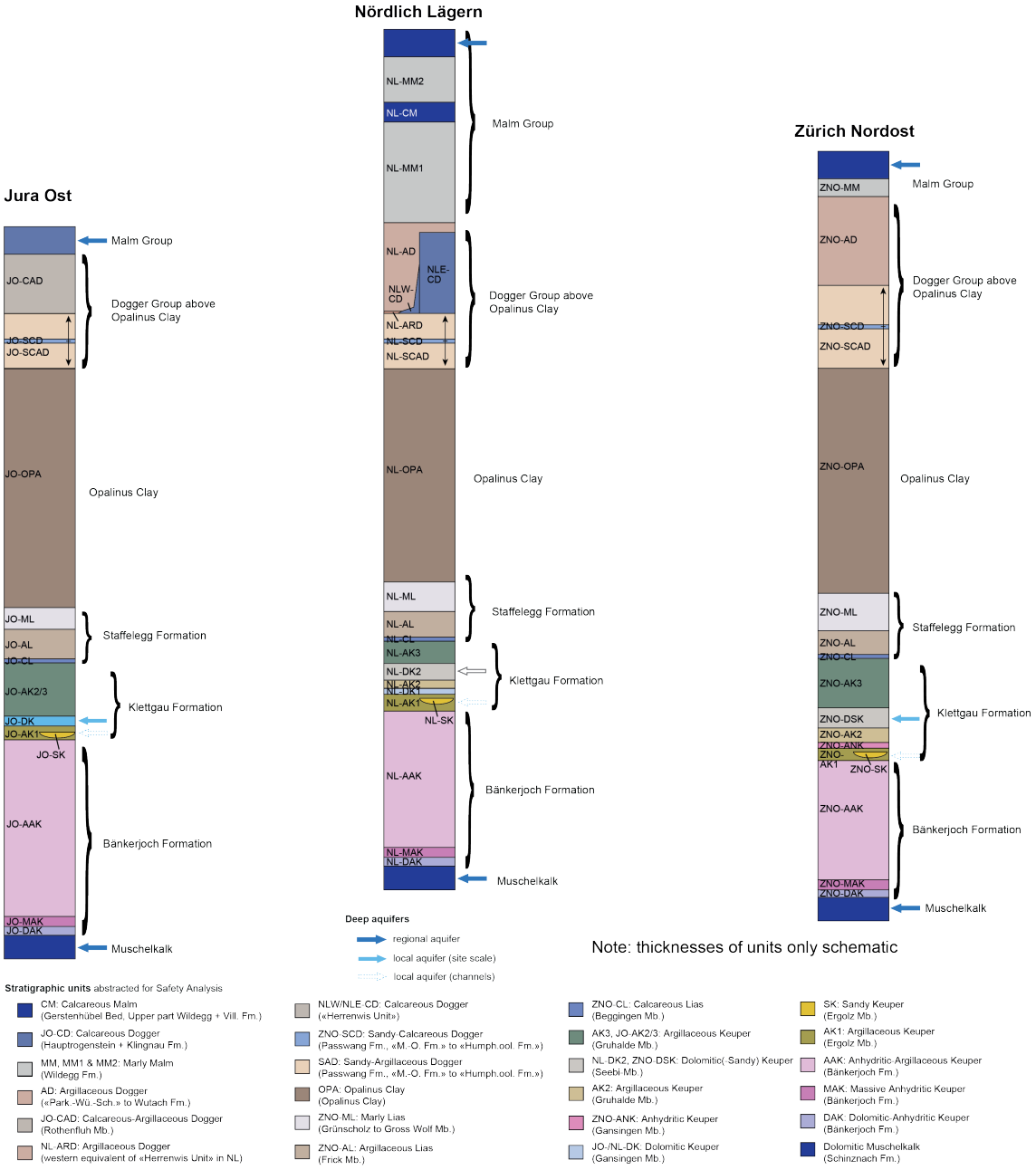

Fig. A-3: Abstracted model illustration of JO, NL, and ZNO

Tab. A-1: Tabulated formation and abstracted units used for transport model calculations for the three siting regions JO, NL, and ZNO

SA & PA: Safety and performance analysis

Jura Ost (JO)		
Lithostrat. Unit	Abstract	SA & PA
Dogger Group above Opalinus Clay	CAD	**CAD**
	SCD	**SCAD+SCD**
	SCAD	
Opalinus Clay	OPA	**OPA**
Staffelegg Fm	ML	**ML**
	AL	**AL**
	CL	**KEU**
	AK2/3	
Klettgau Fm	DK	**KAL**
	AK1/SK	
Bänkerjoch Fm	AAK	**AAK**
	MAK	**KAK**
	DAK	

Nördlich Lägern (NL)		
Lithostrat. Unit	Abstract	SA & PA
Dogger Group above Opalinus Clay	MM2	**MM2**
	CM	**CM**
	MM1	**MM1**
	AD	**AD**
	E-CD / W-CD	**E-CD / W-CD***
	SCD	**SCAD+SCD**
	SCAD	
Opalinus Clay	OPA	**OPA**
Staffelegg Fm	ML	**ML**
	AL	**AL**
	CL	**KEU**
	AK3	
Klettgau Fm	DK2	**KAU**
	AK2	
	DK1	**KAL**
	AK1/SK	
Bänkerjoch Fm	AAK	**AAK**
	MAK	**KAK**
	DAK	

Zürich Nordost (ZNO)		
Lithostrat. Unit	Abstract	SA & PA
Dogger Group above Opalinus Clay	MM	**MM**
	AD	**AD**
	SCD	**SCAD+SCD**
	SCAD	
Opalinus Clay	OPA	**OPA**
Staffelegg Fm	ML	**ML**
	AL	**AL**
	CL	**KEU**
	AK3	
Klettgau Fm	DSK	**KAU**
	AK2	
	ANK	**KAL**
	AK1/SK	
Bänkerjoch Fm	AAK	**AAK**
	MAK	**KAK**
	DAK	

* ARD is not considered separately.